CHARACTERIZING THE TRANSPORT AND DISPOSITION OF RESVERATROL AND ITS METABOLITES IN THE PRESENCE OF MRP2, BCRP AND ENTEROHEPATIC CIRCULATION INHIBITORS

A Dissertation Submitted to

the Temple University Graduate Board

In Partial Fulfillment

of the Requirements for the Degree

DOCTOR OF PHILOSOPHY

---

by

Aneesh A. Argikar

July 2016

Examining Committee Members:

Dr. Swati Nagar, Advisory Chair, Department of Pharmaceutical Science
Dr. Kenneth Korzekwa, Department of Pharmaceutical Science
Dr. Ho-Lun Wong, Department of Pharmaceutical Science
Dr. Konstatine Skordos, Director Clinical Pharmacology Translational Clinical Oncology, Novartis Corporation

ABSTRACT

My research deals with the interplay between metabolism and transport of resveratrol and its metabolites. It takes into account the role of uptake and efflux transporters and enterohepatic circulation in the disposition of resveratrol and conjugated metabolites of resveratrol. The issue of enzyme- and transporter-mediated drug-drug interaction (DDI) is also addressed.

Chapter 1 presents an introduction to resveratrol, its biological activities as well as its interactions with enzymes and transporters. It provides a background for enzyme inhibition. It also explains the hypotheses and describes in short, the studies performed.

Chapter 2 is based on P450 enzyme inhibition. In the first part of this chapter, we explored the ability of sandwich cultured cryopreserved human hepatocytes to predict inhibition parameters and drug-drug interaction (DDI) values. Two lots of cryopreserved human hepatocytes were used to predict inhibition parameters. The predicted DDI values were compared with those reported in literature and clinical studies and were found to be within 1.5 fold of those reported in clinical studies.

The second part of this chapter focuses on the potential of resveratrol or resveratrol-3-glucuronide (R3G) to inhibit CYP2C8. CYP2C8 has been found to be inhibited by glucuronide metabolite such as gemfibrozil-O-β-glucuronide and clopidogrel-β-glucuronide. Hence, we examined the potential of resveratrol, R3G and resveratrol-3-sulfate (R3S) to inhibit CYP2C8. We found that resveratrol, R3G and R3S inhibited CYP2C8 in a reversible manner.

Chapter 3 details studies performed in human cancer cell lines (HT-29 and Caco-2) to study the role of uptake transporters in the disposition of resveratrol and R3G. Western blotting was initially performed to examine the expression of OATP1B

transporters in cancer cell lines. Uptake studies were performed in HT-29 and Caco-2 cell lines with atorvastatin as a positive control. Both, western blots and uptake studies were inconclusive in detecting the presence of OATP1B transporters. Our studies showed that resveratrol undergoes passive diffusion and sulfation in Caco-2 cell line. The uptake of R3G in Caco-2 cell line was not detectable.

In chapter 4, we evaluated the impact of inhibition of efflux transporters on the disposition of resveratrol, R3G and R3S. Mrp2 and bcrp inhibition studies were performed in mice and resveratrol, R3G and R3S were monitored using LC-MS/MS. Non-compartmental analysis was performed to obtain pharmacokinetic parameters. We observed that the inhibition of efflux transporters had a greater impact on area under the curve (AUC) of R3S as compared to R3G and resveratrol.

Resveratrol and R3G have been shown to undergo enterohepatic circulation (EHC). This occurs due to the action of gut bacterial β-glucuronidase. This enzyme converts the glucuronide metabolite into parent, which is reabsorbed into enterocytes. The impact of inhibition of gut bacterial β-glucuronidase due to antibiotics was studied in chapter 5. Elimination of gut microbiome was attempted by using a combination of neomycin and bacitracin. Non-compartmental analysis was performed on the observed data. There was no observable difference in the AUCs of resveratrol, R3G and R3S.

Chapter 6 deals with simulations performed using an existing pharmacokinetic model to explain the data obtained upon transporter and EHC inhibition. The simulations showed that the inhibition of transporters seemed to decrease the elimination rate constant of R3G and R3S.

In summary, we investigated the impact of transporters on pharmacokinetics of resveratrol and its major metabolites. We also investigated P450 inhibition in sandwich

cultured human hepatocytes and the potential of resveratrol, R3G and R3S to inhibit rCYP2C8. We were able to show that inhibition of transporters does impact pharmacokinetics of R3S and R3G.

ACKNOWLEDGEMENTS

My journey began in Fall 2007 and has been a long one as a graduate student. I met many people, made a lot of friends and learnt a whole lot more. As I near the end of this journey, I have learnt that I will always be a student of science and I will continue to learn because whatever I've learnt so far is just a drop in the ocean. I would like to say a big thank you to my advisor-Dr. Swati Nagar who supported and encouraged me throughout my PhD program. Dr. Nagar has been a great professor and a mentor to me since 2009 when I joined her laboratory as a research associate and later as a graduate student. She helped me to develop scientific skills and critical thinking which benefited me to become a scientist. It was my great fortune to be a part of her laboratory. I would also like to thank Dr. Nagar and the department of Pharmaceutical Science for giving me the opportunity to enter the PhD program. I would like to say a special thanks to Dr. Kenneth Korzekwa. Dr. Korzekwa has been a great professor and a huge wealth of knowledge. I deeply appreciate all the discussions I had with him.

I am thankful to Dr. Konstantine Skordos, Ms. Dung Nguyen and Dr. Nagar for giving me the co-op opportunity at GlaxoSmithKline PLC, PA. I am thankful to Dr. Skordos for providing me with scientific insights and to Ms. Nguyen for helping me with mass spectrometry. It was a great experience to work at GSK in a multidisciplinary team of scientists.

I would like to say a big thank Dr. Doukas, Dr. Canney and Dr. Nagar for the financial assistance during my PhD program. I would also like to thank NIH (grant 1R03CA159389) for partially supporting my project. A big thanks to all my professors, fellow graduate students and specially the members of Nagar, Korzekwa laboratories. It

was a delight to share and talk science with each member (Priyanka, Jaydeep, Chuong, Kim and Min). Thanks to Ms. Cutler for her prompt help on many issues throughout my program.

Finally, I would like to thank my family-my grandmother, my father, my mother, my brother and my sister-in-law for their constant support throughout my student life. My parents have always been my pillar of strength. My parents and my grandmother encouraged and supported me through thick and thin and I wouldn't have reached the end of this program without their support.

DEDICATION

To,

SHRISADGURU

The one who nurtured and supported me.

TABLE OF CONTENTS

LIST OF TABLES

LIST OF FIGURES

ABBREVIATIONS

R3G: Resveratrol-3-O-Glucuronide
R4'G: Resveratrol-4'-O-Glucuronide
R3S: Resveratrol-3-O-Sulfate
R4'S: Resveratrol-4'-Sulfate
UGTs: Uridine 5'-diphospho-glucuronosyltransferases
Caco-2: Human colon adenocarcinoma 2
SULTs: Sulfotransferases
THP-1: Human monocytic cell line-1
U937: Histiocytic lymphoma cell line
HT-29: Human colorectal adenocarcinoma-29
HCT 116: Colorectal carcinoma 116
MCF-7: Michigan cancer foundation-7 (breast cancer cell line)
NO: Nitric oxide
ROS: Reactive oxygen species
HLM: Human liver microsomes
i.v.: intra-venous
OATP: Organic anion transporting polypeptide
MRP: Multidrug resistance-associated protein
ABC: ATP binding cassette
SLC: Solute linked carrier
HeLa: Henrietta Lacks (cervical cancer cell line)
Hep G2: Hepatocellular carcinoma cell line
DDI: Drug –Drug Interaction
YAMC: Young adult mouse colon
IMCE: Immorto-Min colonic epithelium
PK: Pharmacokinetic
MDR: Multidrug resistance
LC-MS/MS: Liquid chromatography-tandem mass spectrometer
EHC: Enterohepatic circulation
LS: Low spin
HS: High spin
MBI: Mechanism-based inactivator
SCHH: Sandwich cultured human hepatocytes
NPV: Nucleopolyhedroviruses
DNA: Deoxyribonucleic acid
NME: New molecular entity
RLM: Rat liver microsomes
CAD: Collision gas
CUR: Curtain gas
GS1: Ion source gas
IS: Ion spray
DP: Dispersing potential
CE: Collision energy
CXP: Cell exit potential
EP: Entrance potential
i.p.: intra-peritoneal
i.a.: intra-arterial
AUC: Area under the curve
AIC: Akaike information criterion

TDI: Time dependent inhibition

HCA-7: Human colonic adenocarcinoma-7

HMG-CoA: 3-hydroxy-3-methylglutaryl-coenzyme A

GSH: Glutathione

CDCF: 5(6)-Carboxy-2,'7' dichlorofluorescein

MOPS: [3-(N-Morpholino)propanesulfonic acid]

ATP: Adenosine triphosphate

kDa: kilo Dalton

RIPA: RadioImmunoPrecipitation Assay

CHAPTER 1

INTRODUCTION

1.1 Resveratrol:

1.1.1 Sources:

Resveratrol or trans-3, 5, 4'-trihydroxystilbene (Figure 1.1) is a phytoalexin, which is a naturally occurring compound produced by some plants due to bacterial or fungal infection. Resveratrol is found in grapes, certain nuts, berries etc. Resveratrol was isolated from the roots of white hellebore (*Veratrum grandoflorum O.Loes*) in 1940 and from the roots of *Polygonum cuspidatum* in 1960 (Baur and Sinclair, 2006).

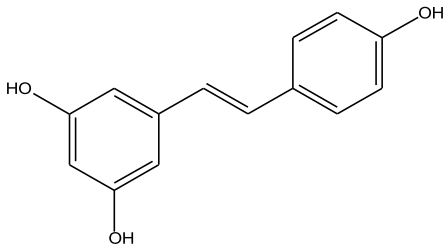

Figure 1.1. Resveratrol

1.1.2 Chemical properties:

Resveratrol is a naturally occurring polyphenol and is characterized by the presence of three hydroxyl groups. Resveratrol exists as two geometric isomers: cis-(Z) and trans-(E) isoforms. Resveratrol is highly photosensitive (Fremont, 2000).

1.1.3 Biological activities:

Resveratrol has been associated with several biological activities. Evidence for some of these activities has been provided while others are still debated. A few examples of the attributed activities will be discussed in this chapter.

(a) Cancer chemopreventive:

Resveratrol was recognized to act on different stages of cancer, which was attributed to its cancer chemopreventive activity (Jang et al., 1997). Resveratrol was shown to inhibit NF-κB in human multiple myeloma cells (Sun et al., 2006) and also in THP-1 and U937 cell lines (Holmes-McNary and Baldwin, 2000).

(i) In-house generated anti-proliferation data:

Resveratrol was tested for its cancer chemopreventive activity based on an in vitro mechanistic assay. Anti-proliferative activity of several phytochemicals was tested in human colorectal adenocarcinoma and breast cancer cell lines such as Caco-2, HT-29, HCT-116 and MCF-7 (Table 1.1). These compounds include resveratrol, pterostilbene, pinosylvin, piceatannol and trimethoxy stilbene. Parameters such as number of cells in each well were optimized. Alamar blue (Abd Serotec, Bio Rad, Raleigh, NC) was used in the anti-proliferation assay as a reagent to assess the growth of cells (Riss et al., 2004; Vega-Avila and Pugsley, 2011). Alamar blue reagent contains resazurin, which is reduced to resorufin. The fluorescence from resorufin is read using a plate reader (Spectramax M2, Molecular Devices Inc., Sunnyvale, CA).The data obtained from these studies was processed to obtain an IC_{50} value for each compound in each cell line. Observations: The predicted IC_{50} for all the compounds are summarized in table 1.1. The IC_{50} values were predicted using Graphpad prism for windows (version 6.0, Graphpad

Software Inc., California). Resveratrol showed more activity against the Caco2 cell line than other cell lines.

Table 1.1. IC_{50} values of phytochemicals in 4 different cell lines

Phytochemicals	IC_{50} (μM)			
	Caco-2	MCF-7	HT-29	HCT-116
trans-Resveratrol	59.8 ± 1.23	373.2 ± 2.0	938 ± 2.23	270.8 ± 1.38
Piceatannol	2032 ± 3.75	65.4 ± 1.31	456 ± 1.74	234.9 ± 1.35
Pinosylvin	87.7 ± 1.28	318.7 ± 1.52	130.7 ± 1.29	114.4 ± 1.63
Trimethoxy stilbene	218.7 ± 1.35	132.4 ± 1.62	213.3 ± 1.5	1104 ± 2.25
Pterostilbene	55 ± 1.17	122 ± 1.22	105 ± 1.35	67.24 ± 1.25

Data is expressed ± standard error.

(b) Cardio-protective:

Resveratrol has been thought to be responsible for the phenomenon known as the 'French paradox' (Renaud and de Lorgeril, 1992; Jang et al., 1997; Furimsky et al., 2008; Canistro et al., 2009; Yang et al., 2014), which shows a reduced incidence of cardiovascular disease in people with high fat intake and moderate consumption of wine. Various mechanisms have been proposed for this effect. These include prevention of platelet aggregation (Kirk et al., 2000; Bertelli et al., 2001; Wang et al., 2002b; Lin et al., 2009; Wu et al., 2011), prevention of low-density lipoprotein (LDL) oxidation (Belguendouz et al., 1997; Zou et al., 1999; Zou et al., 2000) and reduced areas of atherosclerotic plaques (Wang et al., 2005b; Wu et al., 2011). It has been shown that cardiomyocyte survival decreases in ischemic conditions leading to numerous alterations in myocardium (Hearse, 1994). Reperfusion of ischemic conditions also leads to

disruption of regular cell functions. Increased reactive oxygen species (ROS) or increased intracellular calcium has been suggested to be some of the underlying causes (Zweier, 1988; Brooks et al., 1995). Resveratrol has been proposed to be cardio- protective by facilitating an increase in the production of NO in endothelial cells and by serving as an antioxidant against reactive oxygen species (Fitzpatrick et al., 1993; Hung et al., 2000).

(c) Antioxidant:

Resveratrol has been shown to be an antioxidant (Hung et al., 2000). Several biological activities attributed to resveratrol indirectly relate to its antioxidant property. Resveratrol has been suggested to scavenge reactive oxygen species (ROS) (Leonard et al., 2003) and modulate enzymes, which play a role in production or elimination of ROS (Leonard et al., 2003; Carrizzo et al., 2013). Contrary to this belief, there have been reports of antioxidants such as resveratrol, genistein and quercetin inducing genotoxicity and mutagenesis in mammalian cell lines (Kulling and Metzler, 1997; Stopper et al., 2005; Gatz and Wiesmuller, 2008; Lu et al., 2013).

1.1.4 In vivo and in vitro metabolism of resveratrol:

(a) Cytochrome P450 (P450s):

Several P450 enzymes metabolize resveratrol. Resveratrol is metabolized by CYP1A2 and CYP1A1 to piceatannol and a tetrahydroxystilbene metabolite in recombinant P450 and human liver microsomes (HLM) (Piver et al., 2004). Resveratrol is also metabolized by human lymphoblast expressed CYP1B1 microsomes to piceatannol (Potter et al., 2002). Resveratrol has been shown to be an inhibitor of P450s as well, which will be discussed later in this chapter (section 1.1.5).

(b) Uridine 5'-diphosphoglucuronosyltransferases (UGTs):

The presence of three hydroxyl groups on 3, 4' and 5 positions of resveratrol make it an excellent candidate for glucuronidation and sulfation. Resveratrol undergoes extensive conjugative metabolism resulting in low oral bioavailability. Oral dose of labeled resveratrol in humans yielded isomeric glucuronide metabolites and a sulfate metabolite. Resveratrol-3-O-glucurinide (R3G) is the major metabolite (fig. 1.2) (Walle et al., 2004).

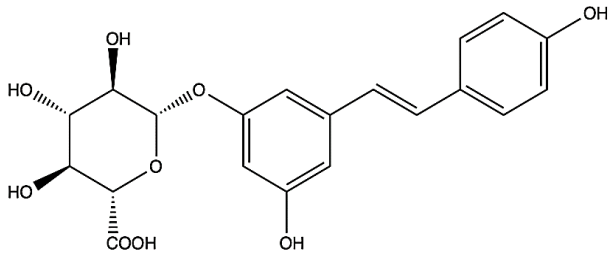

Figure 1.2. Resveratrol-3-glucuronide (R3G)

The rate of glucuronidation of resveratrol was calculated in human liver samples and was observed to be higher than the rate of sulfation (0.58-0.96 nmole/min/mg and 90 pmole/min/mg respectively) (de Santi et al., 2000a). In vitro glucuronidation in human liver microsomes (HLM) of trans- and cis-resveratrol led to the formation of R3G (fig.1.2) and R4'G. In vitro studies in recombinant UGTs indicated the contribution of UGT1A1, UGT1A6, UGT1A7, UGT1A9 and UGT1A10 towards the glucuronidation of resveratrol (Aumont et.al. 2001). UGT1A6 has been shown to metabolize resveratrol in a regio and stereo selectivive manner at 3-O position (Aumont et al., 2001).

(c) Sulfotransferases (SULTs):

Resveratrol undergoes sulfation in addition to glucuronidation (De Santi et al., 2000b; Otake et al., 2000). Three resveratrol sulfate metabolites have been reported in experiments involving incubations with S9 fraction and recombinant SULTs. These metabolites were found to be resveratrol-3-O-sulfate (fig. 1.3), resveratrol-4'-O-sulfate and resveratrol-3-O-4'-O-disulfate (Furimsky et al., 2008).

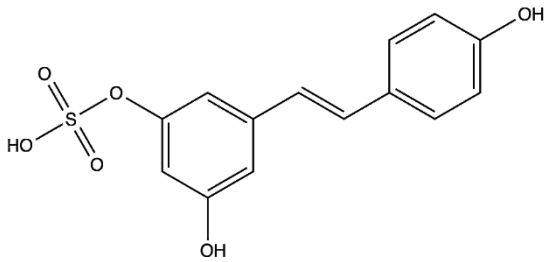

Figure 1.3. Resveratrol-3-sulfate (R3S)

Multiple SULTs such as SULT1A2, SULT1A1*1, SULT1E1 and SULT1A3 have been reported to be involved in resveratrol metabolism (Furimsky et al., 2008). Resveratrol undergoes sulfation in liver as well as duodenum with a K_m of 0.6µM and 0.5µM respectively (De Santi et al., 2000b).

1.1.5 Inhibition of enzymes by resveratrol:

Resveratrol has been shown to be a reversible and mechanism-based enzyme inactivator of several P450s. Resveratrol was reported to inhibit CYP1A1 in a bicistronic system (system simultaneous expressing 2 systems simultaneously) incubation via a mixed type inhibition (Chun et.al. 1999). Resveratrol inhibited CYP1A1 mediated ethoxyresorufin-O-deethylation (EROD) formation with IC_{50} of 23µM while

methoxyresorufin-o-demethylation (MROD) was inhibited with an IC_{50} of 11µM (Chun et.al. 1999). The IC_{50} values for CYP1A1 inhibition of EROD and MROD were 50 fold higher than CYP1A2 (Chun et al., 1999). Similar studies in recombinant enzymes and HLM revealed that resveratrol inhibited CYP1A1 and 1B1 by reversible inhibition while CYP1A2 was inhibited by mechanism-based inactivation with a K_I of 2.4 ± 0.4µM and k_{inact} of 0.43 ± 0.02min^{-1} (Chang et al., 2001). Another phenotyping study reported resveratrol to be a reversible inhibitor of human CYP1A1 and 1B1, and a mechanism-based inactivator of CYP1A2. Resveratrol derivatives were also shown to be P450 inhibitors (Mikstacka et al., 2008). Inhibition of CYP3A4 by resveratrol has been also reported in recombinant CYP incubation. Inhibition of CYP3A4 by resveratrol occurs by mechanism-based inactivation (K_I: 20µM, k_{inact}: 0.20min^{-1}) (Chan and Delucchi, 2000). Resveratrol was also suggested to inhibit CYP1A1 and 1A2 by inhibiting aryl-hydrocarbon induced CYP1A activity (Ciolino and Yeh, 1999). Resveratrol inhibited paclitaxel metabolism by inhibiting CYP2C8 (IC_{50}: 28.5 ± 4.6µM) but the mechanism of inhibition is not known (Vaclavikova et al., 2003). At high concentrations, resveratrol was found to inhibit estradiol sulfation in HLM by inhibition of SULT1E1 (Ung et.al. 2009).

1.1.6 Pharmacokinetics of resveratrol:

Absorption and metabolism of resveratrol was studied by rat intestinal perfusion (Andlauer et al., 2000). After luminal perfusion, 46% of administered dose was extraction and eliminated by lumen, while 20% of resveratrol was absorbed and reached the vascular side. The major metabolite to appear on the vascular side was resveratrol

glucuronide while resveratrol sulfate was the minor metabolite. The metabolism and enterohepatic circulation of resveratrol has been studied in rodents (Marier et al., 2002; Maier-Salamon et al., 2013). Following an i.v. dose, the decrease in resveratrol concentration followed a monoexponential profile with a sudden increase in resveratrol concentration due to enterohepatic circulation. The exposure of resveratrol glucuronide was 7 fold higher than resveratrol itself. For an oral dose, the exposure of resveratrol glucuronide was 48 fold higher than resveratrol. Thus, resveratrol was thought to undergo glucuronidation and secreted via bile into the intestine. In the intestine, resveratrol was thought to be absorbed as unconjugated resveratrol. Rapid absorption was reported in another study (Asensi et al., 2002) in which resveratrol (20mg/kg) was dosed orally to mice, rats and i.v. to rabbits. C_{max} for resveratrol was observed within 5 minutes of resveratrol administration. Extravascular concentrations of resveratrol were also measured. After oral administration, resveratrol concentration was found to be 1nmol/gm of tissue. So, the authors concluded that resveratrol did not accumulate in tissues (Asensi et al., 2002). Resveratrol concentrations in extravascular tissues such as brain, lung, liver and kidney in rabbit, rat and mouse were assessed (Asensi et al., 2002). Intra-arterial administration of preformed resveratrol metabolites was performed to distinguish between the kinetics of preformed and in vivo formed metabolites (Sharan et al., 2012).

A compartmental modeling approach was used to set up independent models for resveratrol (3-compartment open model), R3G (enterohepatic circulation open model) and R3S (2-compartment model). These three models were combined to form a more comprehensive model to predict the pharmacokinetics of in vivo formed metabolites (Sharan et al., 2012). ^{14}C-resveratrol, when administered at 25mg oral dose in humans

volunteers, showed a C_{max} of 10ng/ml after 1 hour with a second peak at around 6 hours, which, indicated enterohepatic circulation (Walle et al., 2004). The elimination half-life ranged from 7 to 14 hours. The percent of dose absorbed was found to be 70% (Walle et al., 2004). Goldberg et.al. conducted a study in human volunteers to assess the concentration of polyphenols after oral dosage of white wine, grape juice and vegetable extract (Goldberg et al., 2003). All the polyphenols were rapidly absorbed. The maximum concentration of resveratrol (416-471µg/l) was reached in 30 minutes. The concentration of free resveratrol in serum was low (1.7%-1.9%) as compared to the total resveratrol (conjugated + free) concentration (Goldberg et al., 2003).

1.1.7 Resveratrol, R3G, R3S and transporters:

Numerous biological activities have been attributed to resveratrol. The evidence of these biologically beneficial activities has not been prominent in in vivo studies. This is attributed to the extensive conjugation of resveratrol and the major metabolites being inactive. A new line of thinking proposes (Patel et al., 2013; Andreadi et al., 2014) that the metabolites of resveratrol, especially R3G and R3S may accumulate in tissues and serve as reservoirs for the parent thereby increasing the exposure of resveratrol. This accumulation in tissues, especially in eliminating tissues such as liver, may involve uptake transporters, which facilitate the flux of glucuronide and sulfate metabolites (Tamai et al., 2001; Sai et al., 2006). Bearing this in mind, and although a clear evidence of such uptake of resveratrol glucuronide or resveratrol sulfate is lacking, further investigations are required on uptake of resveratrol metabolites. A recent report on such uptake was published using HT-29 cell line as a system to study uptake of resveratrol

sulfate (Patel et al., 2013). Taking into account the active protein expression level and gene expression levels, it was hypothesized that an OATP transporter may be involved in the flux of resveratrol sulfate into the cell. Not much research has been performed on the uptake of resveratrol glucuronide into the cell. Resveratrol was shown to have transported across HepG2 cells by passive diffusion and also by uptake transporters (Lancon et al., 2007). Concentration and temperature dependence was shown in HepG2 cells.

There have been few reports on the transport of resveratrol, R3G and R3S by ABC (ATP binding cassette) transporters (van de Wetering et al., 2009). The transport of R3G and R3S was observed in MRP3 (multiple resistance associated protein-3) and BCRP (breast cancer resistance protein) vesicles prepared from transporter overexpressed cell line. Resveratrol-3-glucuronide was observed to be a substrate (K_m: 14 ± 2.2μM and V_{max}: 72 ± 4.5pmol/mg/min) and a competitive inhibitor (10μM) of estradiol glucuronide transport (K_i: 8μM) by MRP3 and showed a weak affinity for BCRP. BCRP was shown to transport R3G (K_m: 120±15μM and V_{max}: 340 ± 22 pmol/mg/min) (van de Wetering et al., 2009). Resveratrol sulfate and disulfate (Res di-S) metabolites were found to be a substrate (R3S, K_m: 5.0 ± 1.3μM, V_{max}: 1060 ± 69 pmol/mg/min and Res di-S, K_m: 10 ± 2.0μM, V_{max}: 1600 ± 94 pmol/mg/min) and competitive inhibitors of BCRP. At 10μM, R3S and Res di-S, inhibited transport of [^{3}H] methotrexate by BCRP (van de Wetering et al., 2009).

Mrp3 and bcrp lacking mice showed a profound difference in the pharmacokinetic profiles of resveratrol and its metabolites. Mice lacking mrp3 showed a 10-fold decrease in plasma levels of R3G while mice lacking bcrp showed only a slight increase of R3G and R3S plasma levels. Jejunum perfusion studies indicated that conjugation and

subsequent efflux of resveratrol glucuronide and sulfate by mrp2 and bcrp limit the bioavailability of resveratrol (Juan et al., 2010). A liver perfusion study in normal and mutant mrp2 wistar rats showed significant mrp2 related efflux of resveratrol glucuronide (Maier-Salamon et al., 2008; Maier-Salamon et al., 2011). The role of P-glycoprotein in the transport of resveratrol has been investigated as well. Resveratrol and other phytochemicals such as curcumin and capsaicin were evaluated as Pgp (P-glycoprotein) inhibitors in KB-C2 cells (Nabekura et al., 2005). These phytochemicals increased the accumulation of rhodamine 123 and daunorubicin. Resveratrol (10µg/ml) also led to increased accumulation of P-gp substrate doxorubicin in three cancer cell lines upon 2 hour incubation (MCF 7-15.9%, HeLa- 119.1% and HepG2- 40.5%) (Al-Abd et al., 2011). Resveratrol, in combination with doxorubicin and docetaxel was also shown to decrease mdr1a gene expression. Resveratrol (100µM) increased the accumulation of rhodamine 123 in P-gp overexpressed MCF-7 cell line. In vivo inhibition study in rats showed an increased exposure (10-11%) of diltiazem when resveratrol was administered as a perpetrator drug (Hong et al., 2008). The reason for this increase was proposed to be due to inhibition of CYP3A4 and P-gp in gut and/or liver. Resveratrol (2.5 and 10mg/kg) increased the oral bioavailability of diltiazem with increase in $AUC_{0-\infty}$ and C_{max} by 47-59%. The enzymes, which contribute to the metabolism of resveratrol, are summarized in table 1.2.

Table 1.2. Enzymes and transporters involved in metabolism of resveratrol

Protein involved	Substrate/victim	Kinetic parameters	Reference
CYP1A1	7-ethoxy resorufin methoxy resorufin	IC_{50}=23μM, IC_{50}=11μM	(Chun et al., 1999)
CYP1A2	7-ethoxy resorufin methoxy resorufin	IC_{50}=1200μM, IC_{50}=580μM	(Chun et al., 1999)
CYP1A2	7-ethoxy resorufin	K_I=2.4±0.4μM, k_{inact}=0.43±0.02min^{-1}	(Chun et al., 1999)
CYP1A1 CYP1A2 CYP1B1	7-ethoxy resorufin	K_{iapp}=1.2±0.1μM K_{iapp}=15.5±1.1μM K_{iapp}=0.8±0.1μM	(Chang et al., 2001)
CYP3A4	Testosterone	K_I=20μM, k_{inact}=0.20min^{-1}	(Chan and Delucchi, 2000)
CYP2C8	Paclitaxel	IC_{50}=26.5±2μM, (6α-hydroxylation)	(Vaclavikova et al., 2003)
SULT1E1	Estradiol	At 500μM resveratrol: 69%↓ in V_{max}/K_m	(Ung and Nagar, 2007)

1.2 Hypotheses:

This thesis deals with the interplay between metabolism and transport of resveratrol and its metabolites. It takes into account the role of uptake and efflux transporters and enterohepatic circulation in the disposition of resveratrol and conjugated metabolites of resveratrol. The issue of enzyme- and transporter-mediated drug drug interaction (DDI) is also addressed.

The hypotheses we sought to substantiate were:

1. (a) Cryopreserved sandwich culture human hepatocytes serve as a holistic system to predict DDI and (b) CYP2C8 could be inhibited by resveratrol or R3G.

2. As R3G is excreted via bile, it will be transported by intestinal uptake transporters and will be absorbed into systemic circulation. Also, uptake transporters present in liver will transport the circulating resveratrol and R3G.

3. The inhibition of efflux transporters such as mrp2 and bcrp will affect the disposition of resveratrol.

4. Resveratrol has been shown to undergo enterohepatic circulation. The inhibition of β-glucuronidase affects the disposition of resveratrol, R3G and R3S and may lead to decreased exposure of resveratrol and its conjugated metabolites.

5. A pharmacokinetic (PK) model could be used to simulate and explain in vivo transporter and enterohepatic circulation inhibition.

The hypotheses were tested with the following studies.

1. (a) Evaluate the use of sandwich cultured human hepatocytes to study time dependent inhibition; use the predicted KI and kinact to calculate DDI values using a static model, (b) Evaluate the inhibition of CYP2C8 by resveratrol, R3G and R3S.

2. Evaluate the transport of resveratrol, resveratrol-3-glucuronide by uptake transporters in HT-29 and Caco-2 cell lines.

3. Evaluate the influence of inhibition of mrp2 and bcrp in mice on the disposition of resveratrol, R3G and R3S.

4. Evaluate the impact of inhibition of enterohepatic circulation (EHC) on the disposition of resveratrol, R3G and R3S.

5. Use a PK model to simulate and provide possible explanations for the observed data.

The rationale for the above studies is explained below.

1. Enzyme inhibition in sandwich culture human hepatocytes and recombinant CYP2C8.

S9 fraction, HLM and recombinant enzymes are routinely used as enzyme systems to evaluate the metabolic profile of compounds. These systems are extremely valuable to study inhibition of P450s (Cytochrome P450s), UGTs, SULTs and other enzymes. The advantages of these systems include cost, simplicity with respect to use, ability to study one enzyme at a time and less experimental time. But these systems also face some disadvantages. These systems are artificial systems and hence do not resemble in vivo conditions. Induction of proteins cannot be studied in these systems. The study of complex interplay between transporters and enzymes is not captured. The enzymes are easily accessible in these systems, which often lead to over prediction of kinetic parameters. Hence, the use of hepatocytes helps in such cases.

To date, few studies have been done in cryopreserved sandwich cultured hepatocytes in order to predict time dependent inhibition and drug-drug interactions (DDIs) between CYP3A4 inhibitor and midazolam. In chapter 2, we explored the feasibility of using this system in a routine analysis to predict time dependent inhibition of a new chemical entity. A set of 8 compounds comprising of true positive, true negative, false positive and negative control was selected.

Given below is the list of these compounds:

1. Troleandomycin
2. Mibefradil
3. Ketoconazole
4. Verapamil
5. Diltiazem
6. Tamoxifen
7. Dihydralazine
8. Raloxifene

2. Evaluation of CYP2C8 inhibition by R3G

Next, we used the knowledge obtained about inhibition from the above assay and utilized it to evaluate CYP2C8 inhibition by resveratrol and R3G. Since it was revealed to be inhibited by gemfibrozil, gemfibrozil-O-β-glucuronide and clopidogrel glucuronide, CYP2C8 has been investigated for potential inhibition by many glucuronides (Ogilvie et al., 2006; Baer et al., 2009; Jenkins et al., 2011; Tornio et al., 2014). Inhibition of CYP2C8 due to gemfibrozil affects the metabolism of paclitaxel (Rahman et al., 1994), amodiaquine (Karonen et al., 2010), cerivastatin (Backman et al., 1994; Shitara et al., 2004), repaglinide (Kajosaari et al., 2005; Honkalammi et al., 2011) and rosiglitazone (Niemi et al., 2003). The acyl-β-D-glucuronide of clopidogrel was also found to inhibit CYP2C8 in a time dependent manner (Tornio et al., 2014). Current literature on inhibition of CYP2C8 exists for compounds such as gemfibrozil (Rahman et al., 1994), gemfibrozil glucuronide (Ogilvie et al., 2006), montelukast (Walsky et al., 2005), pioglitazone (Sahi et al., 2003), trimethoprim (Wen et al., 2002; Niemi et al., 2004; Hruska et al., 2005) and six herbal extracts such as garlic, echinacea, saw palmetto, valerian, black cohosh and cranberry (Albassam et al., 2014). Resveratrol is one of the

constituents of wine and commonly occurs in food. The intake of resveratrol is not monitored. In addition to this, it is also marketed as a nutraceutical. Resveratrol-3-glucuronide is one of the major metabolites and its exposure relative to parent is reported to be 46-fold higher (7.1μmol.h/l as compared to 324.7μmol.h/l) after oral administration (Marier et al., 2002). Considering the exposure R3G and the reported susceptibility of CYP2C8 to gemfibrozil-1-O-β-glucuronide, we explored the possibility of the inhibition of CYP2C8 due to resveratrol, R3G and R3S in chapter 2.

3. Evaluation of resveratrol and R3G uptake:

The OATP transporters are located on the apical membrane of enterocytes and on the basolateral membrane of the hepatocytes. OATP transporters are responsible for the uptake of numerous endogenous substrates and also xenobiotics. Substrates of OATP include statins and conjugated and unconjugated bile salts (Hagenbuch, 2010; Sharma et al., 2012). OATP has come into focus due to the potential of some compounds to inhibit OATP and cause a drug-drug interaction in gut as well as in liver (Shitara et al., 2004; Lau et al., 2007; Nakagomi-Hagihara et al., 2007; Sharma et al., 2012).

Resveratrol metabolites are hypothesized to serve as reserve pools for resveratrol (Patel et al., 2013). Transport of these metabolites by passive diffusion may be difficult due to the polar nature of the conjugates. Hence, the role of uptake transporters such as OATP1B1/1B3/1A2/2B1 in liver and OATP2A1/1A2/2B1 in gut needs further investigation. OATP uptake transporters have been reported to transport glucuronide and sulfate metabolites such as estrone-3-sulfate and estradiol-17-β-glucuronide (Tamai et al., 2001). Anionic compounds are thought to be absorbed via enterocytes by passive diffusion due to the acidic microenvironment (Shiau et al., 1985). But there has been

strong evidence of glucuronide and sulfate metabolite transport by human as well as rodent OATPs (Bossuyt et al., 1996; Kanai et al., 1996; Konig et al., 2000). In addition to these two metabolites, dehydroepiandrosterone sulfate was also shown to be transported by OATP in overexpressed oocytes (Kullak-Ublick et al., 1998; Konig et al., 2000). In this study we attempted to study the role of uptake transporters by using HT-29 and Caco-2 cells. A system with OATP transporter expression was not readily available. Hence, in chapter 3, we performed western blot to assess the expression of OATP1B transporters in HT-29 cell line. We also performed uptake assays for resveratrol and R3G in plated HT-29 and Caco-2 cells using atorvastatin as a positive control.

Considering the polar nature of the metabolites, the role of MRP2, BCRP was also investigated. MRP2 and BCRP are known to transport glucuronide and sulfate metabolites in liver and gut. Research has been ongoing to uncover the role of efflux transporters in the disposition of resveratrol and its major metabolites.

The possible role of ABCC2 (MRP2), ABCC3 (MRP3), ABCB1 (MDR1) and ABCG2 (BCRP) in the disposition of resveratrol, R3G and R3S has been evaluated in perfusion models, transporter vesicles and transporter knockout rodents (Maier-Salamon et al., 2008; van de Wetering et al., 2009; Juan et al., 2010; Maier-Salamon et al., 2011; Maier- Salamon et al., 2013). In chapter 4 of my thesis, an in vivo study was conducted in mice to study the impact of mrp2 and bcrp inhibition on the disposition of resveratrol, R3S and R3G. The data obtained from this study was used to perform simulations and understand the impact of transporter inhibition.

4. Impact of inhibition of mrp2, bcrp transporter and enterohepatic circulation (EHC):

(a) Inhibition of efflux transporters:

Resveratrol is extensively metabolized to glucuronide and sulfate metabolites. The fate of these metabolites is not entirely known. Upon oral dosing, resveratrol is metabolized in gut and the conjugates may be effluxed into the lumen. The fraction, which escapes gut metabolism, subsequently undergoes metabolism in liver. These metabolites are effluxed across apical membrane into the bile.

Mrp2 and bcrp inhibition experiments were conducted in mice. Inhibitors were administered intraperitoneally 30 minutes prior to administration of resveratrol. Blood samples were collected from both groups and the concentration of resveratrol, R3G and R3S was measured by using LC-MS/MS. The pharmacokinetic parameters were calculated using non-compartmental analysis.

(b) Impact of inhibition of bacterial β-glucuronidase:

As the glucuronides enter the small intestine, β-glucuronidase converts resveratrol-glucuronides into resveratrol, which is reabsorbed as parent. This is often seen as a second peak in the pharmacokinetic profile of resveratrol. In this way, enterohepatic circulation leads to an increased exposure of resveratrol (Marier et al., 2002; Sharan et al., 2012). Inhibition of enterohepatic circulation may lead to increased elimination of resveratrol as resveratrol glucuronide and sulfate via feces thus decreasing its total exposure. Enterohepatic circulation serves as a distribution pathway for resveratrol instead of a clearance pathway, which may complicate the prediction of bioavailability, clearance and volume of distribution for resveratrol.

The experiment to observe the impact of enterohepatic circulation (EHC) was conducted in C57BL/6 mice. Gut β-glucuronidase was eliminated by dosing oral antibiotics for four days prior to resveratrol administration and were also administered during the experiment. The control group was not treated with antibiotics. Blood samples were collected from both groups and the concentration of resveratrol, R3G and R3S was measured by using LC-MS/MS. The measured concentrations were used to calculate pharmacokinetic parameters for resveratrol, R3S and R3G. The data obtained from EHC inhibition was used to perform simulations using a pharmacokinetic model.

A previously developed pharmacokinetic model for resveratrol and its metabolites was used to simulate several in vivo scenarios (Sharan et al., 2012). These simulations were used to explain the data obtained from in vivo inhibition of transporters and enterohepatic circulation.

1.3 Significance of work:

Use of sandwich cultured cryopreserved human hepatocytes to predict drug interactions due to mechanism-based inactivation of metabolic enzymes is one of the newer techniques to study drug interactions. Although, this system has its disadvantages, it could be refined further. It will be extremely advantageous to identify a new chemical entity as a true/false positive and true/false negative. Hence, it could serve as a valuable tool in a preclinical setting. Development of a robust method to evaluate mechanism-based inactivation using sandwich cultured cryopreserved human hepatocytes was the first step toward using this technique as a tool in routine analysis of new chemical entities. As it expresses the entire range of metabolic enzymes, it could be used further to

study enzyme-transporter interplay, inhibition of transporters and compounds that cause enzyme inhibition and induction. The use of this technique to study time dependent inhibition is covered in the first part of chapter 2.

The second half of chapter 2 involves the evaluation of resveratrol, R3S and R3G as inhibitors of CYP2C8. Resveratrol being a naturally occurring compound which, is present in the daily diet. It has also been marketed as a nutraceutical due to its numerous beneficial biological actions. Based on previous observations about mechanism-based inactivation of P450s by resveratrol and high exposure of its metabolites, the following questions assume importance. 1. Does resveratrol or its metabolites inhibit CYP2C8? and 2.What is the mechanism of this inhibition? This information will serve in two ways: (a) it will make researchers aware of the interaction and importance of glucuronide metabolites with respect to CYP2C8 and (b) it will provide further evidence of the susceptibility of CYP2C8 with respect to glucuronide metabolites.

Recent research has provided evidence of the role of uptake transporters in the transport of glucuronides and sulfates. As resveratrol is metabolized to R3G and R3S, both of which could be transported by OATPs, the study to evaluate the role of uptake transporters may provide valuable insights into the disposition of resveratrol, R3G and R3S. In addition to this, R3G is secreted via bile into intestine, which has a significant expression of OATP transporter. Hence, the role of uptake transporters gains importance for compounds which, are subject to EHC. These studies are reported in chapter 3. One of the limitations of chapter 3 was to find a system that could be used to study uptake by OATP. Uptake activity and western blot studies in HT-29 cell line did not provide any

clear evidence of the presence of OATP transporter. Caco-2 cell line was used to perform uptake studies.

Considering the research already done on the role of efflux transporters in the disposition of resveratrol and its major metabolites, chapter 4 of the thesis, contains in vivo studies involving efflux transporter activity inhibition in mice.

The role of EHC in the disposition of resveratrol has been recognized from previous in vivo studies. The impact of inhibition of EHC has not been fully evaluated. An in vivo study was conducted in mice to evaluate the role of EHC. Inhibiting EHC was attempted by eliminating the gut bacteria that produce β-glucuronidase. Neomycin and bacitracin were dosed concomitantly in this study. Thus, chapter 5 serves to add to the current knowledge about the importance of gut β-glucuronidase for drugs that undergo enterohepatic circulation, and the use of simulation to explain the impact of inhibition of EHC on the disposition of resveratrol.

Chapter 6 of this thesis uses a previously developed pharmacokinetic model to simulate scenarios involving enzyme and transporter modulation. A simulation approach was used to explain the effect of inhibition of transporters and EHC on the disposition of resveratrol and its metabolites in the in vivo studies performed in chapter 4 and 5. The simulations were performed by varying the rate constants and matching the AUCs of resveratrol and its metabolites. The shape of the pharmacokinetic profile was also taken into account while performing the simulations.

REFERENCES

Al-Abd AM, Mahmoud AM, El-Sherbiny GA, El-Moselhy MA, Nofal SM, El-Latif HA, El-Eraky WI, and El-Shemy HA (2011) Resveratrol enhances the cytotoxic profile of docetaxel and doxorubicin in solid tumour cell lines in vitro. Cell Prolif 44:591-601.

Albassam AA, Mohamed ME, and Frye RF (2014) Inhibitory effect of six herbal extracts on CYP2C8 enzyme activity in human liver microsomes. Xenobiotica:1-7.

Andlauer W, Kolb J, Siebert K, and Furst P (2000) Assessment of resveratrol bioavailability in the perfused small intestine of the rat. Drugs Exp Clin Res 26:47-55.

Andreadi C, Britton RG, Patel KR, and Brown K (2014) Resveratrol-sulfates provide an intracellular reservoir for generation of parent resveratrol, which induces autophagy in cancer cells. Autophagy 10:524-525.

Asensi M, Medina I, Ortega A, Carretero J, Bano MC, Obrador E, and Estrela JM (2002) Inhibition of cancer growth by resveratrol is related to its low bioavailability. Free Radic Biol Med 33:387-398.

Aumont V, Krisa S, Battaglia E, Netter P, Richard T, Merillon JM, Magdalou J, and Sabolovic N (2001) Regioselective and stereospecific glucuronidation of trans- and cis- resveratrol in human. Arch Biochem Biophys 393:281-289.

Backman JT, Kyrklund C, Neuvonen M, and Neuvonen PJ (2002) Gemfibrozil greatly increases plasma concentrations of cerivastatin. Clin Pharmacol Ther 72:685-691.

Backman JT, Olkkola KT, Aranko K, Himberg JJ, and Neuvonen PJ (1994) Dose of Midazolam Should Be Reduced during Diltiazem and Verapamil Treatments. Br J Clin Pharmacol 37:221-225.

Baer BR, DeLisle RK, and Allen A (2009) Benzylic oxidation of gemfibrozil-1-O-beta-glucuronide by P450 2C8 leads to heme alkylation and irreversible inhibition. Chem Res Toxicol 22:1298-1309.

Baur JA and Sinclair DA (2006) Therapeutic potential of resveratrol: the in vivo evidence. Nat Rev Drug Discov 5:493-506.

Belguendouz L, Fremont L, and Linard A (1997) Resveratrol inhibits metal ion-dependent and independent peroxidation of porcine low-density lipoproteins. Biochem Pharmacol 53:1347-1355.

Bertelli AA, Baccalini R, Battaglia E, Falchi M, and Ferrero ME (2001) Resveratrol inhibits TNF alpha-induced endothelial cell activation. Therapie 56:613-616.

Bossuyt X, Muller M, Hagenbuch B, and Meier PJ (1996) Polyspecific drug and steroid clearance by an organic anion transporter of mammalian liver. J Pharmacol Exp Ther 276:891-896.

Breedveld P, Pluim D, Cipriani G, Dahlhaus F, van Eijndhoven MA, de Wolf CJ, Kuil A, Beijnen JH, Scheffer GL, Jansen G, Borst P, and Schellens JH (2007) The effect of low pH on breast cancer resistance protein (ABCG2)-mediated transport of methotrexate, 7-hydroxymethotrexate, methotrexate diglutamate, folic acid, mitoxantrone, topotecan, and resveratrol in in vitro drug transport models. Mol Pharmacol 71:240-249.

Brooks WW, Conrad CH, and Morgan JP (1995) Reperfusion induced arrhythmias following ischaemia in intact rat heart: role of intracellular calcium. Cardiovasc Res 29:536-542.

Canistro D, Bonamassa B, Pozzetti L, Sapone A, Abdel-Rahman SZ, Biagi GL, and Paolini M (2009) Alteration of xenobiotic metabolizing enzymes by resveratrol in liver and lung of CD1 mice. Food Chem Toxicol 47:454-461.

Carrizzo A, Forte M, Damato A, Trimarco V, Salzano F, Bartolo M, Maciag A, Puca AA, and Vecchione C (2013) Antioxidant effects of resveratrol in cardiovascular, cerebral and metabolic diseases. Food Chem Toxicol 61:215-226.

Chan WK and Delucchi AB (2000) Resveratrol, a red wine constituent, is a mechanism-based inactivator of cytochrome P450 3A4. Life Sci 67:3103-3112.

Chang TK, Chen J, and Lee WB (2001) Differential inhibition and inactivation of human CYP1 enzymes by trans-resveratrol: evidence for mechanism-based inactivation of CYP1A2. J Pharmacol Exp Ther 299:874-882.

Chun YJ, Kim MY, and Guengerich FP (1999) Resveratrol is a selective human cytochrome P450 1A1 inhibitor. Biochem Biophys Res Commun 262:20-24.

Ciolino HP and Yeh GC (1999) Inhibition of aryl hydrocarbon-induced cytochrome P-450 1A1 enzyme activity and CYP1A1 expression by resveratrol. Mol Pharmacol 56:760-767.

de Santi C, Pietrabissa A, Mosca F, and Pacifici GM (2000a) Glucuronidation of resveratrol, a natural product present in grape and wine, in the human liver. Xenobiotica 30:1047-1054.

De Santi C, Pietrabissa A, Spisni R, Mosca F, and Pacifici GM (2000b) Sulphation of resveratrol, a natural product present in grapes and wine, in the human liver and duodenum. Xenobiotica 30:609-617.

Fitzpatrick DF, Hirschfield SL, and Coffey RG (1993) Endothelium-dependent vasorelaxing activity of wine and other grape products. Am J Physiol 265:H774-778.

Fremont L (2000) Biological effects of resveratrol. Life Sci 66:663-673.

Furimsky AM, Green CE, Sharp LE, Catz P, Adjei AA, Parman T, Kapetanovic IM, Weinshilboum RM, and Iyer LV (2008) Effect of resveratrol on 17beta-estradiol sulfation by human hepatic and jejunal S9 and recombinant sulfotransferase 1E1. Drug Metab Dispos 36:129-136.

Gatz SA and Wiesmuller L (2008) Take a break--resveratrol in action on DNA. Carcinogenesis 29:321-332.

Goldberg DM, Yan J, and Soleas GJ (2003) Absorption of three wine-related polyphenols in three different matrices by healthy subjects. Clin Biochem 36:79-87.

Hagenbuch B (2010) Drug uptake systems in liver and kidney: a historic perspective. Clin Pharmacol Ther 87:39-47.

Hearse DJ (1994) Myocardial ischaemia: can we agree on a definition for the 21st century? Cardiovasc Res 28:1737-1744: discussion 1745-1736.

Holmes-McNary M and Baldwin AS, Jr. (2000) Chemopreventive properties of trans-resveratrol are associated with inhibition of activation of the IkappaB kinase. Cancer Res 60:3477-3483.

Hong SP, Choi DH, and Choi JS (2008) Effects of resveratrol on the pharmacokinetics of diltiazem and its major metabolite, desacetyldiltiazem, in rats. Cardiovasc Ther 26:269- 275.

Honkalammi J, Niemi M, Neuvonen PJ, and Backman JT (2011) Dose-dependent interaction between gemfibrozil and repaglinide in humans: strong inhibition of CYP2C8 with subtherapeutic gemfibrozil doses. Drug Metab Dispos 39:1977-1986.

Hruska MW, Amico JA, Langaee TY, Ferrell RE, Fitzgerald SM, and Frye RF (2005) The effect of trimethoprim on CYP2C8 mediated rosiglitazone metabolism in human liver microsomes and healthy subjects. Br J Clin Pharmacol 59:70-79.

Hung LM, Chen JK, Huang SS, Lee RS, and Su MJ (2000) Cardioprotective effect of resveratrol, a natural antioxidant derived from grapes. Cardiovasc Res 47:549-555.

Jang M, Cai L, Udeani GO, Slowing KV, Thomas CF, Beecher CW, Fong HH, Farnsworth NR, Kinghorn AD, Mehta RG, Moon RC, and Pezzuto JM (1997) Cancer chemopreventive activity of resveratrol, a natural product derived from grapes. Science 275:218-220.

Jenkins SM, Zvyaga T, Johnson SR, Hurley J, Wagner A, Burrell R, Turley W, Leet JE, Philip T, and Rodrigues AD (2011) Studies to further investigate the inhibition of human liver microsomal CYP2C8 by the acyl-beta-glucuronide of gemfibrozil. Drug Metab Dispos 39:2421-2430.

Juan ME, Gonzalez-Pons E, and Planas JM (2010) Multidrug resistance proteins restrain the intestinal absorption of trans-resveratrol in rats. J Nutr 140:489-495.

Kajosaari LI, Laitila J, Neuvonen PJ, and Backman JT (2005) Metabolism of repaglinide by CYP2C8 and CYP3A4 in vitro: effect of fibrates and rifampicin. Basic Clin Pharmacol Toxicol 97:249-256.

Kanai N, Lu R, Bao Y, Wolkoff AW, Vore M, and Schuster VL (1996) Estradiol 17 beta-D-glucuronide is a high-affinity substrate for oatp organic anion transporter. Am J Physiol 270:F326-331.

Karonen T, Filppula A, Laitila J, Niemi M, Neuvonen PJ, and Backman JT (2010) Gemfibrozil markedly increases the plasma concentrations of montelukast: a previously unrecognized role for CYP2C8 in the metabolism of montelukast. Clin Pharmacol Ther 88:223-230.

Kirk RI, Deitch JA, Wu JM, and Lerea KM (2000) Resveratrol decreases early signaling events in washed platelets but has little effect on platelet in whole blood. Blood Cells Mol Dis 26:144-150.

Konig J, Cui Y, Nies AT, and Keppler D (2000) A novel human organic anion transporting polypeptide localized to the basolateral hepatocyte membrane. Am J Physiol Gastrointest Liver Physiol 278:G156-164.

Kullak-Ublick GA, Fisch T, Oswald M, Hagenbuch B, Meier PJ, Beuers U, and Paumgartner G (1998) Dehydroepiandrosterone sulfate (DHEAS): identification of a carrier protein in human liver and brain. FEBS Lett 424:173-176.

Kulling SE and Metzler M (1997) Induction of micronuclei, DNA strand breaks and HPRT mutations in cultured Chinese hamster V79 cells by the phytoestrogen coumoestrol. Food Chem Toxicol 35:605-613.

Lancon A, Delmas D, Osman H, Thenot JP, Jannin B, and Latruffe N (2004) Human hepatic cell uptake of resveratrol: involvement of both passive diffusion and carrier- mediated process. Biochem Biophys Res Commun 316:1132-1137.

Lau YY, Huang Y, Frassetto L, and Benet LZ (2007) effect of OATP1B transporter inhibition on the pharmacokinetics of atorvastatin in healthy volunteers. Clin Pharmacol Ther 81:194-204.

Leonard SS, Xia C, Jiang BH, Stinefelt B, Klandorf H, Harris GK, and Shi X (2003) Resveratrol scavenges reactive oxygen species and effects radical-induced cellular responses. Biochem Biophys Res Commun 309:1017-1026.

Lin KH, Hsiao G, Shih CM, Chou DS, and Sheu JR (2009) Mechanisms of resveratrol-induced platelet apoptosis. Cardiovasc Res 83:575-585.

Lu LY, Ou N, and Lu QB (2013) Antioxidant induces DNA damage, cell death and mutagenicity in human lung and skin normal cells. Sci Rep 3:3169.

Maier-Salamon A, Bohmdorfer M, Riha J, Thalhammer T, Szekeres T, and Jaeger W (2013) Interplay between metabolism and transport of resveratrol. Ann N Y Acad Sci 1290:98-106.

Maier-Salamon A, Hagenauer B, Reznicek G, Szekeres T, Thalhammer T, and Jager W (2008) Metabolism and disposition of resveratrol in the isolated perfused rat liver: role of Mrp2 in the biliary excretion of glucuronides. J Pharm Sci 97:1615-1628.

Marier JF, Vachon P, Gritsas A, Zhang J, Moreau JP, and Ducharme MP (2002) Metabolism and disposition of resveratrol in rats: extent of absorption, glucuronidation, and enterohepatic recirculation evidenced by a linked-rat model. J Pharmacol Exp Ther 302:369-373.

Mikstacka R, Baer-Dubowska W, Wieczorek M, and Sobiak S (2008) Thiomethylstilbenes as inhibitors of CYP1A1, CYP1A2 and CYP1B1 activities. Mol Nutr Food Res 52 Suppl 1:S77-83.

Nabekura T, Kamiyama S, and Kitagawa S (2005) Effects of dietary chemopreventive phytochemicals on P-glycoprotein function. Biochem Biophys Res Commun 327:866- 870.

Nakagomi-Hagihara R, Nakai D, Tokui T, Abe T, and Ikeda T (2007) Gemfibrozil and its glucuronide inhibit the hepatic uptake of pravastatin mediated by OATP1B1. Xenobiotica 37:474-486.

Niemi M, Backman JT, Granfors M, Laitila J, Neuvonen M, and Neuvonen PJ (2003) Gemfibrozil considerably increases the plasma concentrations of rosiglitazone. Diabetologia 46:1319-1323.

Niemi M, Kajosaari LI, Neuvonen M, Backman JT, and Neuvonen PJ (2004) The CYP2C8 inhibitor trimethoprim increases the plasma concentrations of repaglinide in healthy subjects. Br J Clin Pharmacol 57:441-447.

Ogilvie BW, Zhang D, Li W, Rodrigues AD, Gipson AE, Holsapple J, Toren P, and Parkinson A (2006) Glucuronidation converts gemfibrozil to a potent, metabolism- dependent inhibitor of CYP2C8: implications for drug-drug interactions. Drug Metab Dispos 34:191-197.

Otake Y, Nolan AL, Walle UK, and Walle T (2000) Quercetin and resveratrol potently reduce estrogen sulfotransferase activity in normal human mammary epithelial cells. J Steroid Biochem Mol Biol 73:265-270.

Patel KR, Andreadi C, Britton RG, Horner-Glister E, Karmokar A, Sale S, Brown VA, Brenner DE, Singh R, Steward WP, Gescher AJ, and Brown K (2013) Sulfate metabolites provide an intracellular pool for resveratrol generation and induce autophagy with senescence. Sci Transl Med 5:205ra133.

Piver B, Fer M, Vitrac X, Merillon JM, Dreano Y, Berthou F, and Lucas D (2004) Involvement of cytochrome P450 1A2 in the biotransformation of trans-resveratrol in human liver microsomes. Biochem Pharmacol 68:773-782.

Potter GA, Patterson LH, Wanogho E, Perry PJ, Butler PC, Ijaz T, Ruparelia KC, Lamb JH, Farmer PB, Stanley LA, and Burke MD (2002) The cancer preventative agent resveratrol is converted to the anticancer agent piceatannol by the cytochrome P450 enzyme CYP1B1. Br J Cancer 86:774-778.

Prueksaritanont T, Zhao JJ, Ma B, Roadcap BA, Tang C, Qiu Y, Liu L, Lin JH, Pearson PG, and Baillie TA (2002) Mechanistic studies on metabolic interactions between gemfibrozil and statins. J Pharmacol Exp Ther 301:1042-1051.

Rahman A, Korzekwa KR, Grogan J, Gonzalez FJ, and Harris JW (1994) Selective biotransformation of taxol to 6 alpha-hydroxytaxol by human cytochrome P450 2C8. Cancer Res 54:5543-5546.

Renaud S and de Lorgeril M (1992) Wine, alcohol, platelets, and the French paradox for coronary heart disease. Lancet 339:1523-1526.
Robicsek F and Schaper J (1997) Reperfusion injury: fact or myth? J Card Surg 12:133- 137; discussion 138.

Sahi J, Black CB, Hamilton GA, Zheng X, Jolley S, Rose KA, Gilbert D, LeCluyse EL, and Sinz MW (2003) Comparative effects of thiazolidinediones on in vitro P450 enzyme induction and inhibition. Drug Metab Dispos 31:439-446.

Sai Y, Kaneko Y, Ito S, Mitsuoka K, Kato Y, Tamai I, Artursson P, and Tsuji A (2006) Predominant contribution of organic anion transporting polypeptide OATP-B (OATP2B1) to apical uptake of estrone-3-sulfate by human intestinal Caco-2 cells. Drug Metab Dispos 34:1423-1431.

Sharma P, Butters CJ, Smith V, Elsby R, and Surry D (2012) Prediction of the in vivo OATP1B1-mediated drug-drug interaction potential of an investigational drug against a range of statins. Eur J Pharm Sci 47:244-255.

Shiau YF, Fernandez P, Jackson MJ, and McMonagle S (1985) Mechanisms maintaining a low-pH microclimate in the intestine. Am J Physiol 248:G608-617.

Shitara Y, Hirano M, Sato H, and Sugiyama Y (2004) Gemfibrozil and its glucuronide inhibit the organic anion transporting polypeptide 2 (OATP2/OATP1B1:SLC21A6)- mediated hepatic uptake and CYP2C8-mediated metabolism of cerivastatin: analysis of the mechanism of the clinically relevant drug-drug interaction between cerivastatin and gemfibrozil. J Pharmacol Exp Ther 311:228-236.

Stopper H, Schmitt E, and Kobras K (2005) Genotoxicity of phytoestrogens. Mutat Res 574:139-155.

Sun C, Hu Y, Liu X, Wu T, Wang Y, He W, and Wei W (2006) Resveratrol downregulates the constitutional activation of nuclear factor-kappaB in multiple myeloma cells, leading to suppression of proliferation and invasion, arrest of cell cycle, and induction of apoptosis. Cancer Genet Cytogenet 165:9-19.

Tamai I, Nozawa T, Koshida M, Nezu J, Sai Y, and Tsuji A (2001) Functional characterization of human organic anion transporting polypeptide B (OATP-B) in comparison with liver-specific OATP-C. Pharm Res 18:1262-1269.

Tornio A, Filppula AM, Kailari O, Neuvonen M, Nyronen TH, Tapaninen T, Neuvonen PJ, Niemi M, and Backman JT (2014) Glucuronidation converts clopidogrel to a strong time-dependent inhibitor of CYP2C8: a phase II metabolite as a perpetrator of drug-drug interactions. Clin Pharmacol Ther 96:498-507.

Vaclavikova R, Horsky S, Simek P, and Gut I (2003) Paclitaxel metabolism in rat and human liver microsomes is inhibited by phenolic antioxidants. Naunyn Schmiedebergs Arch Pharmacol 368:200-209.

van de Wetering K, Burkon A, Feddema W, Bot A, de Jonge H, Somoza V, and Borst P (2009) Intestinal breast cancer resistance protein (BCRP)/Bcrp1 and multidrug resistance protein 3 (MRP3)/Mrp3 are involved in the pharmacokinetics of resveratrol. Mol Pharmacol 75:876-885.

Walle T, Hsieh F, DeLegge MH, Oatis JE, Jr., and Walle UK (2004) High absorption but very low bioavailability of oral resveratrol in humans. Drug Metab Dispos 32:1377-1382.

Walsky RL, Obach RS, Gaman EA, Gleeson JP, and Proctor WR (2005) Selective inhibition of human cytochrome P4502C8 by montelukast. Drug Metab Dispos 33:413- 418.

Wang JS, Neuvonen M, Wen X, Backman JT, and Neuvonen PJ (2002a) Gemfibrozil inhibits CYP2C8-mediated cerivastatin metabolism in human liver microsomes. Drug Metab Dispos 30:1352-1356.

Wang Z, Zou J, Cao K, Hsieh TC, Huang Y, and Wu JM (2005) Dealcoholized red wine containing known amounts of resveratrol suppresses atherosclerosis in hypercholesterolemic rabbits without affecting plasma lipid levels. Int J Mol Med 16:533-540.

Wang Z, Zou J, Huang Y, Cao K, Xu Y, and Wu JM (2002b) Effect of resveratrol on platelet aggregation in vivo and in vitro. Chin Med J (Engl) 115:378-380.

Wen X, Wang JS, Backman JT, Laitila J, and Neuvonen PJ (2002) Trimethoprim and sulfamethoxazole are selective inhibitors of CYP2C8 and CYP2C9, respectively. Drug Metab Dispos 30:631-635.

Wu JM, Hsieh TC, and Wang Z (2011) Cardioprotection by resveratrol: a review of effects/targets in cultured cells and animal tissues. Am J Cardiovasc Dis 1:38-47.

Yang X, Li X, and Ren J (2014) From French Paradox to cancer treatment: anti-cancer activities and mechanisms of resveratrol. Anticancer Agents Med Chem 14:806-825.

Zou J, Huang Y, Chen Q, Wei E, Cao K, and Wu JM (2000) Effects of resveratrol on oxidative modification of human low density lipoprotein. Chin Med J (Engl) 113:99-102.

Zou JG, Huang YZ, Chen Q, Wei EH, Hsieh TC, and Wu JM (1999) Resveratrol inhibits copper ion-induced and azo compound-initiated oxidative modification of human low density lipoprotein. Biochem Mol Biol Int 47:1089-1096.

Zweier JL (1988) Measurement of superoxide-derived free radicals in the reperfused heart. Evidence for a free radical mechanism of reperfusion injury. J Biol Chem 263:1353-1357.

CHAPTER 2

CYTOCHROME P450 INHIBITION OF CYP3A4 IN SANDWICH CULTURED CRYOPRESERVED HUMAN HEPATOCYTES AND RECOMBINANT CYP2C8

2.1 Background:

2.1.1 Cytochrome P450:

Cytochrome P450 (P450) is a superfamily of heme containing proteins (Meunier et al., 2004). The term P450 stands for "pigment 450" as the CO bound pigment gives a characteristic absorption band at 450nm (Omura and Sato, 1962).

2.1.2 Catalytic cycle:

The first step of the P450 catalytic cycle involves the binding of the substrate (Luthra et al., 2011). This binding triggers the conversion of the P450 from a low spin state (LS) to a high spin state (HS). This is followed by reduction by addition of the first electron and the conversion of ferric to ferrous state (Johnston et al., 2011; Luthra et al., 2011). The ionic radius of iron in HS state is greater than that of iron in LS state which makes the iron to move out of its original place (Luthra et al., 2011). This is followed by binding of a molecular oxygen to iron (superoxide anion: $O2^-$). The step is followed by the addition of second electron followed by addition of hydrogen ion (reduction at β oxygen) to form Compound 0 (Jung, 2011; Jung et al., 2011). Compound 0 undergoes heterolytic cleavage of dioxygen bond, releasing a molecule of water and forming a

reactive oxygen species commonly called as Compound 1 (Jung, 2011; Jung et al., 2011). The oxidation of substrate proceeds with abstraction of hydrogen ion from the substrate, followed by the rebound attack of substrate radical and release of hydroxylated substrate. The iron returns to the ferric form (Jones and Korzekwa, 1996; Isin and Guengerich, 2006; Luthra et al., 2011).

2.1.3 Cytochrome P450 family:

(a) Clinically important P450s:

Drug-drug interactions (DDIs) resulting from time dependent inhibition display a delayed onset and can persist even after the inhibitor is eliminated from the body (Grimm et al., 2009). Such type of inhibition is a major concern due to its potential to cause clinically significant DDIs (Grimm et al., 2009; Albaugh et al., 2012). P450s are a superfamily of hemoprotein responsible for oxidative metabolism of xenobiotics and endogenous compounds (Ma et al., 2004). P450 metabolism generally leads to detoxification of xenobiotics by forming hydrophilic metabolic products, thus facilitating the elimination of these metabolites. This metabolism may also lead to the formation of reactive intermediates leading to toxicity or reaction with P450s (Hollenberg et al., 2008). A total of eighteen cytochrome P450 families with 43 subfamilies have been recognized (Nelson, 2009). The clinically significant P450s are CYP3A4, CYP2D6, CYP1A2, CYP2C8, CYP2C9, CYP2C19, and CYP2E1 (Wrighton and Stevens, 1992).

(b) CYP3A4:

CYP3A4 is one of the most important P450 enzyme due to its wide substrate specificity. It is also the most abundant P450 in liver and intestine (Guengerich, 2005).

CYP3A4 is known to metabolize a wide variety of compounds with wide range of molecular weights. CYP3A consists of 72% of P450 protein content in human liver samples (Shimada et al., 1994).

(c) CYP2C8:

The CYP2C subfamily consists of four isozymes namely 2C8, 2C9, 2C18 and 2C19. CYP2C8 protein has been detected in lungs (Ding and Kaminsky, 2003), liver and kidneys (Guengerich, 2005). CYP2C8 mRNA has been detected in liver (Nakajima et al., 1994), kidneys, lungs (Nakajima et al., 1994), adrenal gland, breast cancer (Knupfer et al., 2004), heart (Thum and Borlak, 2000), uterus, brain, mammary gland, ovary (Klose et al., 1999; Totah and Rettie, 2005) and duodenum (Totah and Rettie, 2005). CYP2C8 is responsible for metabolism of 5% of drugs (Totah and Rettie, 2005). CYP2C8 metabolizes various classes of drugs such as amiodarone (Ohyama et al., 2000), carbamazepine (Kerr et al., 1994), troglitazone (Yamazaki et al., 1999), paclitaxel (Rahman et al., 1994), repaglinide (Bidstrup et al., 2003), and retinoic acid (Marill et al., 2002; Williams and Feely, 2002).

(d) Inhibition of CYP2C8:

Paclitaxel was recognized as a substrate of CYP2C8 and has been used as a probe substrate for CYP2C8 (Rahman et al., 1994). The major metabolite of paclitaxel was found to be 6α-hydroxypaclitaxel. The reported K_m in rCYP2C8 was 5.4 ± 1μM and the limiting velocity was 30 ± 1.5μM (Rahman et al., 1994). Retinoic acid was found to be an inhibitor of rosiglitazone and paclitaxel metabolism by CYP2C8 (competitive inhibition with K_i: 27μM) (Rahman et al., 1994; Baldwin et al., 1999). Quercetin competitively inhibited CYP2C8 mediated 6α-hydroxylation of taxol with K_i of 1.3μM (Rahman et al.,

1994). Gemfibrozil (600mg) increased systemic concentration of cerivastatin by inhibiting CYP2C8 in healthy non-smoking volunteers. $AUC_{0-\infty}$ of cerivastatin in the presence of gemfibrozil increased 5-fold (Backman et al., 1994). In HLM, gemfibrozil inhibited 6α- hydroxylation of paclitaxel by inhibiting CYP2C8 with K_i of 75μM (Wang et al., 2002a). CYP2C8 was found to be the main enzyme involved in the metabolism of amodiaquine (fig. 2.1), an anti-malarial. N-desethylamodaiquine (fig. 2.2) was found to be the major metabolite (Li et al., 2002). With a low K_m (2.4μM) and high V_{max} (1462pmol/min/mg) in HLM, amodiaquine was observed to be a high affinity substrate for CYP2C8 and has been routinely used as a probe substrate (Li et al., 2002).

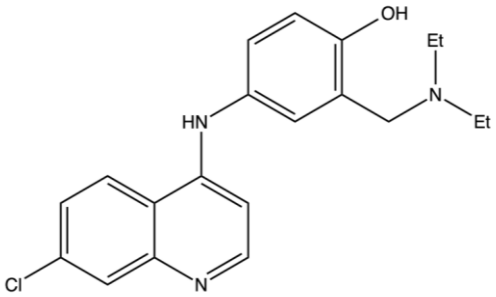

Figure 2.1. Amodiaquine

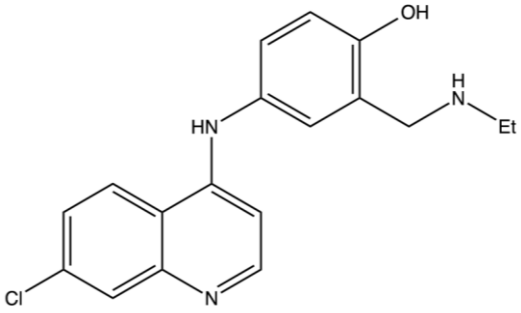

Figure 2.2. N-desethylamodiaquine

Gemfibrozil (fig. 2.3) and gemfibrozil-O-β-glucuronide (fig. 2.4) inhibited cerivastatin metabolism with an IC_{50} of 28 ± 4.3μM and 4.07 ± 1.23μM respectively (Shitara et al., 2004). Ogilvie et.al. reported gemfibrozil-O-β-glucuronide as a mechanism-based inactivator of CYP2C8 (Ogilvie et al., 2006). The predicted K_I and k_{inact} values were 20 to 52μM (variable due to change in protein concentration) and 0.21min^{-1}, respectively. Clopidogrel acyl-β-D-glucuronide was also found to be a mechanism-based inactivator of CYP2C8 with a K_I of 9.9μmol/l and k_{inact} of 0047 min^{-1} (Tornio et al., 2014), which made it a second example of a glucuronide metabolite being a mechanism-based inactivator of CYP2C8.

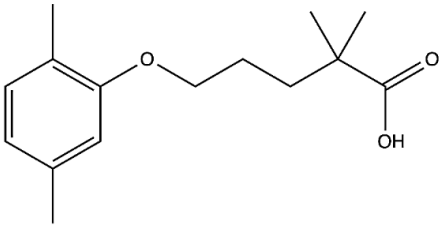

Figure 2.3. Gemfibrozil

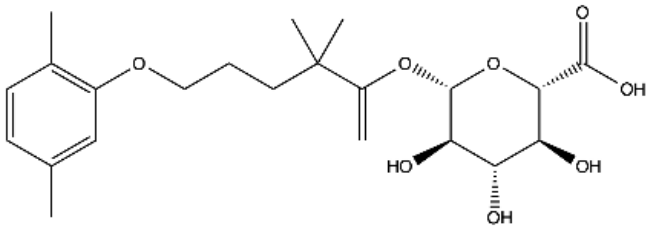

Figure 2.4. Gemfibrozil-O-β-glucuronide

The proposed mechanism of inactivation by gemfibrozil-O-β-glucuronide was through the production of a hydroxylated gemfibrozil-O-β-glucuronide moiety (Ogilvie et al., 2006; Parkinson et al., 2010). The hydroxylation was observed to occur on the

dimethylphenoxy moiety and not on the glucuronide moiety. But the exact location of hydroxylation was not discernable (Ogilvie et al., 2006). Further research provided stronger evidence, which confirmed a hydroxylation on the 2', 5'-dimethylphenoxy moiety and the formation of benzylic radical. The benzylic radical further alkylated the heme moiety in CYP2C8, thereby irreversibly inactivating CYP2C8 (Ogilvie et al., 2006; Baer et al., 2009; Parkinson et al., 2010). Although the exact position of hydroxylation was not confirmed, oxidation on 2'- or 5'- or 2', 5'- positions were considered to be the likely inactivating species (Baer et al., 2009). Thus, the inhibitory capacity of gemfibrozil increased after glucuronidation (Ogilvie et al., 2006; Baer et al., 2009; Parkinson et al., 2010; Jenkins et al., 2011).

2.1.4 Enzyme inhibition:

Cytochrome P450 inhibition is one of the most common causes of DDIs. Inhibition can be divided into three broad categories: reversible inhibition, quasi-irreversible inhibition and irreversible inhibition (Silverman, 1995; Kalgutkar et al., 2007b).

(a) Reversible inhibition:

Reversible inhibition is the most commonly observed inhibition (Hollenberg, 2002). It is classically considered to be of three types- 1. Competitive inhibition, 2.Non-competitive inhibition, 3.Uncompetitve inhibition (Segel, 1993b; Cornish-Bowden, 2012). Various steps of the P450 catalytic cycle are susceptible to reversible inhibition (Hollenberg, 2002).

(b) Mechanism-based inactivation:

Mechanism-based inactivators (MBIs) depend on the enzyme to cause inhibition. In this type of inhibition, the substrate or its metabolite may form a quasi-irreversible complex with the heme prosthetic group or the reactive intermediate may bind covalently to the apoprotein or the heme group to cause inactivation of the enzyme (Zhang et al.). Selected examples of clinically observed DDI due to mechanism-based inactivation are (a) erythromycin and midazolam (Zhang et al.; Olkkola et al., 1993), and (b) troleandomycin and triazolam (Warot et al., 1987), among many others. A list of few mechanism-based inactivators of human cytochrome P450s is provided in Table 2.1.

Table 2.1: Mechanism-based inhibitors of CYP enzymes

Irreversible inhibitor	Enzyme inactivated	Reference
Troleandomycin	CYP3A4	(Franklin, 1991; Periti et al., 1992)
Mibefradil	CYP3A4	(Prueksaritanont et al., 1999)
Verapamil	CYP3A4	(Ma et al., 2000; Wang et al., 2005a)
Gemfibrozil and 1-glucuronide	CYP2C8	(Ogilvie et al., 2006)
Erythromycin	CYP3A4	(Franklin, 1991; Periti et al., 1992)
Fluoxetin	CYP3A4,	(Mayhew et al., 2000)
Diltiazem	CYP3A4	(Ma et al., 2000; Yeo and Yeo, 2001)
Tienilic acid, Amiodarone	CYP2C9	(Guengerich, 2005; Guengerich, 2009)
Furafylline, Phenacetin	CYP1A2	(Guengerich, 2009)
Isoniazid, Paroxetine	CYP2D6	(Mohutsky and Hall, 2014)

2.1.5 Mechanisms of mechanism-based inhibition:

The mechanism behind mechanism-based inactivation has been understood in recent years, and significant advances have been made in order to estimate more accurate kinetic parameters in vitro. MBIs require at least one catalytic cycle of P450s, hence they demonstrate NADPH, time and concentration dependent inhibition (Kalgutkar et al., 2007b; Zhou, 2008). MBIs are quasi-irreversible or irreversible inhibitors. In quasi-irreversible inhibition, the reactive intermediate co-ordinates with the heme group leading to a metabolite-inhibitor complex (MI complex) formation with the enzyme (Kalgutkar et al., 2007b). In irreversible inhibition, the reactive intermediates covalently bind to the active site in the apoprotein or lead to alkylation/arylation of heme group. Some chemical compounds which are associated with mechanism based inhibition are furans, thiophenes, substituted imidazoles, and substituted pyridines (Kalgutkar et al., 2007b). A general kinetic scheme of mechanism-based inactivation is depicted as shown in Scheme 2.1 (Silverman, 1995; Kalgutkar et al., 2007b; Grimm et al., 2009).

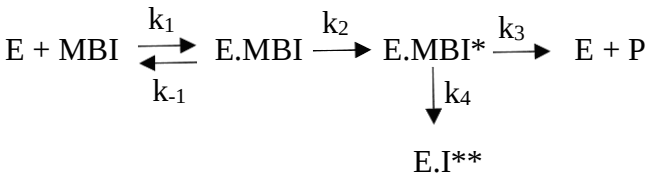

Scheme 2.1: Kinetic depiction of mechanism-based inhibition (Silverman, 1995; Hollenberg et al., 2008) E: enzyme concentration, MBI: inhibitor concentration, E.MBI: enzyme-inhibitor complex, E.MBI*: enzyme-reactive intermediate complex, E.I**: enzyme inactivated complex, P: concentration of product, k_1, k_{-1}, k_2, k_3, k_4: rate constants.

2.1.6 Characteristics of MBIs include (Silverman, 1995):

Several characteristics for mechanism-based inactivators have been proposed. Some, but not all, of them are routinely evaluated in order to ascertain the type of inhibition.

(a) Time dependence of inactivation

The extent of inhibition increases with time. The time dependence is due to the slow rate of formation of the active intermediate, which is responsible for the inactivation of enzyme. This characteristic is usually evaluated to characterize a compound as a mechanism-based inactivator.

(b) Saturation

The rate of inactivation is dependent on the concentration of inactivator. This is characterized by a first order decline in active enzyme. The rate of inactivation reaches maximum when the enzyme is saturated with the inactivator resulting in no further inactivation.

(c) Substrate protection

Addition of the substrate concomitantly with the mechanism-based inactivator decreases the rate of inactivation due to the binding of the substrate to the enzyme active site.

(d) Irreversibility

Mechanism-based inactivators form a covalent bond (co-ordinate in case of quasi-irreversible inactivators). Such a bond cannot be broken by dialysis or filtration or under any in vivo conditions. This makes the inactivator-enzyme complex inactive and permanently removes the enzyme from the active pool of enzyme.

(e) Stoichiometry

It was proposed that one molecule of inactivator binds to one enzyme molecule. Enzymes with multiple active sites or binding sites may bind to more than one molecule of enzyme. Current evidence shows that P450s could bind to multiple inactivator molecules in spite of a single binding site.

(f) Catalytic step

This is one of the important characteristics of mechanism-based inactivation. This is one of the characteristics, which separate mechanism-based inactivators from tight, slow binding inhibitors, which may also show time dependent inhibition.

(g) Inactivation prior to release

The reactive intermediates formed as a result of catalytic step of P450s have two fates. They may either inactivate the enzyme or may diffuse out of the active site to bind with glutathione of extra-endoplasmic reticulum components. Instead of binding to glutathione, the reactive intermediates may return and inactivate the active site. Such inactivation may not be categorized as a mechanism-based inactivation. Hence, the reactive intermediate should inactivate the enzyme before it diffuses from the active site.

For more elaborate description of properties of mechanism-based inactivators, the reader is encouraged to refer to Mechanism-Based enzyme inactivation: chemistry and enzymology, Vol. 1 (Silverman, 1988).

2.1.7 Analysis of data:

The parameter k_{obs} is calculated from the slope of the plot of natural logarithm of the percent of enzyme activity remaining after pre-incubation, corrected for loss of

enzyme activity in absence of inhibitor, for each concentration of inhibitor, against pre-incubation time (Grimm et al., 2009). Using non-linear regression, the plot of k_{obs} against inhibitor gives a hyperbolic curve (Eq.2.1, section 2.3.1), typically observed for a Michaelis-Menten type reaction. The kinetic parameters of inhibition, K_I and k_{inact}, are obtained from such a plot (Ghanbari et al., 2006; Hanna, 2014).

The static model is one of the models used to compute the extent of DDI. This model (eq. 2.2, section 2.3.1) uses K_I, k_{inact}, k_{deg}, and in vivo inhibitor concentration among other parameters (Ito et al., 1998; Ito et al., 2004; Ghanbari et al., 2006; Venkatakrishnan and Obach, 2007; Hanna, 2014). The model makes few assumptions: 1. the model assumes that the substrate is metabolized by a single P450. Metabolism by the intestinal enzymes was included later in the model. 2. the model also assumes that the enzyme concentration is at steady state and the fold decrease in the enzyme concentration is due to the inhibition. 3. the inhibitor does not affect the rate of enzyme synthesis or enzyme degradation (k_{syn} or k_{deg}) (Mayhew et al., 2000; Hanna, 2014).

2.1.8 In vitro assays to evaluate time dependent inhibition:

(a) Time dependent inhibition assay in microsomes:

A preliminary screen for mechanism based inactivation is performed using 3 incubations. 1. with a pre-incubation step, 2. with co-incubation of substrate and inhibitor and 3. with pre-incubation step in presence of substrate without inhibitor and NADPH. The first condition indicates if the inhibition requires a catalytic step. The second condition assesses the possibility of reversible inhibition. The third condition exploits the

substrate protection characteristic of inhibitor. Inhibition of enzyme activity in all 3 incubations may indicate reversible inhibition.

(b) Kinetic assay:

This assay involves the estimation of two kinetic parameters (K_I), concentration of inhibitor at half maximal inactivation and k_{inact}, rate constant of inactivation at maximum inactivation. It is a two-step assay, 1. pre-incubation step, and 2. incubation step. The pre-incubation step is performed in the presence of multiple inhibitor concentrations and at multiple time points. The incubation step is performed in the presence of a probe substrate for a fixed time. The analysis of data is discussed above (section 2.1.6).

2.1.9 In vitro systems:

(a) Recombinant P450s - Baculovirus expressed system:

Baculoviruses are circular DNA viruses, which infect nonvertebrates but are non-infectious in vertebrates. Nucleopolyhedroviruses (NPVs) are generally used as expression vectors. These viruses infect insect cell lines one of which is Spodoptera frugiperda (Sf 9). Recombinant baculoviruses are used as vectors to produce foreign proteins using insect cell lines. The ease, speed and safety of using insect cell lines make this a desirable system to use (Altmann F et.al.1999).

(b) Sandwich cultured human hepatocytes (SCHH):

Human liver microsomes (HLM) have been widely accepted and used as a model system to study enzyme kinetics and predict extent of enzyme inhibition (Xu et al., 2009b). But SCHH display some major advantages over HLM. As SCHH express all

drug metabolizing enzymes and transporters, they are considered to be a holistic cell system and more closely replicate the in vivo situation. SCHH are cultured between layers of collagen in a sandwich formation (fig.2.5) (Chandra et al., 2001).

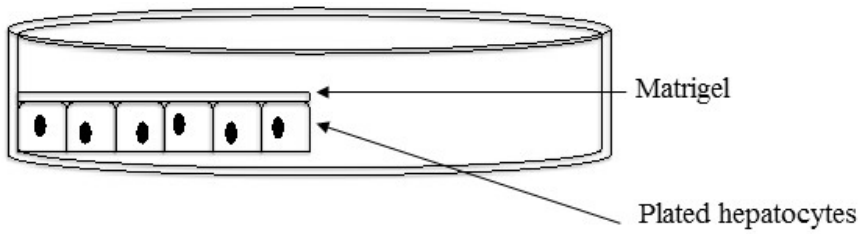

Figure 2.5. Sandwich cultured hepatocyte culture. Matrigel^{TM} is overlaid on the hepatocytes. The hepatocytes form a monolayer on a collagen coated plate. The hepatocytes are polarized thus promoting the formation of bile canaliculi (fig. 2.6).

The presence of collagen facilitates the formation of bile canaliculi and maintains the cuboidal shape of hepatocytes (LeCluyse et al., 1994; Chandra et al., 2001). SCHH configuration also facilitates tight junctions and polarization of hepatocytes with an apical membrane and a basolateral membrane (LeCluyse et al., 1994; Chandra et al., 2001; Swift et al., 2010). Hence, SCHH are also used to study biliary excretion (Bi et al., 2006). The sandwich cultured configuration is considered to be conducive for the expression of drug metabolizing enzymes and transporters (LeCluyse et al., 1994; Chandra et al., 2001; Kemp and Brouwer, 2004; Turncliff et al., 2006; Hewitt et al., 2007; Abe et al., 2009; Swift et al., 2010), hence proving to be a more holistic in nature than HLM (Brouwer et al., 2013).

2.1.10 Unresolved issues:

As the preclinical evaluation of all new molecular entities (NMEs) for time dependent inhibition becomes a norm, certain unresolved scientific issues in experimental techniques, models used to assess TDI and the use of right parameters in these models need to be addressed. Precise information about all the factors used in the static model is necessary to make accurate DDI predictions. Thus, K_I, k_{inact}, $[I]_{invivo}$, k_{deg}, and fraction metabolized by CYP3A4 in the liver and intestine need more precise values (Grimm et al., 2009). The experimental design used to obtain the inhibition kinetic parameters may also need further refinement. The inhibitory activity of the perpetrator compound in the pre-incubation step of the experiment is assumed to have diminished due to the dilution step in HLM or washing step in SCHH. But it has been observed that the inhibitor tends to remain in the incubation step and may continue to inhibit the enzyme, the consequence of which is over prediction of DDI value.

2.2 Experimental Section:

2.2.1 Materials:

The materials used in sandwich cultured hepatocyte assay will not be mentioned here (Xu et al., 2009a; Albaugh et al., 2012).

Recombinant CYP2C8 microsomes were purchased from Corning Inc. (Corning, NY). Monobasic potassium phosphate and dibasic potassium phosphate were purchased from Fisher Scientific (Fair Lawn, NJ). Regenerating NADPH solution A and solution B were purchased from Corning Inc. (Corning, NY). Amodiaquine, N-desethyl-

amodiaquine hydrochloride, gemfibrozil-1-O-β-glucuronide, R3G and R3S were purchased from Toronto Research Chemicals (Toronto, CA). The mobile phase used to analyze samples was composed of methanol and formic acid. Methanol was purchased from two vendors: Honeywell B & J (Muskegon, MI), EMD Chemicals (Gibbstown, NJ). Formic acid was purchased from EMD Chemicals (Gibbstown, NJ). The instruments used in this assay were LC and MS/MS. LC was an Agilent 1100 instrument. MS/MS was ABSciex API 4000 instrument. Atorvastatin was purchased from TCI Chemicals (Montgomeryville, PA). The phytochemicals used for anti-proliferation assays (table 1.1) (resveratrol, trimethoxy stilbene, pterostilbene, pinosylvin and piceatannol) were purchased from Cayman Chemicals (Ann Arbor, MI).

2.2.2 Development of cryopreserved sandwich cultured human hepatocyte assay:

Cryopreserved human hepatocytes from several lots were evaluated for enzyme activity. The formation of 1'-hydroxymidazolam was analyzed over time. A multiday enzyme activity assay was conducted in order to select the day of the experiment. Several other parameters such as concentration of Matrigel^{TM}, day of conducting the assay and number of viable cells to be plated were optimized. A set of 8 compounds was selected (table 2.2) (Kalgutkar et al., 2007b; Hollenberg et al., 2008).

Table 2.2 Set of 8 compounds used in 2 different hepatocyte donor lots.

Tested market drugs	P450 inactivation mechanism	Tested Hepatocyte lots		
		Lot 1	Lot 2	Lot 3
Troleandomycin	Quasi irreversible	✓	✓	✓
Mibefradil	Irreversible	✓	✓	✓
Ketoconazole	Direct inhibitor	✓	✓	✓
Verapamil	Quasi irreversible	✓	✓	---
Diltiazem	Quasi irreversible	✓	✓	---
Raloxifene	Irreversible inactivator	✓	✓	---
Tamoxifen	Quasi irreversible	✓	✓	---
Dihydralazine	Irreversible inactivator	✓	✓	---

2.2.3 Sandwich cultured human hepatocyte assay:

1. The cryopreserved cells were thawed for 90 seconds and poured into hepatocyte maintenance medium. The hepatocytes were counted for viability using trypan blue and a desired concentration of viable hepatocyte/ml was obtained by dilution. The hepatocytes were plated (Day 0) in 48 well plates using the plating medium. The cells were incubated overnight at 37^0C with 5% CO_2 and the inhibition assay was performed the next day (Day 1).

2. The pre-incubation step was performed at different concentrations of inhibitor at different time points (see appendix A 1 for experiment design). Table 2.2 lists the inhibitors that were used. At the end of the pre-incubation step, the inhibitor was pipetted out, cell layer was given a quick wash and 20µM of midazolam was added. Midazolam was incubated for 20 minutes and the formation of 1'-hydroxymidazolam was monitored.

3. The samples were analyzed on UPLC-MS/MS using an already developed and validated method.

4. k_{obs} values were calculated using linear regression analysis. K_I and k_{inact} were obtained from k_{obs} vs. inhibitor concentration plot. DDI values were calculated by using the predicted K_I and k_{inact} and the static model. Graphpad prism for windows (version 6.0, Graphpad Software Inc., California)

2.2.4 CYP2C8 assay:

For CYP2C8 inhibition assays, an initial experiment for assessing time and protein linearity was performed.

1. An initial screen to detect mechanism-based inactivation was performed with resveratrol, R3G and R3S. CYP2C8 inactivation was assessed in three incubations, (a) effect of preincubation with a single high concentration of MBI for 30 minutes with rCYP2C8 in the presence of NADPH, (b) effect of same concentration of MBI coincubated with NADPH, substrate and rCYPC8 (preincubation time of 0 minute) and (c) effect of single high concentration of MBI when substrate was preincubated with enzyme for 30 minutes prior to addition of MBI. The control incubations included the above 3 incubations without MBI (negative control) and with gemfibrozil-O-β-glucuronide (positive control).

2. Further experiments were performed to assess reversible inhibition of CYP2C8 by resveratrol. Two experiments were performed, (a) an enzyme activity assay was performed to obtain kinetic parameters (K_m and V_{max}) and (b) an assay to assess reversible inhibition in the presence of inhibitor (resveratrol) was performed. Amodiaquine was used as a probe substrate for all the inhibition experiments involving CYP2C8. The formation of N-desethylamodiaquine was monitored. The total percent of

organic solvent did not exceed 1.0%. Gemfibrozil-1-O-β-glucuronide (30μM), a known mechanism based inhibitor of CYP2C8, was used as a positive control. The concentration of resveratrol, R3G and R3S used in the MBI screen was 1mM, 50μM and 1mM respectively. The CYP2C8 enzyme assay for the metabolism of amodiaquine was performed at 12 concentrations of amodiaquine (0.05μM-15μM). The incubation time was set to 5 minutes. Each incubation contained 195μg/ml protein concentration. For the CYP2C8 inhibition assay, eight concentrations of resveratrol (0.5μM-250μM) were used. Amodiaquine concentration was set to 0.5μM.

2.2.5 Amodiaquine LC-MS/MS method validation:

An LC-MS/MS method was developed for analyzing the metabolite, N-desethylamodiaquine. (See appendix B 2 for N-desethylamodiaquine compound optimization details).

(a) Preparation of calibration standards and quality control standards:

The stock solutions of resveratrol, gemfibrozil-O-β-glucuronide, N-desethylamodiaquine, amodiaquine, R3G and R3S were prepared in methanol. Calibration standards were prepared by spiking stock solutions in rat liver microsomes (RLM). A set of eight calibration standards was prepared within a concentration range of 3.93nM to 250nM and a set of 4 quality control samples was prepared within a concentration range of 30nM-240nM. (See appendix B 1 for a representative chromatogram of N-desethylamodiaquine).

(b) LC-MS/MS conditions:

Liquid chromatography-triple quadrapole mass spectrometer (LC-MS/MS) analysis was performed on an Agilent liquid chromatography system (HPLC-1100) equipped with a degasser, binary pump system, autosampler and a thermostat coupled to a ABSciex API-4000 tandem mass spectrometer. Analyst (Ver: 6.1) software was used for acquisition and processing of LC-MS/MS data.

A Zorbax SB-C18 (5µm, 4.6 mm x 12.5 mm) column with an Extend-C18 (3.5µm, 4.6 mm x 50 mm) guard column was used for analytical separation. Atorvastatin was used as an internal standard (IS). A gradient elution was used to separate atorvastatin (71.7nM) and N-desethylamodiaquine. The mobile phase consisted of solution A: 0.1% formic acid in water and solution B: 0.1% formic acid in methanol. The gradient elution started with 90% of A at 0 minute to 10% of A at 2 to 6.5 minutes and was increased back to 90% at 9.5 minutes and was maintained at 90% A for further 1.5 minutes. The total run time was 11 minutes. The flow rate was set to 0.5 ml/min. The retention time for N-desethylamodiaquine was ~ 4 minutes and for atorvastatin was ~ 6 minutes. ESI (electrospray ionization) was used in positive ion mode. Nitrogen was used as an ion source, curtain gas and collision gas. The optimized tandem MS parameters are summarized below in table 2.3. (See appendix B 1 for representative chromatogram and appendix B 2 for compound optimization of N-desethylamodiaquine).

(c) LC-MS/MS assay validation:

Calibration curves were constructed using peak area ratios of the analyte and internal standard. The calibration curves were constructed using the linear least square method and weighting of $1/x^2$ was applied. Intraday and interday accuracy was

determined using n=3 and n=6 replicates respectively. Accuracy was calculated by the following equation:

% accuracy = ((observed mean concentration-nominal concentration)/nominal concentration)* 100.

Table 2.3 ESI tandem MS parameters for N-desethylamodiaquine and atorvastatin.

Operating parameters	Settings
Collision gas (CAD) (psi)	10
Curtain gas (CUR) (psi)	40
Ion source gas (GS1) (psi)	40
IonSpray voltage (IS) (V)	4500
Temperature (TEM) (^{0}C)	400
Entrance potential (EP) (V)	10

	N-desethyl amodiaquine D1*	N-desethyl amodiaquine D2*	Atorvastatin
Precursor ion	328.1	330.1	559.407
Product ion (m/z)	283.1	285.1	440.537
Dwell time (ms)	400	400	400
DP (V)	62	62	76
CE (V)	21	21	31
CXP (V)	10	10	12

The following precursor-product ion transitions were monitored: 328.1→ 283.1 (D1) and 330.1→ 285.1 (D2) for N-desethyl amodiaquine (Perloff et.al., 2009) and 559.407 → 440.537 for atorvastatin (internal standard). The m/z transition monitored for N-desethylamodiaquine was previously reported by Perloff et.al. (2009).

2.3 Data Analysis:

2.3.1 Data analysis for SCHH:

The data obtained from incubation with inhibitor was normalized with respect to data obtained without inhibitor (100% enzyme activity). Using linear regression, a plot of natural logarithm of enzyme activity remaining against time gave straight lines. Each line was indicative of first order decrease in enzyme activity due to inactivation at that inhibitor concentration. The slope of natural logarithm of remaining enzyme activity and time gave the rate of inactivation (k_{obs}) at each inhibitor concentration. The kinetic parameters were obtained by using Eq, 2.1. Graphpad prism windows (v.6.0, Graphpad Software Inc., California) was used for linear and nonlinear regression.

$$k_{obs} = \frac{k_{inact} \cdot [I]}{K_I + [I]}$$

where, (Eq.2.1)

k_{obs}: pseudo first order rate of inactivation at inactivator concentration [I], k_{inact}: maximum inactivation rate constant, K_I: inactivator concentration when the rate of inactivation reaches half k_{inact}.

2.3.2 DDI prediction using a static model:

The kinetic parameters K_I and k_{inact} were used in the static model to calculate a DDI value (Eq. 2.2). A DDI value is the ratio of AUC in the presence of inhibitor to the AUC in the absence of inhibitor. The static model which includes metabolism by hepatic and gut CYP3A4 is as follows:

$$AUC_i/AUC = \frac{1}{F_g + \left[1 - F_g \frac{1}{1 + \left[\frac{K_{inact} \cdot [I]_g}{k_{degCYP3Agut}(K_I + [I]_g)}\right]}\right]} \cdot \frac{1}{(1 - f_{mCYP3A}) + \frac{1}{\left[\frac{f_{mCYP3A}}{1 + \frac{k_{inact} \cdot [I]_{invivo}}{K_I \cdot k_{degCYP}}}\right]}}$$

(Eq.2.2)

where,

AUC: area under the curve of victim drug (no inactivator), AUC_i: area under the curve of victim drug in the presence of an inactivator, F_g: fraction of victim drug, which escapes gut metabolism, $[I]_g$: concentration of inactivator in gut following oral administration, $k_{degCYP3Agut}$: natural degradation rate constant for gut CYP3A, f_{mCYP3A}: fraction of substrate metabolized by CYP3A, $[I]_{invivo}$: concentration of inactivator at enzyme site, $k_{degCYP3Ahep}$: natural degradation rate constant for hepatic CYP3A.

2.3.3 Data analysis for CY2C8 assay:

Time and protein linearity assays were performed. The linearity of product formation with respect to time and protein amount were assessed using linear regression. The Michaelis-Menten equation was fit to the CYP2C8 activity data. The following equation (Eq. 2.3) was used to calculate V_{max} (limiting rate of velocity or maximum velocity) and K_m, the Michaelis constant (substrate concentration at half the limiting rate of velocity) (Segel, 1993a; Cornish-Bowden, 2011):

$v = V_{max} * [S] / (K_m + [S])$ (Eq. 2.3)

where,

v = velocity or rate of reaction, [S] = substrate concentration, V_{max} = limiting rate of velocity or maximum velocity, K_m = Michaelis constant.

The substrate inhibition model was also fit to the data. The equation (Eq.2.4) used was:

$v = V_{max} * [S] / (K_m + [S] * (1 + [S] / K_i)$ (Eq. 2.4)

where,

K_i = substrate inhibition constant.

Nonlinear regression was performed using Graphpad Prism for Windows (Ver. 6.0, Graphpad Software Inc., San Diego, CA). The Akaike information criterion (AIC) values between the two models were compared. Sy.x is computed by Graphpad prism using the following equation (Eq. 2.5):

$$Sy.x = \sqrt{\frac{(residuals)^2}{n-K}} \quad \text{(Eq. 2.5)}$$

where,

n = number of data points, K = number of parameters fit, n-K = degrees of freedom. Sy.x is the standard deviation of the residuals. If the number of parameters being estimated is two or more, Sy.x gives a better goodness-of-fit. Similar to AIC, a smaller value of Sy.x for the model means a better fit of the model to the data.

2.4 Results:

TDI assay in SCHH was performed in all 8 compounds (table 2.2). SCHH was plated on Day 0 and the enzyme activity on Day 1 was monitored to assess enzyme activity. On day 1, SCHH formed a monolayer as well as bile canaliculi (figure 2.6).

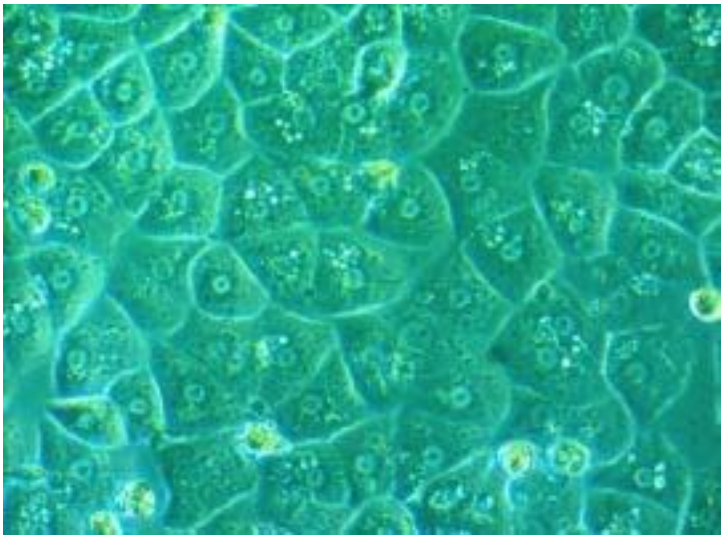

Figure 2.6. Sandwich cultured human hepatocytes plated in monolayer. The bright cell junctions depict bile canaliculi (from work done at GSK, King of Prussia, PA).

2.4.1 Enzyme activity on Day 1:

The enzyme activity on Day 1 in SCHH was assessed by monitoring the formation of 1'-hydroxymidazolam (fig.2.7). The assay was performed for 60 minutes with midazolam (20µM) as the probe substrate.

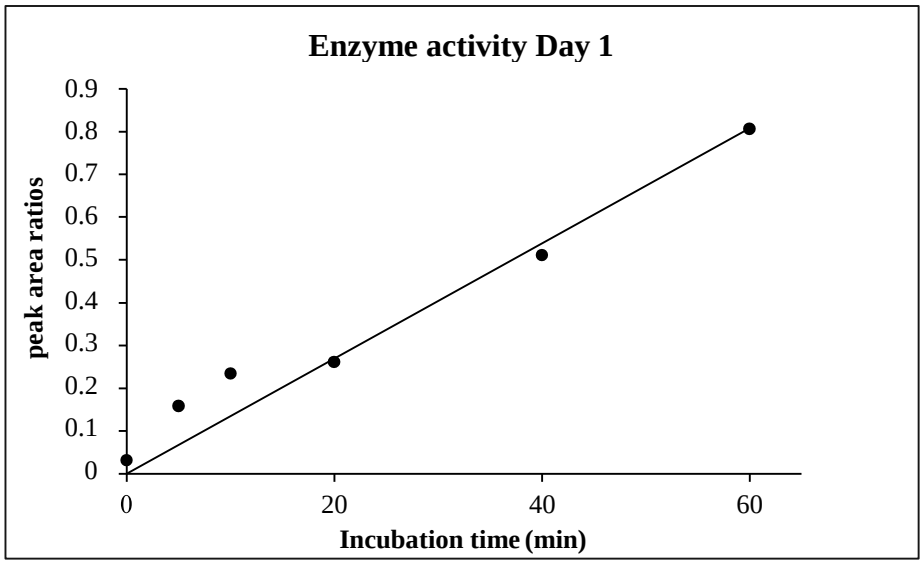

Figure 2.7. CYP3A4 activity on Day 1. The formation of 1'-hydroxy midazolam was monitored (n=1).

2.4.2 Estimation of k_{obs}:

k_{obs} for each inhibitor concentration was estimated from the slope of natural logarithm of percent remaining enzyme activity and pre-incubation time. The plots for percent remaining enzyme activity vs inhibitor concentration are displayed in fig. 2.8(A-H). The kinetic parameters for inactivation (K_I and k_{inact}) (table 2.4) were calculated using nonlinear regression plots displayed in figures 2.9(A-E).

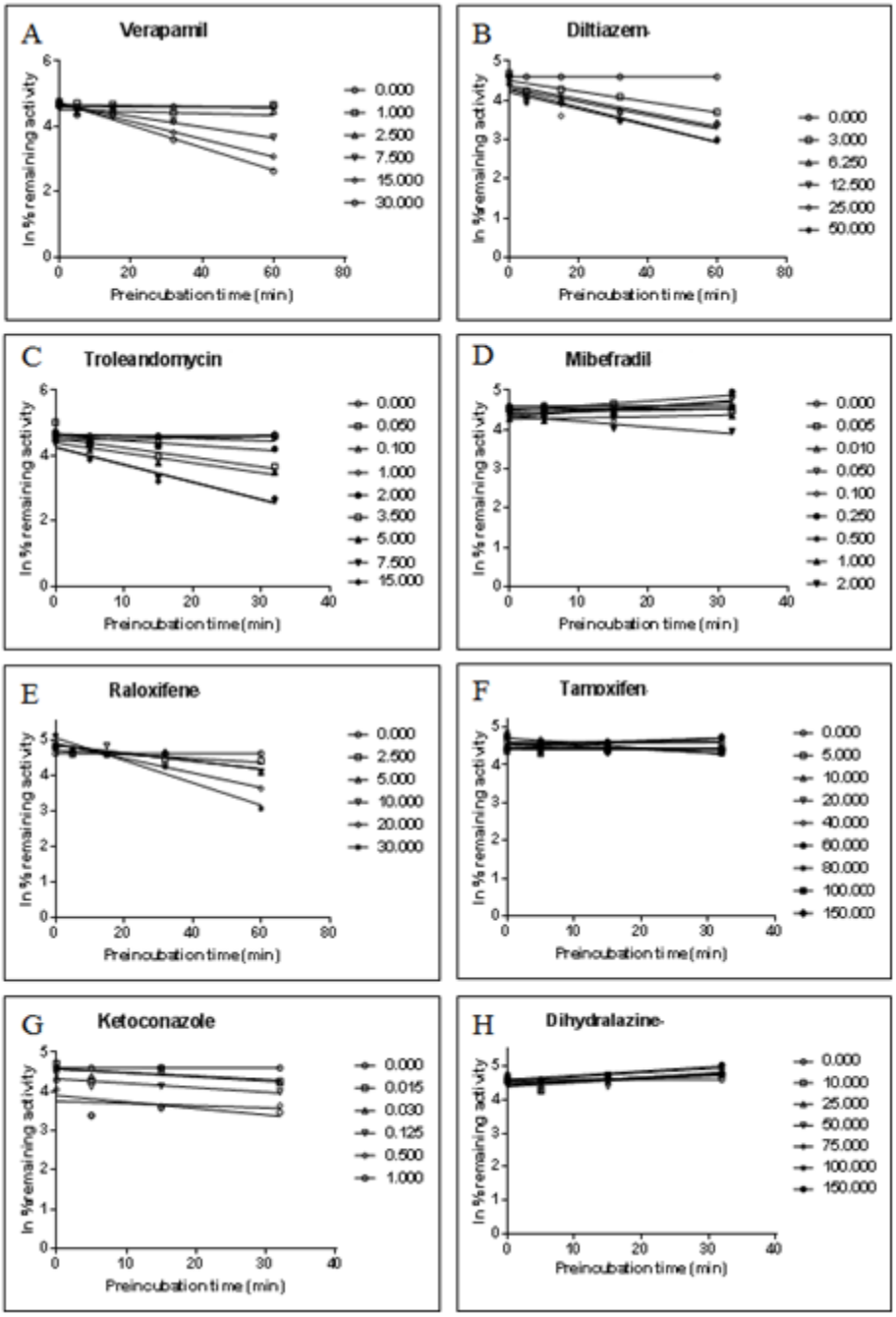

Figure 2.8(A-H). Plot of percent enzyme activity remaining vs pre-incubation time for lot 1. (A) verapamil (0-30µM), (B) diltiazem (0-50µM), (C) troleandomycin (0-15µM), (D) mibefradil (0-2µM), (E) raloxifene (0-30µM), (F) tamoxifene (0-150µM), (G) ketoconazole (0-1µM), (H) dihydralazine (0-150µM).

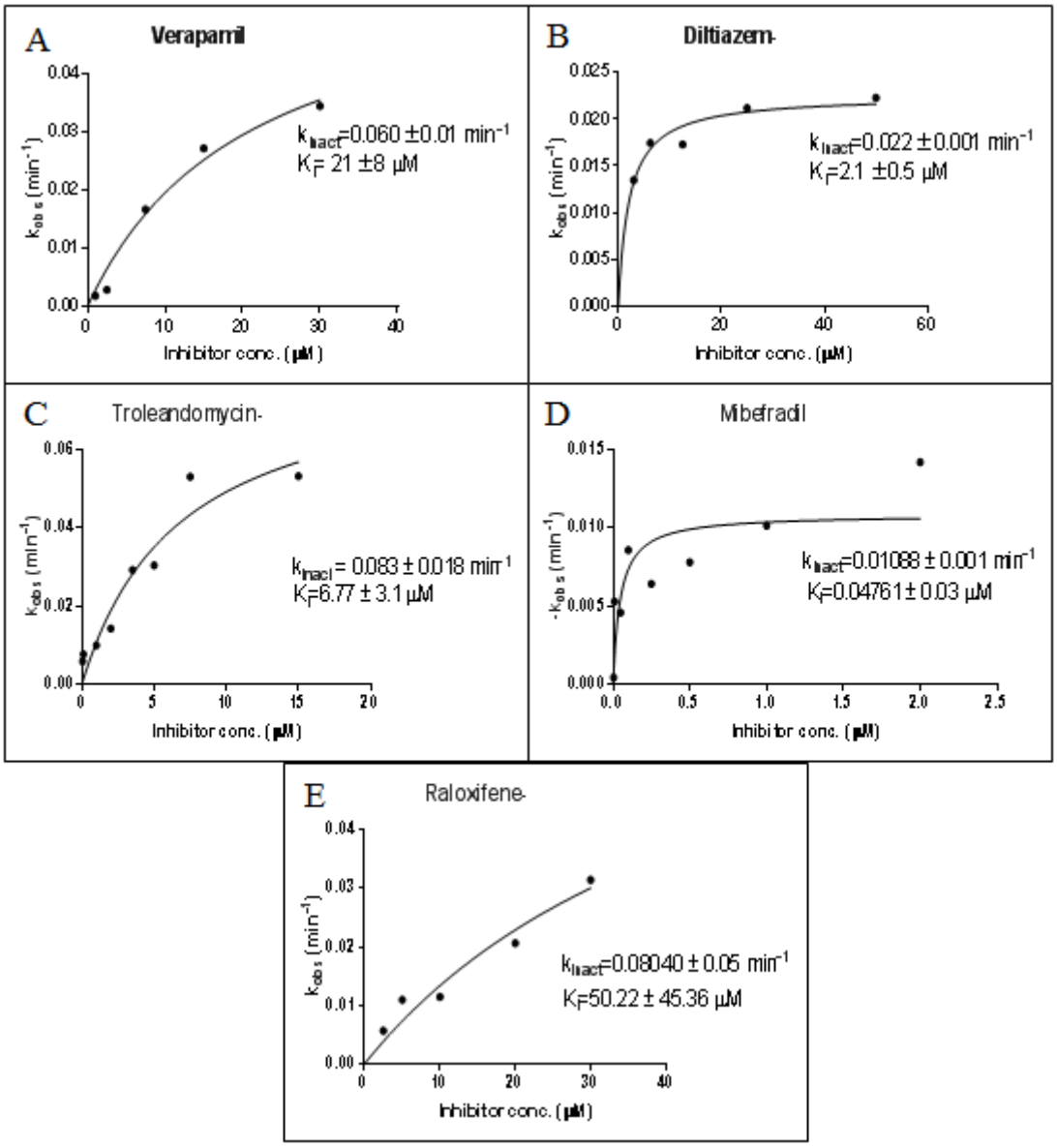

Figure 2.9(A-E). Plot of k_{obs} vs inhibitor concentration for lot 1. Verapamil (0-30µM), diltiazem (0-50µM), troleandomycin (0-15µM), mibefradil (0-2µM), raloxifene (0-30µM).

Table 2.4. Predicted K_I and k_{inact} values in comparison to reported values in human liver microsomes and sandwich cultured human hepatocytes.

Compound	Lot ID	In-house hep. k_{inact} (min^{-1})/ K_I (μM)	Lit. k_{inact} (min^{-1})/K_I (μM) HLM	Ref.	Lit. hep. k_{inact} (min^{-1}) / K_I (μM)	Ref.
Troleandomycin	1	**0.082/ 6.7**	0.065/0.19	(Xu et al., 2009b)	0.08/0.6	(Albaugh et al., 2012)
	2	**0.052/ 1.85**				
Mibefradil	1	**0.011/ 0.047**	0.070/ 1.1	(Albaugh et al., 2012)	0.28/0.2	(Albaugh et al., 2012)
	2	**0.025/ 0.068**				
Verapamil	1	**0.060/ 20.8**	0.053/ 3.5	(Xu et al., 2009b)	0.14/1.9	(Albaugh et al., 2012)
	2	**0.036/ 23.8**				
Diltiazem	1	**0.023/ 2.12**	0.019/0.67			
	2	**0.015/ 1.44**				
Raloxifene	1	**0.08040/ 50**	0.36/19	(Chen et al., 2002)	Not Known	
	2	**0.05178/ 53**				
Tamoxifen (T)	1	N/A	0.04/0.2	(Zhao et al., 2002)	Not Known	
	2					
Dihydralazine (Testosterone as probe substrate)	1	N/A	0.050 / 35	(Masubuchi and Horie, 1999)	Not Known	
	2					
Ketoconazole	1	N/A				
	2					

2.4.3 Calculation of DDI:

DDI was calculated using a static model. The ratio of AUC in the presence of inhibitor and in the absence was calculated. The in house generated values of F_g, $[I]_g$, $k_{degCYP3Agut}$, f_{mCYP3A}, $[I]_{in\ vivo}$, $k_{degCYP3Ahep}$ were used in this model. DDI values calculated for the 8 compounds are shown in table 2.5. DDI values predicted using unbound C_{max} and unbound portal concentrations were compared with DDI values obtained from reported HLM, SCHH and clinically observed values.

Table 2.5. Predicted DDI values using in-house predicted K_I and k_{inact} values and the static model

Compound	Lot #	In-house Predicted DDI (Hep+Gut combined-Free C_{max})	In-house Predicted DDI (Hep+Gut combined-Free Portal C_{max})	Predicted DDI (HLM) from Lit.	Predicted DDI (Hep) from Lit (free systemic C_{max})	Observed Clinical DDI AUC fold change
Troleandomycin	3	---	---	23 (Albaugh et al., 2012)	22 (Albaugh et al., 2012)	13.8 (Kharasch et al., 2004)
	1	**9.2**	**13.6**			
	2	**10.9**	**13.7**			
Mibefradil	3	**6.8**	---	12 (Albaugh et al., 2012)	16 (Albaugh et al., 2012)	8.0 (Veronese et al., 2003)
	1	**6.6**	**9.6**			
	2	**8.6**	**11.5**			
Verapamil	1	**2.2**	**3.2**	4.0 (Albaugh et al., 2012)	10 (Albaugh et al., 2012)	2.9 (Backman et al., 1994)
	2	**2.0**	**2.5**			
Diltiazem	1	**4**	**11.4**	6.3 (Xu et al., 2009b)	---	3.8 (Backman et 1994)
	2	**3.9**	**10.7**			
Raloxifene	1	**1.2**	**1.2**	1.6 (Zhao et al., 2005)	Not Known	No observed DDI reported
	2	**1.1**	**1.1**			
Tamoxifen (dosed to steady state) (Testosterone)	1	Not showed TDI		5.1 (Zhao et al., 2002)	Not Known	Not Known
	2					

2.4.4 N-desethylamodiaquine LC-MS/MS method validation:

The interday valiation was performed at four N-desethylamodiaquine concentrations (30nM, 60nM, 120nM and 240nM) with n=6 at each concentration on 3

separate days. Table 2.6 shows the interday assay validations. The LLOQ for N-desethylamodiaquine was about 3.9nM.

Table 2.6 Interday validation for N-desethylamodiaquine.

Nominal concentration (nM)	Average observed concentration			Mean	SD	% CV	% RE
	Day 1	Day 2	Day 3				
30	31.4	40.35	27.15	32.97	7.06	21.4	9.89
60	60.7	63.05	62.05	61.93	4.38	7.07	3.22
120	120	174.5	121.5	138.67	28.76	20.74	15.56
240	259	282.5	254.5	265.33	28.8	10.86	10.56

SD: standard deviation, CV: coefficient of variation, RE: relative error

The intraday validation was performed using the same concentrations with n=3 at each concentration on the same day. Table 2.7 depicts the intraday assay validations.

Table 2.7 Intraday validation for N-desethylamodiaquine.

Nominal concentration (nM)	Average observed concentration			Mean	SD	% CV	% RE
	Day 1	Day 2	Day 3				
30	22.6	29.5	25.4	25.83	3.47	13.43	-13.89
60	66.3	53.8	67.8	62.63	7.68	12.27	4.39
120	92.3	112	129	111.1	18.37	16.53	-7.42
240	247	265	242	251.33	12.1	4.81	4.72

SD: standard deviation, CV: coefficient of variation, RE: relative error

2.4.5 Amodiaquine time and protein linearity assay:

Time and protein linearity assays were performed with 3 protein concentrations (117µg/ml, 195µg/ml, 292.5µg/ml) and until 7.5 minutes. Figures 2.10 and 2.11 depict the linearity profiles for amodiaquine in rCYP2C8.

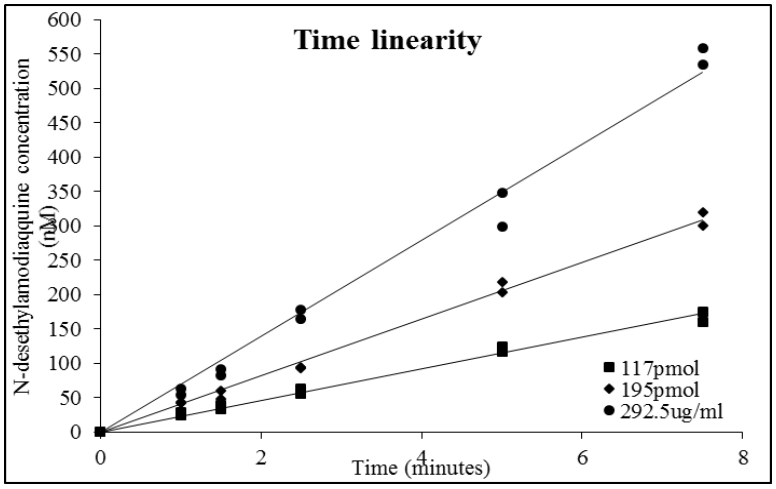

Figure 2.10. Linearity of metabolite formation of amodiaquine with time for 7.5 minutes, at 3 protein concentrations. Data are expressed as mean values (n=2).

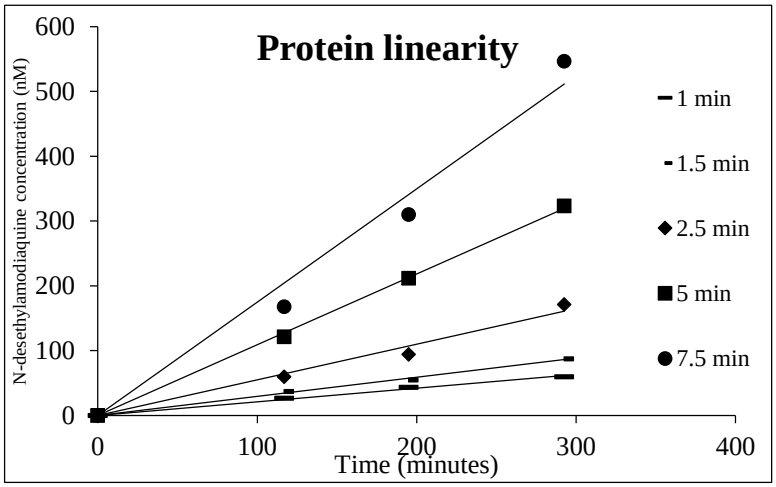

Figure 2.11. Linearity of metabolite formation of amodiaquine with protein concentration of 117µg/ml, 195µg/ml and 292.5µg/ml. Data are expressed as mean values (n=2).

2.4.6 Preliminary MBI screen:

MBI screen was used to assess time dependent inhibition. The table below (fig. 2.12) showed the percent remaining enzyme activity. The enzyme activity is normalized with the activity in control incubation (control incubation: incubation with methanol + 0 minute pre-incubation time). The enzyme activity in control incubation in considered to be 100%.

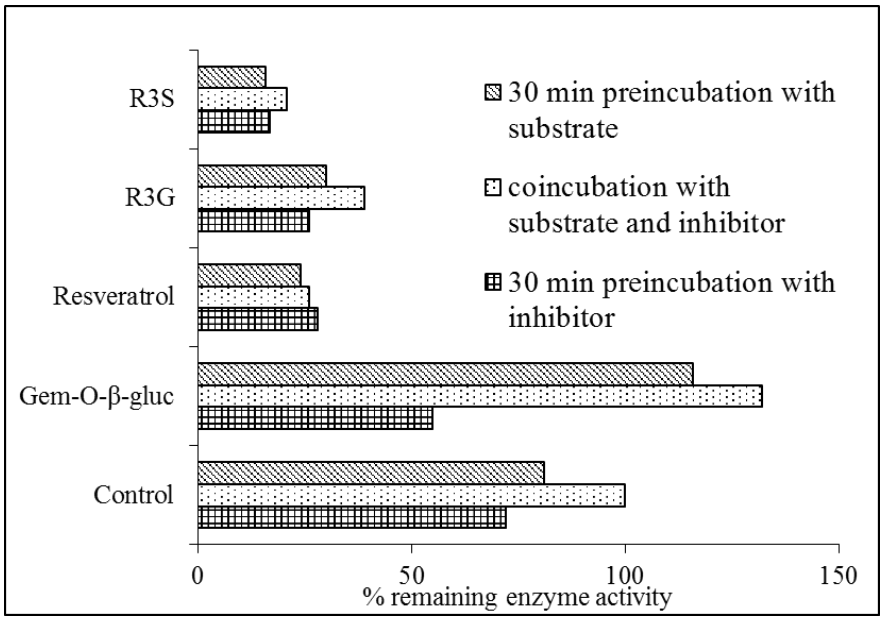

Figure 2.12 MBI screening assay conducted for resveratrol (1mM), R3G (50µM) and R3S (1mM). Gemfibrozil-O-β-glucuronide (30µM) and methanol (solvent) used as controls. Incubation 1: rCYP2C8 is pre-incubated for 30 minute with the test compound, incubation, 2: rCYP2C8 is co-incubated with substrate and the test compound, incubation 3: rCYP2C8 is pre-incubated for 30 min with substrate with absence of the test compound. Data expressed as n=2, Gem-O- β-gluc: Gemfibrozil-O-β-glucuronide.

Gemfibrozil-O-β-glucuronide displayed time dependent inhibition with % enzyme inhibition decreased to 55% as compared to the control. A decrease in percent enzyme activity in control incubations depicted enzyme loss (~21%) due to 30 minutes pre-incubation. The test compounds, resveratrol, R3G and R3S inhibited the enzyme activity in all three incubations, which suggested reversible inhibition rather than mechanism-based inactivation.

2.4.7 Amodiaquine enzyme activity assay:

The kinetic profiles for the formation of N-desethylamodiaquine in recombinant CYP2C8 are shown in fig 2.13. Commercially available rCYP2C8 was used to construct these kinetic profiles. Michaelis-Menten and substrate inhibition equations were both fit to the data. The kinetic parameters and statistical parameters are shown in table 2.8.

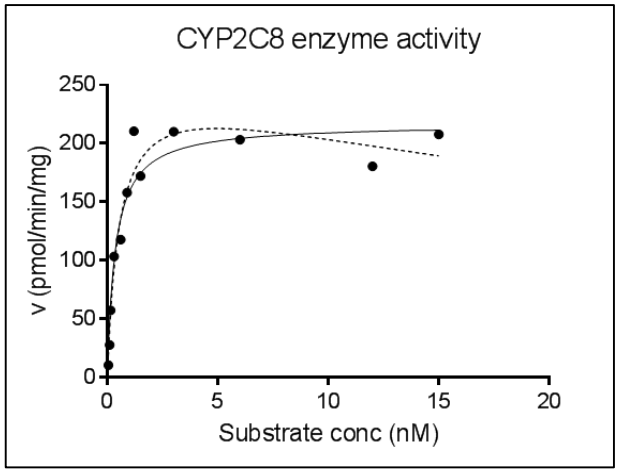

Figure 2.13. Kinetic profiles for the formation of N-desethylamodiaquine in rCYP2C8. (solid line: Michaelis-Menten equation was fit to the data, dashed line: substrate inhibition equation was fit to the data). Data is expressed as mean values (n=2).

Table 2.8. Kinetic parameter estimates for the formation of N-desethylamodiaquine.

Product	V_{max} (pmol/min/mg	K_m (μM)	K_i (μM)	Type of model	R^2	Sy.x	AIC
N-desethyl-amodiaquine	216.6	0.366	na	MM	0.92	20.72	150.6
	259.6	0.54	44.9	SI	0.94	18.13	146

Data are expressed as (n=2). MM: Michaelis Menten, AIC: Akaike information criterion, SI: substrate inhibition, Sy.x: standard deviation for residuals, estimated using Eq. 2.5.

The R^2 and absolute sum of square values for substrate inhibition model were lower than those obtained in Michaelis-Menten model. Although the experiment was performed with n=2 at each concentration which, may prove to be a limitation in order to choose the correct model, AIC values for both models were less than 5 units apart. Hence, the simpler model (Michaelis-Menten model) was preferred over substrate inhibition model.

2.4.8 Lineweaver-Burk plot for reversible inhibition:

Lineweaver-Burk plot was drawn to assess type of reversible inhibition (fig. 2.14). The intersection of lines was observed to be in the second quadrant. As the intersection of lines is not on X or Y axis, the likely inhibition would be a mixed type inhibition. The inhibition experiment was performed with 7 concentrations of resveratrol (0.5μM-250μM) in the presence of 7 concentrations of amodiaquine (0.15μM-3 μM).

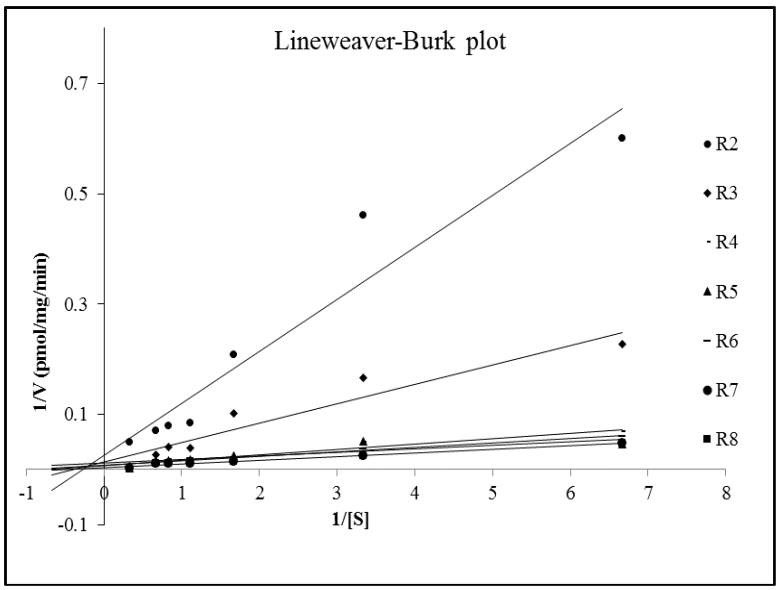

Figure 2.14. Lineweaver-Burk plot for inhibition of rCYP2C8 by resveratrol. Data expressed as mean values (n=2) (7 concentrations of resveratrol include, R2: 250µM, R3: 100µM, R4: 50µM, R5: 25µM, R6: 5µM, R7: 1µM, R8: 0.05µM). Data are expressed as mean values (n=2).

2.5 Discussion:

The U.S. Food and Drug Administration (FDA) has issued a guidance in 2012, which provides the reason to evaluate new chemical entities for enzyme inhibition (http://www.fda.gov/downloads/Drugs/GuidanceComplianceRegulatoryInformation/Guidances/ucm292362.pdf). In addition to this, it provides a decision tree for evaluation of investigational drugs as enzyme inhibitors. Despite the wealth of knowledge on enzyme inhibition, DDI still occur due to limitations in predictive ability of the enzyme inhibition models and in vitro systems. HLM is widely used to conduct inhibition assays (Grimm et al., 2009). But HLM often provides inconsistent DDI predictions for weak time

dependent inhibitors. Additionally, HLM also suffers from loss of enzyme activity when incubations exceed 30 minutes (Foti and Fisher, 2004). Freshly plated human hepatocytes and hepatocyte suspension have also been used to study DDI (Mao et al., 2011; Albaugh et al., 2012). The limitations of these systems are the availability of human hepatocytes, viability of hepatocytes when freshly plated or in suspension and the change in activity of enzymes (Zhao, 2008). The goal of the above hepatocyte study was to assess the utility of SCHH in predicting TDI. The goal of CYP2C8 inhibition study was to assess the potential of resveratrol, R3G and R3S to inhibit CYP2C8.

All SCHH incubations were performed in two lots of hepatocytes. Inter-lot variability (with respect to inhibition parameters and DDI values) was observed. Pooled hepatocyte plating was attempted unsuccessfully using multiple lots of hepatocytes. The in house predicted K_I, k_{inact} and DDI values were compared with literature reported values obtained in SCHH and HLM (table 2.4, table 2.5). The predicted k_{inact} values from SCHH were within two fold as compared to literature reported HLM values except for mibefradil and raloxifene. The in-house predicted SCHH k_{inact} values were 10 fold lower in comparison to literature reported SCHH k_{inact} values, except for troleandomycin. The predicted K_I values were lower as compared to literature reported K_I values in HLM except for troleandomycin (at least 10 fold higher) and raloxifene (2.5 fold higher). The predicted K_I values for troleandomycin and verapamil were higher than the reported SCHH K_I values while K_I values were lower in case of mibefradil. The DDI values obtained using in-house predicted kinetic parameters and static model were compared to literature reported DDI values generated by using HLM and SCHH. In-house generated DDI values were two fold lower than those reported in SCHH (Albaugh et al., 2012). The

calculated DDI values were within two fold of clinically reported DDI value for verapamil, troleandomycin, mibefradil and diltiazem.

The set of compounds used in the above TDI assays were a combination of true positive in vivo time dependent inhibitors (troleandomycin, mibefradil, verapamil, diltiazem) (Backman et al., 1994; Veronese et al., 2003; Kharasch et al., 2004; Xu et al., 2009b; Albaugh et al., 2012), true negative in vivo time dependent inhibitors (dihydralazine) and two false positive in vivo time dependent inhibitor (raloxifene and tamoxifen). Here, false positive time dependent inhibitor indicates a compound, which shows a DDI value greater than 1.25 in in vitro microsomal incubations and a DDI value less than 1.25 in vivo. Rigorous validation of SCHH using a larger set of time dependent inhibitors will increase confidence in this system.

A static model was used for the calculation of DDI values (Obach, 2009). The static model makes some important assumptions (discussed in section 2.1.7). The predictions obtained by using the static model are for steady state concentrations of inhibitor and victim drug (Grimm et al., 2009). Hence, the static model fails to account for changing concentrations of both the drugs. Several estimates of inhibitor concentration at enzyme active site have been used. These estimates include total C_{max}, unbound C_{max}, portal inlet concentration [I_{inlet}], systemic total or unbound concentration [I_{sys}, I_u] and inhibitor concentration in small intestine [I_{gut}] (Grimm et al., 2009; Peters et al., 2012). Also, other parameters included in the static model such as k_{deg}, f_{gut}, f_h, are difficult to calculate in vivo and precise values of these parameters would improve DDI predictions (Grimm et al., 2009). For example, the measurement of k_{deg} is not presently ethical to measure in vivo in humans (Grimm et al., 2009). The k_{deg} value used in the

current SCHH assay was $0.024h^{-1}$ (Quinney et al., 2010). This k_{deg} value was calculated from the recovery of CYP3A4 following clarithromycin treatment (Gorski J, 2002; Wang Y-H, 2004; Quinney et al., 2010). Considering these disadvantages, SCHH could serve as a valuable preclinical tool in conjunction with HLM to assess DDI.

Ogilvie et.al. (2006) reported that the glucuronidated product of gemfibrozil was a more potent mechanism-based inactivator than its parent (Ogilvie et al., 2006). Further exploration of this inhibition phenomenon showed that the inactivator is formed via hydroxylation on 2', 5'-dimethylphenoxy moiety and that glucuronide moiety remained intact. Tornio et.al. reported that glucuronidation converted clopidogrel to a strong mechanism-based inactivator (Tornio et al., 2014). Since, resveratrol is extensively metabolized to R3G and the reported exposure of R3G in vivo is greater than resveratrol, we considered the possibility of R3G being a mechanism-based inactivator of CYP2C8. Hence, we assessed this possibility for resveratrol, R3G and R3S.

The kinetic parameters of amodiaquine were first estimated. The kinetic profile of CYP2C8 provided K_m of 0.36μM and V_{max} of 216.6pmol/mg/min. The substrate inhibition model was also fit to the data, which provided K_m of 0.54μM and V_{max} of 259.6pmol/mg/min.

A preliminary MBI screen was run using gemfibrozil-O-β-glucuronide as a positive control and methanol (solvent) as a negative control. As expected, gemfibrozil-O-β-glucuronide showed mechanism-based inactivation with percent remaining enzyme activity reduced to 55% after 30 minutes pre-incubation. Resveratrol, R3S and R3S showed CYP2C8 inhibition when coincubated with amodiaquine and preincubation with

amodiaquine. So, resveratrol, R3G and R3S reduced the enzyme activity in all three incubations indicating reversible inhibition.

To assess inhibition of CYP2C8 by resveratrol, an assay to assess reversible inhibition study was performed with seven concentrations of resveratrol. A lineweaver-burk plot was used to distinguish type of reversible inhibition. A decrease in apparent V_{max} and an increase in apparent K_m was observed. Thus, the possible type of reversible inhibition is mixed type inhibition characterized by decrease in V_{max} and increase in K_m.

2.6 Conclusions:

Resveratrol is a naturally occurring phytochemical (Fremont, 2000; Baur and Sinclair, 2006). The dose of resveratrol is usually not monitored. It is metabolized extensively into glucuronide and sulfate conjugates. Resveratrol is also known to be a weak time dependent inhibitor of CYP3A4 (Chan and Delucchi, 2000). Glucuronide metabolites of certain compounds such as clopidogrel and gemfibrozil (Ogilvie et al., 2006; Tornio et al., 2014) have been known to inhibit CYP2C8, and hence, the ability of resveratrol and its metabolites to inhibit CYP2C8 was assessed. Resveratrol and its metabolites were not found to be mechanism-based inactivators of CYP2C8. But CYP2C8 was found to be reversibly inhibited by resveratrol and the type of inhibition was mixed type of inhibition.

Sandwich cultured cryopreserved human hepatocytes was used to predict DDI. DDI estimates provided by SCHH were closer to those obtained from literature reported in vivo data than those reported in HLM (Backman et al., 1994; Veronese et al., 2003; Kharasch et al., 2004; Xu et al., 2009b; Albaugh et al., 2012). If the system were

corrected for inter-lot variability and expression of CYP3A4, sandwich cultured cryopreserved human hepatocytes would be a viable choice for routine assessment of time dependent inhibition.

2.7 Future directions:

As discussed earlier, SCHH is often considered to be a more holistic system than HLM to study irreversible enzyme inhibition. But being a more comprehensive system, factors such as partitioning, involvement of transporters, sequestration in lysosomes may affect the predicted DDI value. The TDI experiments in SCHH were performed in duplicates. TDI experiments with more replicates, in several lots and in pooled SCHH would provide with a better estimate of inhibition parameters. The differences in the inhibition parameters obtained from the two hepatocyte lots also indicated inter lot-variability. Thus, using pooled plated hepatocytes would provide a solution to this issue.

The cryopreserved hepatocytes used in these experiments were not characterized with respect to expression of transporters and enzymes. Hence, the difference in expression of enzymes and transporters may have contributed towards the variability of obtained parameters and DDI values. The static model fails to account for changing concentrations of both the victim and the perpetrator. The issues with the parameters used in this model are discussed in detail in sections 2.1.10 and 2.5. A more complex semi-physiological based pharmacokinetic model has been used to predict the effect of diltiazem on midazolam pharmacokinetics (Zhang et.al. 2009) and to predict mechanism-based inactivation by clarithromycin (Quinney et.al. 2010).

ACKNOWLEDGMENTS

The time dependent inhibition assays in sandwich cultured cryopreserved human hepatocytes were funded by GlaxoSmithKline PLC and performed in GlaxoSmithKline PLC, King of Prussia, PA. I would like to acknowledge the help and support of Dr. Nagar and Dr. Skordos for the co- op opportunity at GlaxoSmithKline PLC.

I would like to thank Dr. Konstantine Skordos, Ms. Dung Nguyen and Mr. Cory Watson for the help and guidance throughout my co-op at GlaxoSmithKline PLC. Many thanks to Dr. Skordos and Ms. Nguyen for providing me with insights in TDI as well as technical help. Many thanks to Ms. Nguyen and Mr. Cory Watson for their assistance with UPLC- MS/MS.

REFERENCES

Abe K, Bridges AS, and Brouwer KLR (2009) Use of Sandwich-Cultured Human Hepatocytes to Predict Biliary Clearance of Angiotensin II Receptor Blockers and HMG- CoA Reductase Inhibitors. Drug metabolism and Disposition 37:447-452.

Albaugh DR, Fullenwider CL, Fisher MB, and Hutzler JM (2012) Time-dependent inhibition and estimation of CYP3A clinical pharmacokinetic drug-drug interactions using plated human cell systems. Drug Metab Dispos 40:1336-1344.

Altmann F, Staudacher E, Wilson IBH, and Marz L (1999) Insect cells as hosts of the expression of recombinant glycoproteins. Glycoconjugate Journal 16:109-123.altma

Backman JT, Olkkola KT, Aranko K, Himberg JJ, and Neuvonen PJ (1994) Dose of Midazolam Should Be Reduced during Diltiazem and Verapamil Treatments. Br J Clin Pharmacol 37:221-225.

Baer BR, DeLisle RK, and Allen A (2009) Benzylic oxidation of gemfibrozil-1-O-beta-glucuronide by P450 2C8 leads to heme alkylation and irreversible inhibition. Chem Res Toxicol 22:1298-1309.

Baldwin SJ, Clarke SE, and Chenery RJ (1999) Characterization of the cytochrome P450 enzymes involved in the in vitro metabolism of rosiglitazone. Br J Clin Pharmacol 48:424-432.

Baur JA and Sinclair DA (2006) Therapeutic potential of resveratrol: the in vivo evidence. Nat Rev Drug Discov 5:493-506.

Bi YA, Kazolias D, and Duignan DB (2006) Use of cryopreserved human hepatocytes in sandwich culture to measure hepatobiliary transport. Drug metabolism and Disposition 34:1658-1665.

Bidstrup TB, Bjornsdottir I, Sidelmann UG, Thomsen MS, and Hansen KT (2003) CYP2C8 and CYP3A4 are the principal enzymes involved in the human in vitro biotransformation of the insulin secretagogue repaglinide. Br J Clin Pharmacol 56:305- 314.

Brouwer KL, Keppler D, Hoffmaster KA, Bow DA, Cheng Y, Lai Y, Palm JE, Stieger B, Evers R, and International Transporter C (2013) In vitro methods to support transporter evaluation in drug discovery and development. Clin Pharmacol Ther 94:95-112.

Chan WK and Delucchi AB (2000) Resveratrol, a red wine constituent, is a mechanism-based inactivator of cytochrome P450 3A4. Life Sci 67:3103-3112.

Chandra P, Lecluyse EL, and Brouwer KL (2001) Optimization of culture conditions for determining hepatobiliary disposition of taurocholate in sandwich-cultured rat hepatocytes. In Vitro Cell Dev Biol Anim 37:380-385.

Chen Q, Ngui JS, Doss GA, Wang RW, Cai XX, DiNinno FP, Blizzard TA, Hammond ML, Stearns RA, Evans DC, Baillie TA, and Tang W (2002) Cytochrome P450 3A4- mediated bioactivation of raloxifene: Irreversible enzyme inhibition and thiol adduct formation. Chem Res Toxicol 15:907-914.

Cornish-Bowden A (2011) Fundamentals of enzyme kinetics. Wiley-Blackwell.

Cornish-Bowden A (2012) Fundamentals of Enzyme Kinetics. Wiley-Blackwell.

Ding X and Kaminsky LS (2003) Human extrahepatic cytochromes P450: function in xenobiotic metabolism and tissue-selective chemical toxicity in the respiratory and gastrointestinal tracts. Annu Rev Pharmacol Toxicol 43:149-173.

Foti RS and Fisher MB (2004) Impact of incubation conditions on bufuralol human clearance predictions: enzyme lability and nonspecific binding. Drug Metab Dispos 32:295-304.

Franklin MR (1991) Cytochrome P450 metabolic intermediate complexes from macrolide antibiotics and related compounds. Methods Enzymol 206:559-573.

Fremont L (2000) Biological effects of resveratrol. Life Sci 66:663-673.

Ghanbari F, Rowland-Yeo K, Bloomer JC, Clarke SE, Lennard MS, Tucker GT, and Rostami-Hodjegan A (2006) A critical evaluation of the experimental design of studies of mechanism based enzyme inhibition, with implications for in vitro-in vivo extrapolation. Curr Drug Metab 7:315-334.

Gorski J WZ, and Hall S (2002) Duration of CYP3A inhibition of clarithromycin. Clin Pharmacol Ther 71.

Grimm SW, Einolf HJ, Hall SD, He K, Lim HK, Ling KH, Lu C, Nomeir AA, Seibert E, Skordos KW, Tonn GR, Van Horn R, Wang RW, Wong YN, Yang TJ, and Obach RS (2009) The conduct of in vitro studies to address time-dependent inhibition of drug-metabolizing enzymes: a perspective of the pharmaceutical research and manufacturers of America. Drug Metab Dispos 37:1355-1370.

Guengerich FP (2005) Human Cytochrome P450 Enzymes, in: Cytochrome P450: Structure, Mechanism, and Biochemistry (Ortiz de Montellano PR ed), KluwerAcademic/Plenum Publishers, New Yrok.

Guengerich FP (2009) Inhibition of Drug Metabolizing Enzymes, in: Handbook of Drug Metabolism, pp 203-226.

Hanna HJEaI (2014) Management and Mitigation of Human Drug–drug Interaction Risks in the Drug Discovery and Development Phases, in: Predictive ADMET: Integrated Approaches in Drug Discovery and Development, pp 353.

Hewitt NJ, Lechon MJG, Houston JB, Hallifax D, Brown HS, Maurel P, Kenna JG, Gustavsson L, Lohmann C, Skonberg C, Guillouzo A, Tuschl G, Li AP, LeCluyse E, Groothuis GMM, and Hengstler JG (2007) Primary hepatocytes: Current understanding of the regulation of metabolic enzymes and transporter proteins, and pharmaceutical practice for the use of hepatocytes in metabolism, enzyme induction, transporter, clearance, and hepatotoxicity studies. Drug Metab Rev 39:159-234.

Hollenberg PF (2002) Characteristics and common properties of inhibitors, inducers, and activators of CYP enzymes. Drug Metab Rev 34:17-35.

Hollenberg PF, Kent UM, and Bumpus NN (2008) Mechanism-based inactivation of human cytochromes p450s: experimental characterization, reactive intermediates, and clinical implications. Chem Res Toxicol 21:189-205.

Isin EM and Guengerich FP (2006) Kinetics and thermodynamics of ligand binding by cytochrome P450 3A4. J Biol Chem 281:9127-9136.

Ito K, Brown HS, and Houston JB (2004) Database analyses for the prediction of in vivo drug-drug interactions from in vitro data. Br J Clin Pharmacol 57:473-486.

Ito K, Iwatsubo T, Kanamitsu S, Ueda K, Suzuki H, and Sugiyama Y (1998) Prediction of pharmacokinetic alterations caused by drug-drug interactions: metabolic interaction in the liver. Pharmacol Rev 50:387-412.

Jenkins SM, Zvyaga T, Johnson SR, Hurley J, Wagner A, Burrell R, Turley W, Leet JE, Philip T, and Rodrigues AD (2011) Studies to further investigate the inhibition of

human liver microsomal CYP2C8 by the acyl-beta-glucuronide of gemfibrozil. Drug Metab Dispos 39:2421-2430.

Johnston WA, Hunter DJ, Noble CJ, Hanson GR, Stok JE, Hayes MA, De Voss JJ, and Gillam EM (2011) Cytochrome P450 is present in both ferrous and ferric forms in the resting state within intact Escherichia coli and hepatocytes. J Biol Chem 286:40750- 40759.

Jones JP and Korzekwa KR (1996) Predicting the rates and regioselectivity of reactions mediated by the P450 superfamily. Methods Enzymol 272:326-335.

Jung C (2011) The mystery of cytochrome P450 Compound I: a mini-review dedicated to Klaus Ruckpaul. Biochim Biophys Acta 1814:46-57.

Jung C, de Vries S, and Schunemann V (2011) Spectroscopic characterization of cytochrome P450 Compound I. Arch Biochem Biophys 507:44-55.

Kalgutkar AS, Obach RS, and Maurer TS (2007) Mechanism-based inactivation of cytochrome P450 enzymes: chemical mechanisms, structure-activity relationships and relationship to clinical drug-drug interactions and idiosyncratic adverse drug reactions. Curr Drug Metab 8:407-447.

Kemp DC and Brouwer KL (2004) Viability assessment in sandwich-cultured rat hepatocytes after xenobiotic exposure. Toxicol In Vitro 18:869-877.

Kerr BM, Thummel KE, Wurden CJ, Klein SM, Kroetz DL, Gonzalez FJ, and Levy RH (1994) Human liver carbamazepine metabolism. Role of CYP3A4 and CYP2C8 in 10,11- epoxide formation. Biochem Pharmacol 47:1969-1979.

Kharasch ED, Walker A, Hoffer C, and Sheffels P (2004) Intravenous and oral alfentanil as in vivo probes for hepatic and first-pass cytochrome P450 3A activity:

Noninvasive assessment by use of pupillary miosis. Clinical Pharmacology & Therapeutics 76:452- 466.

Klose TS, Blaisdell JA, and Goldstein JA (1999) Gene structure of CYP2C8 and extrahepatic distribution of the human CYP2Cs. J Biochem Mol Toxicol 13:289-295.

Knupfer H, Schmidt R, Stanitz D, Brauckhoff M, Schonfelder M, and Preiss R (2004) CYP2C and IL-6 expression in breast cancer. Breast 13:28-34.

LeCluyse EL, Audus KL, and Hochman JH (1994) Formation of extensive canalicular networks by rat hepatocytes cultured in collagen-sandwich configuration. Am J Physiol 266:C1764-1774.

Li XQ, Bjorkman A, Andersson TB, Ridderstrom M, and Masimirembwa CM (2002) Amodiaquine clearance and its metabolism to N-desethylamodiaquine is mediated by CYP2C8: a new high affinity and turnover enzyme-specific probe substrate. J Pharmacol Exp Ther 300:399-407.

Luthra A, Denisov IG, and Sligar SG (2011) Spectroscopic features of cytochrome P450 reaction intermediates. Arch Biochem Biophys 507:26-35.

Ma B, Prueksaritanont T, and Lin JH (2000) Drug interactions with calcium channel blockers: possible involvement of metabolite-intermediate complexation with CYP3A. Drug Metab Dispos 28:125-130.

Ma B, Subramanian R, Schrag ML, Rodrigues AD, and Tang C (2004) Cytochrome P450 2C8 (CYP2C8)-mediated hydroxylation of an endothelin ETA receptor antagonist in human liver microsomes. Drug Metab Dispos 32:473-478.

Mao J, Mohutsky MA, Harrelson JP, Wrighton SA, and Hall SD (2011) Prediction of CYP3A-mediated drug-drug interactions using human hepatocytes suspended in human plasma. Drug Metab Dispos 39:591-602.

Marill J, Capron CC, Idres N, and Chabot GG (2002) Human cytochrome P450s involved in the metabolism of 9-cis- and 13-cis-retinoic acids. Biochem Pharmacol 63:933-943.

Masubuchi Y and Horie T (1999) Mechanism-based inactivation of cytochrome P450s 1A2 and 3A4 by dihydralazine in human liver microsomes. Chem Res Toxicol 12:1028- 1032.

Mayhew BS, Jones DR, and Hall SD (2000) An in vitro model for predicting in vivo inhibition of cytochrome P450 3A4 by metabolic intermediate complex formation. Drug Metab Dispos 28:1031-1037.

Meunier B, de Visser SP, and Shaik S (2004) Mechanism of oxidation reactions catalyzed by cytochrome p450 enzymes. Chem Rev 104:3947-3980.

Mohutsky M and Hall S (2014) Irreversible Enzyme Inhibition Kinetics and Drug–Drug Interactions, in: Enzyme Kinetics in Drug Metabolism (Nagar S, Argikar UA, and Tweedie DJ eds), pp 57-91, Humana Press.

Nakajima T, Elovaara E, Gonzalez FJ, Gelboin HV, Raunio H, Pelkonen O, Vainio H, and Aoyama T (1994) Styrene metabolism by cDNA-expressed human hepatic and pulmonary cytochromes P450. Chem Res Toxicol 7:891-896.

Nelson DR (2009) The cytochrome p450 homepage. Hum Genomics 4:59-65.

Obach RS (2009) Predicting drug-drug interactions from in vitro drug metabolism data: challenges and recent advances. Curr Opin Drug Discov Devel 12:81-89.

Ogilvie BW, Zhang D, Li W, Rodrigues AD, Gipson AE, Holsapple J, Toren P, and Parkinson A (2006) Glucuronidation converts gemfibrozil to a potent, metabolism- dependent inhibitor of CYP2C8: implications for drug-drug interactions. Drug Metab Dispos 34:191-197.

Ohyama K, Nakajima M, Nakamura S, Shimada N, Yamazaki H, and Yokoi T (2000) A significant role of human cytochrome P450 2C8 in amiodarone N-deethylation: an approach to predict the contribution with relative activity factor. Drug Metab Dispos 28:1303-1310.

Olkkola KT, Aranko K, Luurila H, Hiller A, Saarnivaara L, Himberg JJ, and Neuvonen PJ (1993) A Potentially Hazardous Interaction between Erythromycin and Midazolam. Clinical Pharmacology & Therapeutics 53:298-305.

Omura T and Sato R (1962) A new cytochrome in liver microsomes. J Biol Chem 237:1375-1376.

Parkinson A, Kazmi F, Buckley DB, Yerino P, Ogilvie BW, and Paris BL (2010) System-dependent outcomes during the evaluation of drug candidates as inhibitors of cytochrome P450 (CYP) and uridine diphosphate glucuronosyltransferase (UGT) enzymes: human hepatocytes versus liver microsomes versus recombinant enzymes. Drug Metab Pharmacokinet 25:16-27.

Periti P, Mazzei T, Mini E, and Novelli A (1992) Pharmacokinetic drug interactions of macrolides. Clinical Pharmacokinetics 23:106-131.

Perloff ES, Mason AK, Dehal SS, Blanchard AP, Morgan L, Ho T, Dandeneau A, Crocker RM, Chandler CM, Boily N, Crespi CL and Stresser DM (2009) Validation of cytochrome P450 time-dependent inhibition assays: a two point IC50 shift spproach facilitates kinact assay design, Xenobiotica 39:99-112.

Peters SA, Schroeder PE, Giri N, and Dolgos H (2012) Evaluation of the use of static and dynamic models to predict drug-drug interaction and its associated variability: impact on drug discovery and early development. Drug Metab Dispos 40:1495-1507.

Prueksaritanont T, Ma B, Tang CY, Meng Y, Assang C, Lu P, Reider PJ, Lin JH, and Baillie TA (1999) Metabolic interactions between mibefradil and HMG-CoA reductase inhibitors: an in vitro investigation with human liver preparations. Br J Clin Pharmacol 47:291-298.

Quinney SK, Zhang X, Lucksiri A, Gorski JC, Li L, and Hall SD (2010) Physiologically based pharmacokinetic model of mechanism-based inhibition of CYP3A by clarithromycin. Drug Metab Dispos 38:241-248.

Rahman A, Korzekwa KR, Grogan J, Gonzalez FJ, and Harris JW (1994) Selective biotransformation of taxol to 6 alpha-hydroxytaxol by human cytochrome P450 2C8. Cancer Res 54:5543-5546.

Segel IH (1993a) Enzyme Kinetics: Behavior and Analysis of Rapid Equilibrium and Steady-State Enzyme Systems.

Segel IH (1993b) Enzyme Kinetics: Behavior and Analysis of Rapid Equilibrium and Steady-State Enzyme Systems Wiley-Interscience.

Shimada T, Yamazaki H, Mimura M, Inui Y, and Guengerich FP (1994) Interindividual variations in human liver cytochrome P-450 enzymes involved in the oxidation of drugs, carcinogens and toxic chemicals: studies with liver microsomes of 30 Japanese and 30 Caucasians. J Pharmacol Exp Ther 270:414-423.

Shitara Y, Hirano M, Sato H, and Sugiyama Y (2004) Gemfibrozil and its glucuronide inhibit the organic anion transporting polypeptide 2

(OATP2/OATP1B1:SLC21A6)- mediated hepatic uptake and CYP2C8-mediated metabolism of cerivastatin: analysis of the mechanism of the clinically relevant drug-drug interaction between cerivastatin and gemfibrozil. J Pharmacol Exp Ther 311:228-236.

Silverman RB (1988) Mechanism-Based Ezyme Inactivators: Chemistry and Enzymology. CRC press.

Silverman RB (1995) Mechanism-based enzyme inactivators. Methods Enzymol 249:240-283.

Swift B, Pfeifer ND, and Brouwer KL (2010) Sandwich-cultured hepatocytes: an in vitro model to evaluate hepatobiliary transporter-based drug interactions and hepatotoxicity.
Drug Metab Rev 42:446-471.

Thum T and Borlak J (2000) Gene expression in distinct regions of the heart. Lancet 355:979-983.

Tornio A, Filppula AM, Kailari O, Neuvonen M, Nyronen TH, Tapaninen T, Neuvonen PJ, Niemi M, and Backman JT (2014) Glucuronidation converts clopidogrel to a strong time-dependent inhibitor of CYP2C8: a phase II metabolite as a perpetrator of drug-drug interactions. Clin Pharmacol Ther 96:498-507.

Totah RA and Rettie AE (2005) Cytochrome P450 2C8: substrates, inhibitors, pharmacogenetics, and clinical relevance. Clin Pharmacol Ther 77:341-352.

Turncliff RZ, Tian X, and Brouwer KL (2006) Effect of culture conditions on the expression and function of Bsep, Mrp2, and Mdr1a/b in sandwich-cultured rat hepatocytes. Biochem Pharmacol 71:1520-1529.

Venkatakrishnan K and Obach RS (2007) Drug-drug interactions via mechanism-based cytochrome P450 inactivation: Points to consider for risk assessment from in vitro data and clinical pharmacologic evaluation. Curr Drug Metab 8:449-462.

Veronese ML, Gillen LP, Dorval EP, Hauck WW, Waldman SA, and Greenberg HE (2003) Effect of mibefradil on CYP3A4 in vivo. J Clin Pharmacol 43:1091-1100.

Wang JS, Neuvonen M, Wen X, Backman JT, and Neuvonen PJ (2002) Gemfibrozil inhibits CYP2C8-mediated cerivastatin metabolism in human liver microsomes. Drug Metab Dispos 30:1352-1356.

Wang Y-H GJ, Hamman MA, and Hall SD (2004) Age and sex effect on the recovery time of CYP3A inhibition by clarithromycin. Drug Metab Rev 36:287.

Wang YH, Jones DR, and Hall SD (2005) Differential mechanism-based inhibition of CYP3A4 and CYP3A5 by verapamil. Drug Metab Dispos 33:664-671.

Warot D, Bergougnan L, Lamiable D, Berlin I, Bensimon G, Danjou P, and Puech AJ (1987) Troleandomycin-triazolam interaction in healthy volunteers: pharmacokinetic and psychometric evaluation. Eur J Clin Pharmacol 32:389-393.

Williams D and Feely J (2002) Pharmacokinetic-pharmacodynamic drug interactions with HMG-CoA reductase inhibitors. Clin Pharmacokinet 41:343-370.

Wrighton SA and Stevens JC (1992) The human hepatic cytochromes P450 involved in drug metabolism. Crit Rev Toxicol 22:1-21.

Xu L, Chen Y, Pan Y, Skiles GL, and Shou M (2009a) Prediction of human drug-drug interactions from time-dependent inactivation of CYP3A4 in primary hepatocytes using a population-based simulator. Drug Metab Dispos 37:2330-2339.

Xu L, Chen YP, Pan Y, Skiles GL, and Shou MG (2009b) Prediction of Human Drug-Drug Interactions from Time-Dependent Inactivation of CYP3A4 in Primary Hepatocytes Using a Population-Based Simulator. Drug metabolism and Disposition 37:2330-2339.

Yamazaki H, Shibata A, Suzuki M, Nakajima M, Shimada N, Guengerich FP, and Yokoi T (1999) Oxidation of troglitazone to a quinone-type metabolite catalyzed by cytochrome P-450 2C8 and P-450 3A4 in human liver microsomes. Drug Metab Dispos 27:1260- 1266.

Yeo KR and Yeo WW (2001) Inhibitory effects of verapamil and diltiazem on simvastatin metabolism in human liver microsomes. Br J Clin Pharmacol 51:461-470.

Zhang X, Jones DR, and Hall SD Mechanism-Based Inhibition of Human Cytochromes P450: In Vitro Kinetics and In Vitro–In Vivo Correlations, in: Drug-Drug Interactions, pp 515-544.

Zhao P (2008) The use of hepatocytes in evaluating time-dependent inactivation of P450 in vivo. Expert Opin Drug Metab Toxicol 4:151-164.

Zhao P, Kunze KL, and Lee CA (2005) Evaluation of time-dependent inactivation of CYP3A in cryopreserved human hepatocytes. Drug metabolism and Disposition 33:853- 861.

Zhao XJ, Jones DR, Wang YH, Grimm SW, and Hall SD (2002) Reversible and irreversible inhibition of CYP3A enzymes by tamoxifen and metabolites. Xenobiotica 32:863-878.

Zhou SF (2008) Potential strategies for minimizing mechanism-based inhibition of cytochrome P450 3A4. Curr Pharm Des 14:990-1000.

CHAPTER 3

EVALUATION OF THE ROLE OF OATP1B AND MRP2 IN RESVERATROL AND RESVERATROL-3-GLUCURONIDE (R3G) TRANSPORT

3.1. Background:

ATP-binding cassette (ABC) transporters are important determinants of bioavailability of a drug. The human genome project identified 400 transporters, which are broadly divided into ABC transporters and solute linked carrier (SLC) transporters (Hillgren et al., 2013). Variability in the expression and activity of transporters may cause DDI. Among them, Pgp, MRP2, MRP3, OATP1B and BCRP are relevant in drug disposition. They are expressed in enterocytes, kidney proximal tubules, blood brain barrier and hepatocytes (Fig.3.1) where they facilitate the efflux of xenobiotics/compounds, thereby limiting the concentration in the cell and decreasing the exposure of compounds.

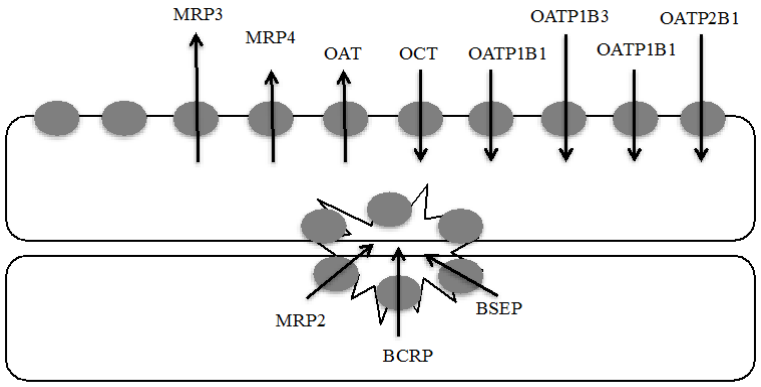

(A) Hepatocyte

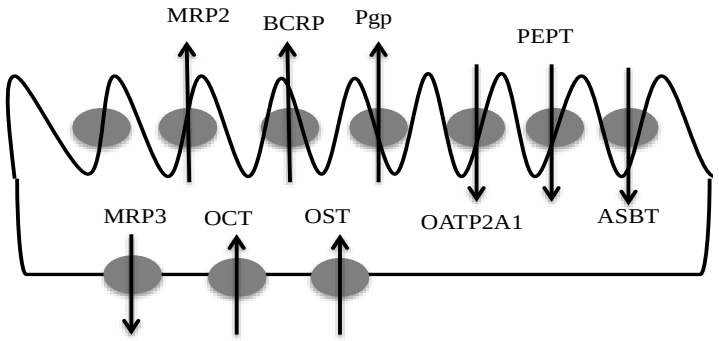

(B) Enterocyte

Figure 3.1. (A) Hepatocyte express BCRP (ABCG2), MRP2 (ABCC2) and BSEP (ABCB11) on apical side while MRP3 (ABCC3), MRP4 (ABCC4), OATP1B1 (SLCO1B1), OATP1B3 (SLCO1B3), SLCO2B1 (OATP2B1) and members of OAT, OCT family on the basolateral side. (B) Enterocyte express BCRP (ABCG2), MRP2 (ABCC2), Pgp (ABCB1), PEPT, ASBT, OATP2A1 (SLCO2A1) on the apical side while MRP3 (ABCC3) and members of OCT, OST family on the basolateral side (Hillgren et al., 2013)

In recent studies (Maier-Salamon et al., 2008; van de Wetering et al., 2009; Alfaras et al., 2010; Juan et al., 2010; Planas et al., 2012), BCRP, MRP3 and MRP2 have been shown to affect the disposition of resveratrol and its conjugated metabolites. Alfaras et.al (Alfaras et al., 2010) showed the involvement of bcrp in the efflux of resveratrol-3-sulfate (R3S) using bcrp -/- mice and suggested that the sulfate metabolite has greater affinity towards bcrp than the glucuronide metabolite. The involvement of Mrp2 (Maier-Salamon et al., 2008; Juan et al., 2010) was studied in rat perfusion studies. The role of OATP in the disposition of resveratrol, R3G and R3S has been recently studied using

human cancer cell lines such as HT-29 and HCA-7 (Patel et al., 2013). Cellular concentrations of resveratrol monosulfate after incubations with 75µM resveratrol monosulfate indicated the role of an uptake transporter. Further studies to evaluate uptake transport indicated the presence of OATP1B3 in HT-29 cell and HCA-7 cell lines (Patel et.al. 2013).

3.1.1. SLC transporters: OATP: Localization, mechanism and structure:

SLC is the second major subfamily of transporter proteins. SLC transporters are considered to be uptake transporters. SLC contain two subfamilies, OATP family (SLC21/SLCO), and the OAT and OCT family (SLC22A). The OATP family is further divided into six subfamilies (OATP1-6) (Hagenbuch and Meier, 2004; Konig et al., 2013). Out of the 11 transporters in the subfamilies, four transporters (OATP1A2, OATP1B1, OATP1B3 and OATP2B1) are considered to play a prominent role in xenobiotic transport. For example, HMG-CoA reductase class of compounds are transported by OATPs (Kalliokoski and Niemi, 2009). OATPs share overlapping substrate specificity (Konig et al., 2013). The OATPs are expressed in renal epithelium, intestinal epithelium, brain capillary endothelial cells and hepatocytes (Konig et al., 2013). In addition to expression in normal tissues, OATPs are expressed in several malignant tissues. For example, OATP1B3 expression occurs in colon polyps and colon cancer (Lee et al., 2008; Konig et al., 2013). OATPs are sodium independent transporting systems. The transport mechanism is based on anion exchange (Hagenbuch and Meier, 2003). A transport study of taurocholate in oatp1- expressing oocytes showed a 1:1

stoichiometry of taurocholate-GSH exchange, indicating an important role of cellular GSH in the transport mechanism of OATP (Li et al., 1998; Hagenbuch and Meier, 2003).

OATPs range from 650 to 750 amino acids with 12 transmembrane domains. OATPs also have multiple N-glycosylation sites on the extracellular domains (Konig et al., 2000; Hagenbuch and Meier, 2003; Niemi et al., 2011; Roth et al., 2012). The molecular weight of OATP1B1 is 84kDa while the deglycosylated protein has a molecular weight of 58kDa (Konig et.al. 2000, Konig et.al. 2000).

Preliminary experiments to evaluate efflux transport were conducted using hMRP2 inside-out vesicles (fig. 3.2) with 5(6)-Carboxy-2', 7'- dichlorofluorescein (CDCF) as the probe substrate and then with resveratrol and R3G as substrates. LC-MS/MS was used to detect and analyze resveratrol and R3G while fluorescence plate reader was used to analyze CDCF.

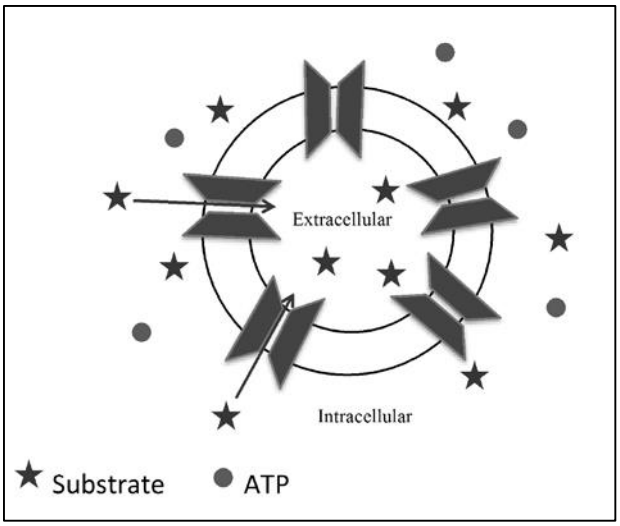

Figure 3.2. Inside-out vesicles (Heredi-Szabo et al., 2008a; Hegedus et al., 2009; Heredi-Szabo et al., 2012). The efflux transporters expressed in the membrane of inside-out vesicles transport substrates from the buffer into the vesicle. Substrate trapped inside is extracted using 0.1N sodium hydroxide (NaOH) and is quantified.

The experiments to study the uptake of resveratrol and R3G were performed in HT-29 and Caco-2 cell line. HT-29 and Caco-2 cell lines have been shown to express mRNA of OATP1B uptake transporters which may play a crucial role in uptake of resveratrol and its metabolites (Seithel et al., 2006; Muto et al., 2007; Ichihara et al., 2010; Imai et al., 2013).

3.2 Experimental section:

3.2.1 Materials:

Human MRP2 (hMRP2) inside-out vesicles were purchased from BD Gentest (San Jose, California). HT-29 and Caco-2 cell lines were purchased from ATCC (Manassas, VA, USA). Sterile DMEM medium and Costar ™ spin X centrifuge tubes were purchased from Corning (New York, USA). RIPA buffer and ATP disodium triphosphate was purchased from Amresco Inc. (Solon, OH). R3G and tariquidar were purchased from Toronoto Research Chemicals Inc. (Toronto, Canada). Atorvastatin was purchased from TCI Chemicals (Montgomeryville, PA). Pitavastatin was purchased from LKT Laboratories, Inc (St. Paul, MN). Sulfasalazine was purchased from Sigma-Aldrich (China). Resveratrol and dexamethasone was purchased from Cayman Chemicals (Ann Arbor, MI). Glycine, tris hydroxymethyl aminomethane hydrochloride, sodium dodecyl sulfate, magnesium chloride and MOPS was purchased from Fisher Scientific (Fair Lawn, NJ). Tris hydroxymethyl aminomethane (Tris base) was purchase from MP Biomedicals (Solon, OH). Fetal bovine serum and McCoy's 5A cell culture medium was purchased from Life Technologies Corporation (Carlsbad, CA). Trypsin with 0.1% EDTA, anti-actin antibody and potassium chloride was purchased from Sigma-Aldrich (St. Louis, MO, USA). Mouse monoclonal OATP2/8 antibody and OATP8 overexpression lysate was purchased from Novus Biological (Littleton, CO, USA). CDCF (5(6)-Carboxy-2,'7'-dichlorofluorescein, sterile DMSO and sodium butyrate was purchased from Santa Cruz Biotechnology, Inc (Dallas, TX). CL-Xposure^{TM} film was purchased from Thermo Fisher Scientific (Rockford, IL). OATP8 overexpressed lysate

(native) and mouse monoclonal OATP2/8 antibody (MDQ) were purchased from Novus Biologicals (Littleton, CO). SuperSignal ™ West Pico chemiluminescent substrate was purchased from Thermo Scientific (Rockford, IL). LC-MS/MS was used for cell uptake assays. LC was an Agilent 1100 instrument. MS/MS was ABSciex API 4000 instrument. SpectraMax M2 (Molecular Devices LLC, Sunnyvale, CA) fluorescence plate reader was used for inside-out vesicle assays. The film developer used was Agfa CP1000 automatic film processor (Agfa healthcare, Medlink Imaging LLC, Pine Brook, NJ).

3.2.2. Preparation of vesicle assay components:

The solutions for vesicle assay were prepared according to table 3.1 below.

Table 3.1 Preparation and components of vesicle assay (protocol modified from assays published in GenoMembrane buffer preparation protocol Ver 1.6, (van Staden et al., 2012).

Solution	Preparation
1.7 M Tris	Dissolve 5.15g of Tris (hydroxymethyl) aminomethane in DI (deionized) water to make 25ml
100mM MOPS-Tris	Dissolve 0.523g of MOPS [3-(N- Morpholino) propanesulfonic acid] in 22.5ml DI water and adjust pH to 7 with 1.7M Tris. Make up the volume to 25ml
1 M KCl	Dissolve 5.08g of potassium chloride in DI water to make 25 ml
200 mM MgATP	Dissolve 1.11g of Na_2ATP in 5ml of DI water and add 2ml of 1M $MgCl_2$. Adjust the pH to 7 using 1.7M Tris and adjust the volume of water to 10ml

3.2.3. Preparation of reaction buffer:

Table 3.2 Components of reaction buffer.

Solution	Volume added	Final concentration
100 mM MOPS-Tris	5ml	50mM
1M KCl	0.7ml	70mM
1M $MgCl_2$	75µl	7.5mM
DI water	q.s	
Final Volume	10ml	

3.2.4 Preparation of stopping buffer:

Table 3.3 Components of stopping buffer

Solution	Volume added	Final concentration
100 mM MOPS-Tris	4ml	40mM
1M KCl	7ml	70mM
DI water	q.s	
Final volume	10ml	

3.2.5 Inside-out vesicle assay:

(a) Linearity and kinetic assays using inside-out vesicles:

The vesicle uptake experiments were performed using filtration tubes. The incubation mix consisted of reaction buffer (Tris-MOPS buffer), vesicle solution (10µg of protein), glutathione and test compound. The incubation mix was incubated at 37^0C for 2 minutes. The reaction was initiated by adding ATP solution (1mM). Once started, the reaction mixture was kept at 37^0C in a shaking water bath for 10 minutes. The reaction mixture (60µl) was transferred on to a tube filter and the reaction was terminated by adding cold stopping buffer. The vesicles were separated on the filter by centrifugation at 9500 rpm for 2 minutes. The filter was washed twice with chilled stopping buffer and

0.1N NaOH was added to the filter tubes and incubated at room temperature for 2 minutes. The filter tubes were centrifuged, the filtered solution was pipetted into 96 well plate and analyzed using a fluorescence plate reader.

CDCF was used as a probe substrate for MRP2 transport experiments (Heredi-Szabo et al., 2008b; Heredi-Szabo et al., 2012; Colombo et al., 2013) because of optimal detection and transport properties. CDCF in vesicles was extracted by using 0.1N NaOH. The extracted CDCF (Ex: 485, Em: 535) was detected and quantitated using the fluorescence plate reader.

For resveratrol transport experiments, the vesicles containing resveratrol were extracted by using methanol. The sample thus collected was analyzed by using LC-MS/MS (Iwuchukwu et al., 2012). Acetaminophen (APAP 80ng/ml) was used as an internal standard. Resveratrol concentrations were calculated using peak area ratios.

3.2.6 Western blot:

(a) Cell culture and generation of cell homogenate:

HT-29 cells were grown in 10cm culture plates with McCoy's complete medium (10% fetal bovine serum + 1% penicillin streptomycin solution). HT-29 cells were grown to 70% confluency until passaging. Plated cells were trypsinized and collected after attaining the required confluency. The collected cells were lysed using a lysis buffer such as Tris buffer and RIPA buffer and were subjected to ultra-sonication of 5 bursts for 20 seconds each with 1 minute resting between each bursts. Homogenization was performed on ice. The homogenates were stored at -80^0C.

(b) Bradford assay and western blot for OATP1B:

Bradford's assay was used to determine the protein content in the cell homogenates using bovine serum albumin as a standard. HT-29 cell homogenates were subjected to western blot analysis to determine the presence of OATP1B uptake transporters. HT-29 cell homogenates were electrophoresed on 8% and 10% SDS-PAGE gels at 150V for 1 hour. The proteins were transferred onto a nitrocellulose membrane at 12V for 70 minutes. Membrane blocking was not performed for OATP1B but was performed for β- actin western blot by using 1% milk in Tris/RIPA buffer containing Tween 20 for 1 hour. The membrane was incubated with 1:50 anti-OATP1B antibody solution overnight at 4^0C. The next day, membrane was rinsed thrice with Tris/RIPA buffer containing Tween-20 followed by 2 hour incubation with secondary antibody (horseradish peroxidase anti- mouse antibody for OATP1B, MRP2 and BCRP detection and horseradish peroxidase anti-rabbit antibody for β-actin detection). The membrane was washed thrice with a solution of Tween-20 in Tris buffer and soaked for 5 minutes in SuperSignal ™ West Pico chemiluminescent substrate. The membrane was exposed to a radiographic film and developed using a film developer. β-actin was used as a loading control. Cell lysate with over expressed OATP1B was used as a positive control.

Due to the possibility of low expression of OATP1B in HT-29 cells, rifampicin and phenytoin was dosed to induce the expression of OATP1B. HT-29 cells were plated in 10cm culture plates and treated with rifampicin (10μM and 30μM) and phenytoin (30 μM) for 7 days. The rifampicin and phenytoin treated medium was changed after every 24 hours. At the end of 7 days, the cell layer was washed, scraped and collected to

generate the cell homogenate. Western blot was performed on the cell homogenates to assess the expression of OATP1B.

(c) Bradford assay and western blot for BCRP and MRP2:

HT-29 cells were grown as described previously. The cell lysate was prepared and the protein content was calculated as before using Bradford's assay. Western blot analysis was performed using OATP1B1/1B3 primary antibodies and OATP1B1/1B3 over-expressed cell lysates as positive controls.

3.2.7 Cell culture for uptake assays using HT-29 and Caco-2 cells:

Uptake assays were performed in HT-29 and Caco-2 cell lines. McCoy's complete medium (10% fetal bovine serum + 1% penicillin streptomycin solution) was used for HT-29 cells and DMEM complete medium (20% fetal bovine serum + 1% penicillin streptomycin solution) was used for Caco-2 cells. Both cell lines were grown to 70% confluency until passaging. Cells were grown in a monolayer in 24 well plates. HT-29 and Caco-2 cells were seeded at a density of 100,000 cells/well. Once seeded, HT-29 cells were allowed to grow for 7 days and form a monolayer while Caco-2 cells took 5 days to form a monolayer.

(a) Uptake assay in HT-29 cells:

Uptake assay in HT-29 cell line was performed for atorvastatin and resveratrol. Rifampicin was used at 10μM as an inducer of OATP transporters. HT-29 cells were plated in 24 well plates at a cell density of 100,000 cells/well. Rifampicin dosing commenced 2 days after cell plating. Fresh medium containing rifampicin was dosed after every 24 hours for 7 days. The uptake experiment was conducted on day 8.

Atorvastatin (1, 2 and 3µM) was dosed in 500µl of Hanks buffer per well and the assay was conducted at different time points. After the determined time point, the cell layer was washed with Hanks buffer, and the reaction was stopped by adding 500µl acetonitrile: water (80%:20%) mixture. The cell layer was scraped and collected (see appendix C 1 for the experiment design of the uptake assay). Atorvastatin was extracted from the scraped cell layer using acetonitrile containing the internal standard (pitavastatin: 250 ng/ml) and was analyzed using LC-MS/MS.

In the case of resveratrol, the quenching solution was methanol and water (80%:20%) mixture containing the internal standard (acetaminophen: 80ng/ml) (Iwuchukwu et al., 2012). All experiments were performed at 37^0C and 4^0C.

(b) Uptake assay in Caco-2 cells:

Similar to HT-29 cell plating, Caco-2 cells were plated in 24 well plates at a cell density of 100,000 cells/well. Unlike HT-29 cells, the uptake assay in Caco-2 cells was performed on the 5^{th} day after plating. Atorvastatin at 2, 4, 6 and 10µM was dosed in 250µl of Hanks buffer per well and the assay was conducted at different time points (see appendix C 1 for experiment design). Dexamethasone and sodium butyrate were also to induce OATP expression in Caco-2 cells. Uptake assays were also performed in the presence of OATP inhibitors (rifampicin and sulfasalazine). In order to minimize the interference of Pgp in the uptake assay, the uptake of atorvastatin was studied in presence of probe Pgp inhibitor, tariquidar (2µM)(Mistry et al., 2001; Fox and Bates, 2007; Kannan et al., 2011). Resveratrol and R3G uptake assays were conducted in Caco-2 cells. All assays were conducted at 37^0C and 4^0C.

3.3 Data analysis:

Inside-out vesicle assays: The concentrations of CDCF were calculated using a standard curve. These concentrations were further used to calculate rate of uptake (pmol/min/mg of total protein). The kinetic parameters of transport were calculated by plotting uptake rate against CDCF concentration (2µM-100µM) using non-linear regression in Graphpad prism for windows (ver. 6.0, Graphpad Software Inc., California). For the HT-29 and Caco-2 cell uptake assays, the concentrations of atorvastatin and resveratrol were calculated from the peak area ratios and respective standard curves.

3.4 Results:

3.4.1 CDCF transport experiments:

The standard curve for CDCF is depicted in fig. 3.3. The standard curve was prepared by serial dilutions and fluorescence was measured in fluorescence units using the plate reader.

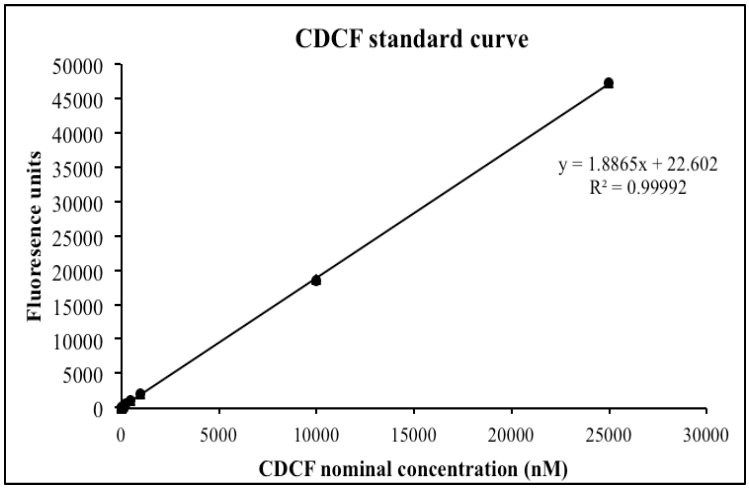

Fig. 3.3 CDCF standard curve (0-25µM). Data is expressed as mean values (n=2).

The kinetic profile of CDCF efflux transport is portrayed in figure 3.4. The concentration used ranged from 0-100μM. The Michaelis-Menten equation was fit to the data to produce a regular hyperbolic curve. The estimated values of kinetic parameters V_{max} and K_m (± S.E.) were 263.6 ± 42.75pmol/min/mg and 38.57 ± 14.86μM.

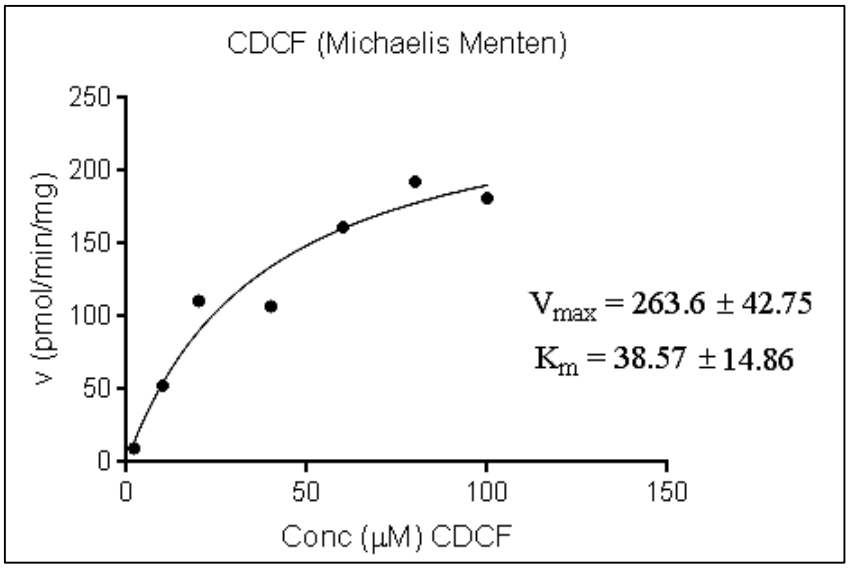

Fig. 3.4. Kinetic profile for CDCF efflux by hMRP2 inside out vesicles (n=2).

3.4.2 Western blot for HT-29 cells:

Due to the lack of OATP1B western blot data in literature, significant time was spent on developing a western blot method for OATP1B protein. Various parameters such as protein concentration, gel type (% of sodium dodecyl sulfate), dilutions of OATP1B antibody, buffers, electrophoresis run time, protein transfer times were changed. As the cells need to be lysed in order to release proteins, lysis buffers are used to disrupt cell membranes and solubilize cellular proteins. RIPA buffer is one of the most suitable buffer to extract proteins from pelleted or suspended mammalian cells. It contains denaturing agents such as sodium dodecyl sulfate and Triton X-100 or NP-40,

which makes RIPA buffer efficient in extracting cytoplasmic, nuclear and membrane proteins (RIPA buffer datasheet, Thermo Scientific and A definitive guide to western blot-Abcam). Hence, as OATP1B1/1B3 are membrane proteins, RIPA buffer was used as a lysis buffer to extract OATP1B1/1B3 proteins.

The western blots obtained for β-actin (loading control) and OATP1B1/1B3 protein is depicted in figure 3.5(A) and (B) respectively.

Fig. 3.5(A)

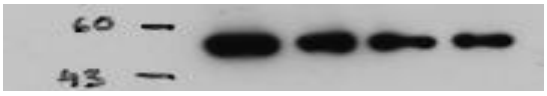

Fig. 3.5(B)

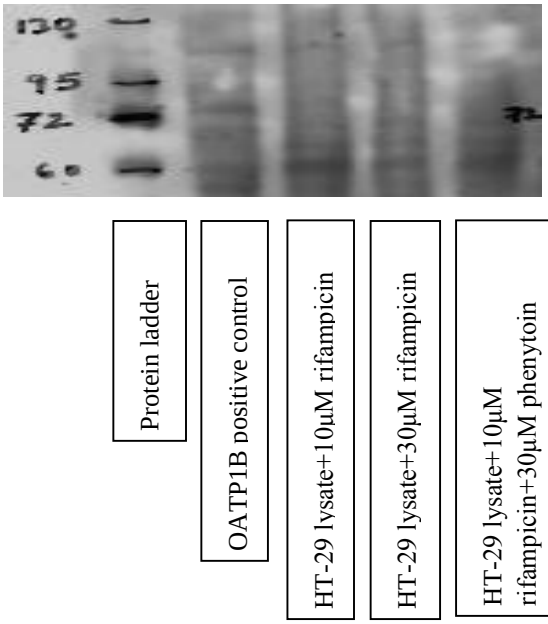

Figure 3.5. Western blots for OATP1B and β-actin. β-actin bands at were observed at 42kDa. OATP1B bands were not observed at 120kDa or 84kDa (as reported in literature). Lanes (from left) in fig. 3.5(A) and (B): Lane 1: protein ladder, Lane 2: OATP1B overexpressed cell lysate [positive control], Lane 3: HT-29 cell lysate (25µg) treated with 10µM rifampicin, Lane 4: HT-29 cell lysate (25µg) treated with 30µM rifampicin, Lane 5: HT-29 cell lysate (25µg) treated with 10µM rifampicin+60µM phenytoin.

The OATP1B protein bands usually appear around 90kDa and120kDa (Novus biologicals data sheet) (Cui et.al. 2003). The blots of control cell lysate and HT-29 cell lysates showed a high degree of uncertainty. Prominent OATP bands were not observed at 84kDa or 120kDa but were observed at 60kDa. Unglycosylated OATP1B bands have been observed previously between 60kDa to100kDa (Cui et al., 2003; Ho et al., 2006). Ambiguous bands were observed at 60kDa and between 95kDa and 130 kDa. The bands observed at 60kDa (fig 3.5B) in lanes 3, 4 and 5 could be the unglycosylated protein in the HT-29 cells.

The western blots performed for the detection of MRP2 and BCRP were not indicative of the expression of BCRP and MRP2 (fig. 3.6(A) and (B) respectively). The positive control used in this case was the inside-out vesicles for MRP2 and BCRP.

Fig. 3.6(A)

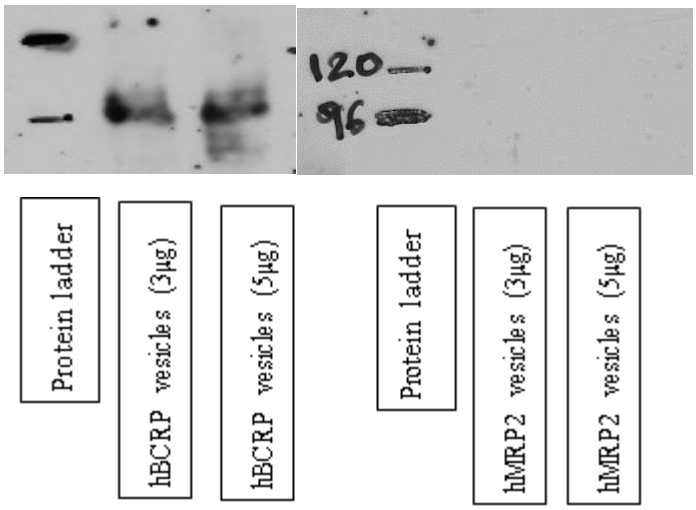

Fig. 3.6(B)

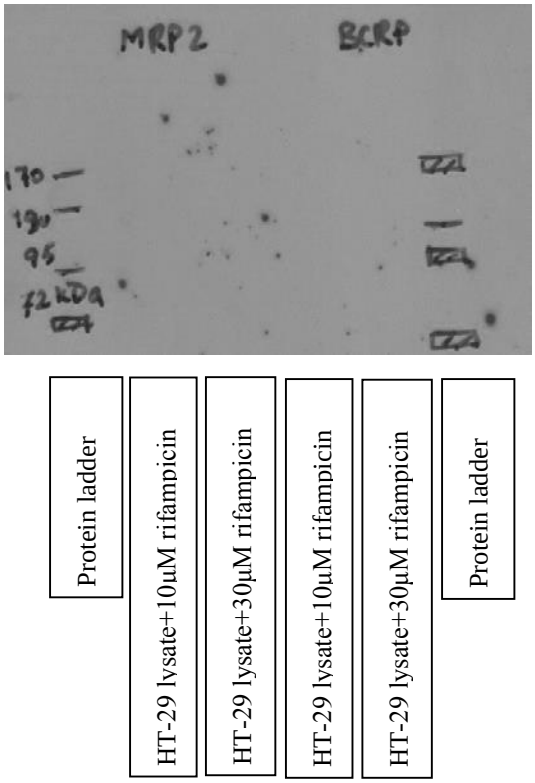

Figure 3.6 BCRP and MRP2 western blots (positive control and HT-29 cells). BCRP bands observed (positive control) near 60kDa. Lanes in fig. 3.6(A) (from left): Lane 1, 4: protein ladder, Lane 2: hBCRP vesicles (3µg), Lane 3: hBCRP vesicles (5µg), Lane 5: hMRP2 vesicles (3µg), Lane 6: hMRP2 vesicles (5µg). Figure 3.6(B) MRP2 and BCRP in HT-29 cells. Lanes 2 and 3 treated with MRP2 antibody, Lanes 4 and 5 treated with BCRP antibody. Lanes 1, 6: protein ladder, Lane 2: HT-29 cell lysate (25µg) treated with 10µM rifampicin, Lane 3: HT-29 cell lysate (25µg) treated with 30µM rifampicin, Lane 4: HT-29 cell lysate (25µg) treated with 10µM rifampicin, Lane 5: HT-29 cell lysate (25µg) treated with 30µM rifampicin.

The molecular weight of ABCG2 (BCRP) is 72kDa. ABCG2 bands reported in the literature are variable ranging from 65kDa to 95kDa (Aronica et al., 2005; Kobayashi et al., 2005; Vander Borght et al., 2006) (Santa Cruz Biotechnology Inc. datasheet, Abcam Biotechnology Inc. datasheet). Although BCRP bands in positive control were prominent, BCRP bands in HT-29 cell lysate were not observed. MRP2 bands were not observed in positive control and HT-29 cell lysate.

3.4.3 Uptake in HT-29 cells:

In order to induce OATP expression, Caco-2 cells were treated with rifampicin for 5 days. Experiments were performed using atorvastatin as the probe substrate (1-3μM). Total cell atorvastatin concentrations (ng/ml) in the absence and presence of rifampicin at 37^0C and 4^0C were calculated. Plots of total cell concentrations of atorvastatin (ng/ml) with respect to time were obtained (fig. 3.7 (A to C)).

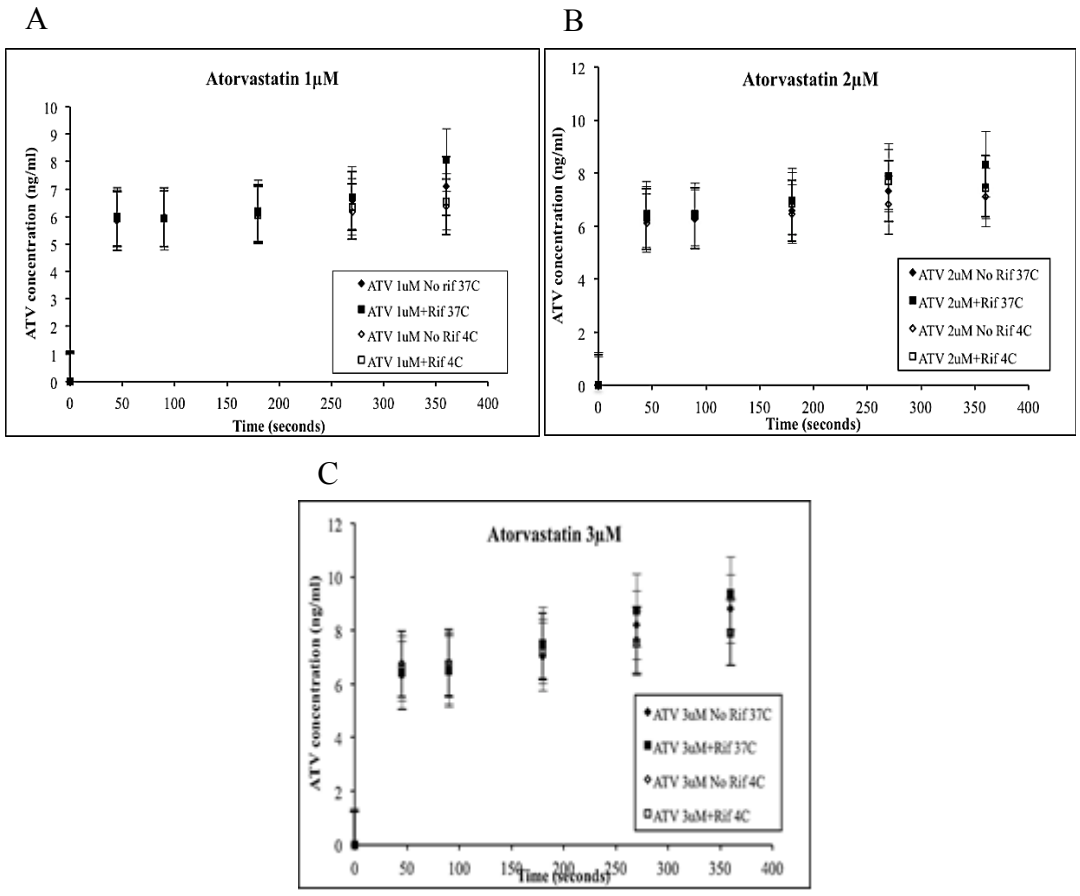

Figure 3.7. Atorvastatin uptake in rifampicin-treated and untreated HT-29 cells. The uptake experiments were performed at 3 concentrations of atorvastatin, (A) 1µM, (B) 2µM, (C) 3µM. The experiments were performed at 37^0C and 4^0C. Data represented as mean values ± standard deviation (n=4).

3.4.4 Uptake in Caco-2 cells:

Uptake experiments in Caco-2 cells were performed using atorvastatin. Figure 3.8(A) is a representative standard curve of atorvastatin used to calculate atorvastatin total cell concentrations. Pitavastatin (20ng/ml) was used an internal standard. An

intraday calibration curve (fig 3.8(B)) was constructed using scraped Caco-2 cells as the matrix.

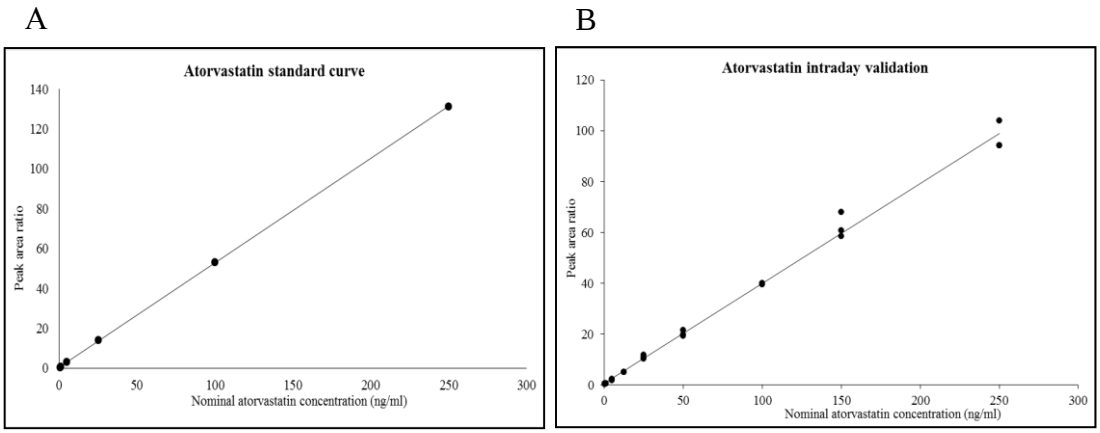

Fig. 3.8(A). A representative standard curve of atorvastatin in Caco-2 cell matrix (n=1) and (B). An intraday validation curve for atorvastatin in Caco-2 cell matrix. Data represented as triplicates (n=3).

3.4.5 Method validation for atorvastatin:

Method validation was performed in the same matrix as the samples (scraped cell layer). Average observed concentration was obtained from 3 replicates of QC samples analyzed on 3 separate occasions. Accuracy was determined by calculating percent relative error (RE %). All QC samples except 1ng/ml passed validation (table 3.4). Interday and intraday validation was performed using quality control samples analyzed on the separate (table 3.4) and same day (table 3.5). The LLOQ was about 1ng/ml.

%CV = (standard deviation/mean)*100 (Eq 3.1)

%RE = [(avg. observed conc.-theoretical conc.)/theoretical conc.]*100 (Eq 3.2)

Table 3.4 Interday method validation for atorvastatin

Nominal concentration (ng/ml)	Average observed concentration (ng/ml)	%CV	RE %
1	0.91 ± 0.39	43.6	-8.6
5	5.46 ± 0.46	8.5	9.2
25	26.22 ± 1.23	4.7	4.8
100	104.6 ± 11.8	11.3	4.6

Data expressed as mean values ± standard deviation (n=3).

Table 3.5 Intraday method validation for atorvastatin:

Nominal concentration (ng/ml)	Avg. observed concentration (ng/ml)	%CV	%RE
5	4.05 ± 0.35	8.5	-18.9
25	23.57 ± 2.6	11	-5.7
50	51.46 ± 3.1	6.1	2.9
100	100.01 ± 4.5	4.5	0.01

Data expressed as mean values ± standard deviation (n=3).

3.4.6 Atorvastatin uptake in Caco-2 cells in the presence of rifampicin and sulfasalazine:

A preliminary study of atorvastatin uptake was performed at 37^0C only with pretreatment with sodium butyrate (Kalgutkar et al., 2007a) and dexamethasone. These pretreatments were performed in order to induce transporter expression in Caco-2 cells. Increased atorvastatin concentration with respect to time was observed in Caco-2 cells. Further experiments were performed at 37^0C and 4^0C.

Uptake studies were performed in the absence of OATP inhibitors (fig. 3.9(A) and 3.9(B)) and in the presence of OATP inhibitors such as sulfasalazine (fig. 3.10(A) and 3.10(B)) and rifampicin (fig. 3.11(A) and 3.11(B)) at 37^0C and 4^0C. Concomitant addition of rifampicin (30µM) or sulfasalazine (30µM) was performed with atorvastatin. Pitavastatin (20ng/ml) was used as an internal standard. Atorvastatin uptake in presence and absence of OATP inhibitors was not significantly different which, provides an unclear picture about the presence of OATP transporters. Atorvastatin uptake at 37^0C and 4^0C was similar indicating a much greater contribution of passive diffusion as compared to active uptake. This also suggests that the expression of OATP1B1/1B3 in Caco-2 cells may be low.

A B

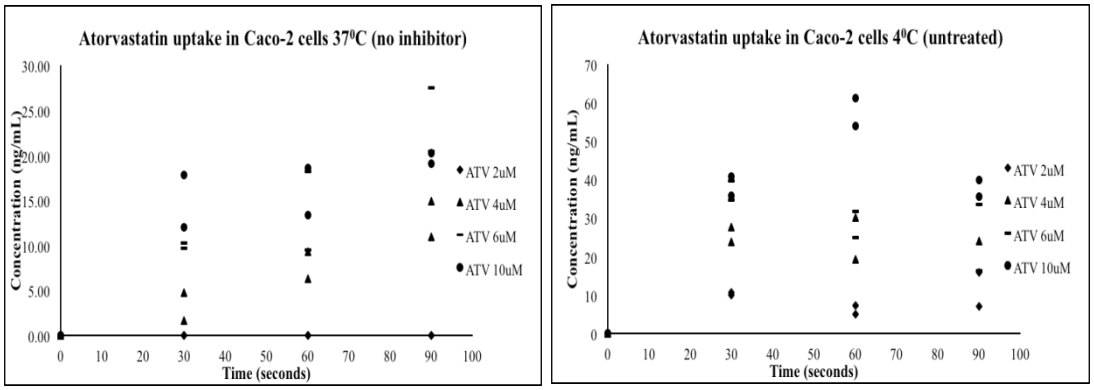

Fig. 3.9. Atorvastatin uptake in Caco-2 cells at (A) 37^0C and (B) 4^0C without inhibitor. Data represented as duplicates (n=2).

A B

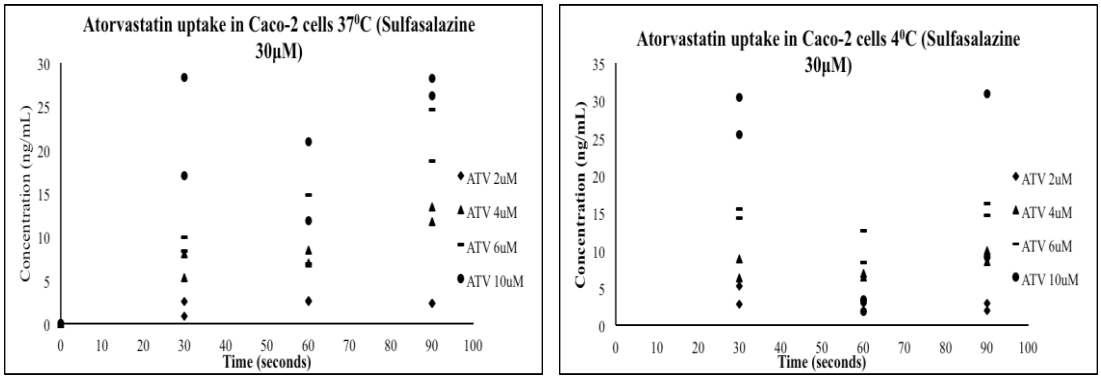

Fig. 3.10. Atorvastatin uptake in presence of sulfasalazine (30µM) at (A) 37^0C and (B) 4^0C. Data represented as duplicates (n=2).

A B

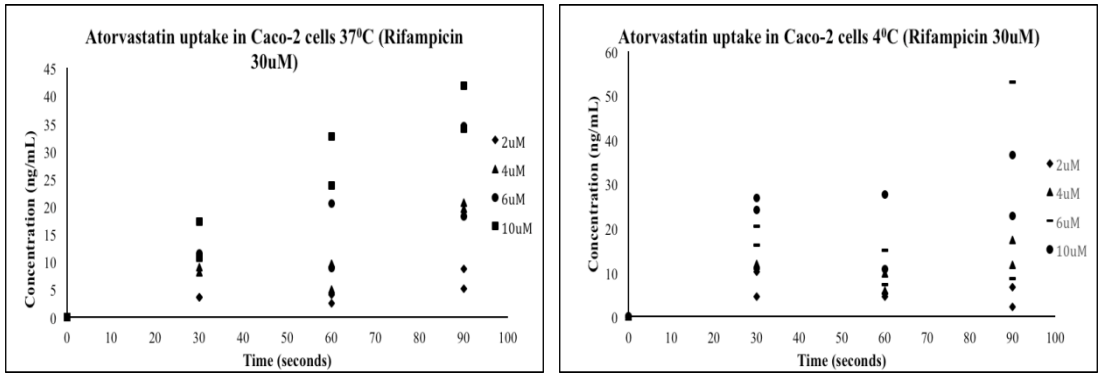

Fig. 3.11. Atorvastatin uptake in presence of rifampicin (30µM) at (A) 37^0C and (B) 4^0C. Data represented as duplicates (n=2).

3.4.7 Atorvastatin uptake in presence of Pgp inhibitor tariquidar:

To determine the involvement and interference of Pgp transporters in the uptake assay, selective Pgp inhibitor, tariquidar (Mistry et al., 2001; Fox and Bates, 2007; Kannan et al., 2011), was used. Tariquidar is reported to be a selective and potent inhibitor of Pgp. Hence; tariquidar (2µM) was added as a competitive inhibitor of Pgp. This study was performed at 37^0C (fig. 3.12(A)) and 4^0C (fig. 3.12(B)) with samples

collected at 0s, 30s, 60s, 90s. Tariquidar (2μM) was concomitantly dosed with atorvastatin (2, 4, 6, 10μM).

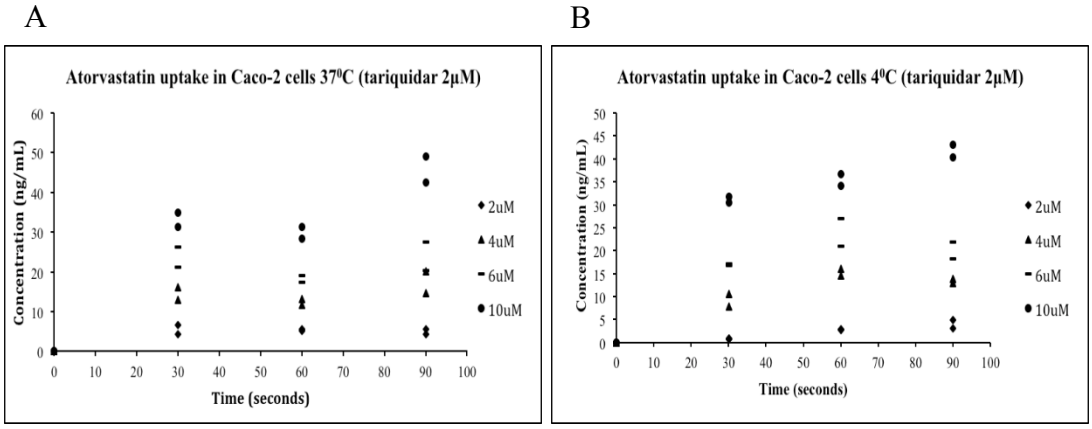

Fig. 3.12. Atorvastatin uptake in Caco-2 cells in presence of Pgp inhibitor, tariquidar (2μM) at (A) 37^0C and (B) 4^0C. Data expressed as duplicates (n=2).

This may indicate less than expected contribution of Pgp efflux in the uptake assay.

3.4.8 Resveratrol and R3G uptake assay:

Resveratrol and R3G uptake was studied using Caco-2 cell. A previously developed LC-MS/MS method was used to construct a standard curve for resveratrol (fig. 3.13) and R3S (fig. 3.14) (Sharan et al., 2012). Acetaminophen (APAP-80ng/ml) was added as an internal standard. The uptake assay samples were analyzed using the above mentioned method (see appendix C 2 for a representative chromatogram of resveratrol uptake in Caco-2 cells).

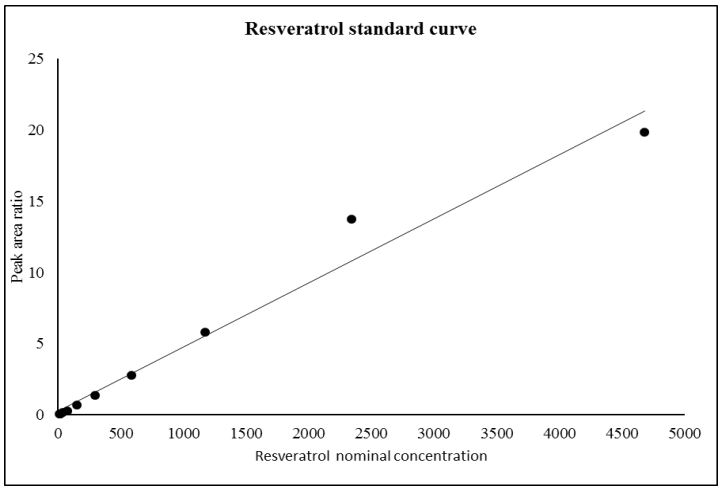

Fig. 3.13. Resveratrol standard curve (0-150µg/ml) (n=1). Standard curve prepared by serial dilution of resveratrol stock solution. Scraped Caco-2 cell layer was used as the matrix.

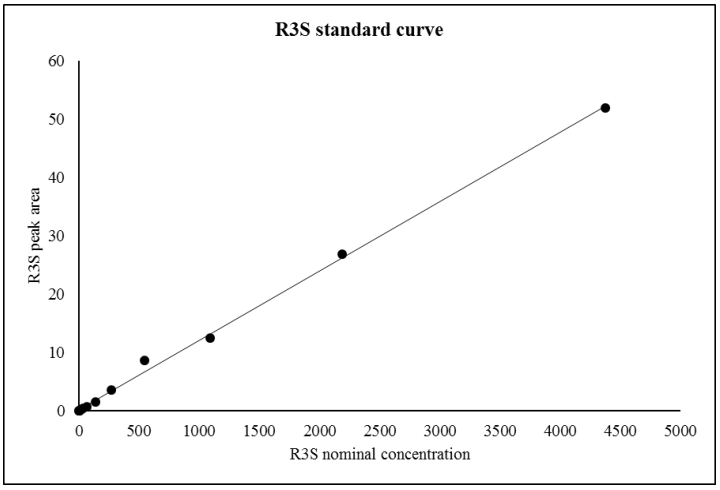

Fig. 3.14. R3S standard curve (0-4500ng/ml) (n=1). Standard curve prepared by serial dilution of resveratrol stock solution. Scraped Caco-2 cell layer was used as the matrix.

Resveratrol was dosed at 4 concentrations (5, 10, 20 and 40µM) (fig. 3.15). R3S was observed due to the metabolism of resveratrol to R3S. Due to high concentration of

internal standard (IS), the concentration of R3S was estimated by using peak area of R3S instead of a peak area ratio. R3S was observed after 5, 10, 20 and 40μM dose of resveratrol. R3S was also observed for experiments performed at 4^0C (except for 5μM) though at lower concentrations (fig. 3.16(A), 3.16(B)). The assay for R3G uptake was performed at three R3G concentrations (5, 10 and 25μM). Total cell concentration of R3G after completion of uptake assay were not detectable (see appendix C 3 for a representative chromatogram portraying the absence of R3G uptake in Caco-2 cells).

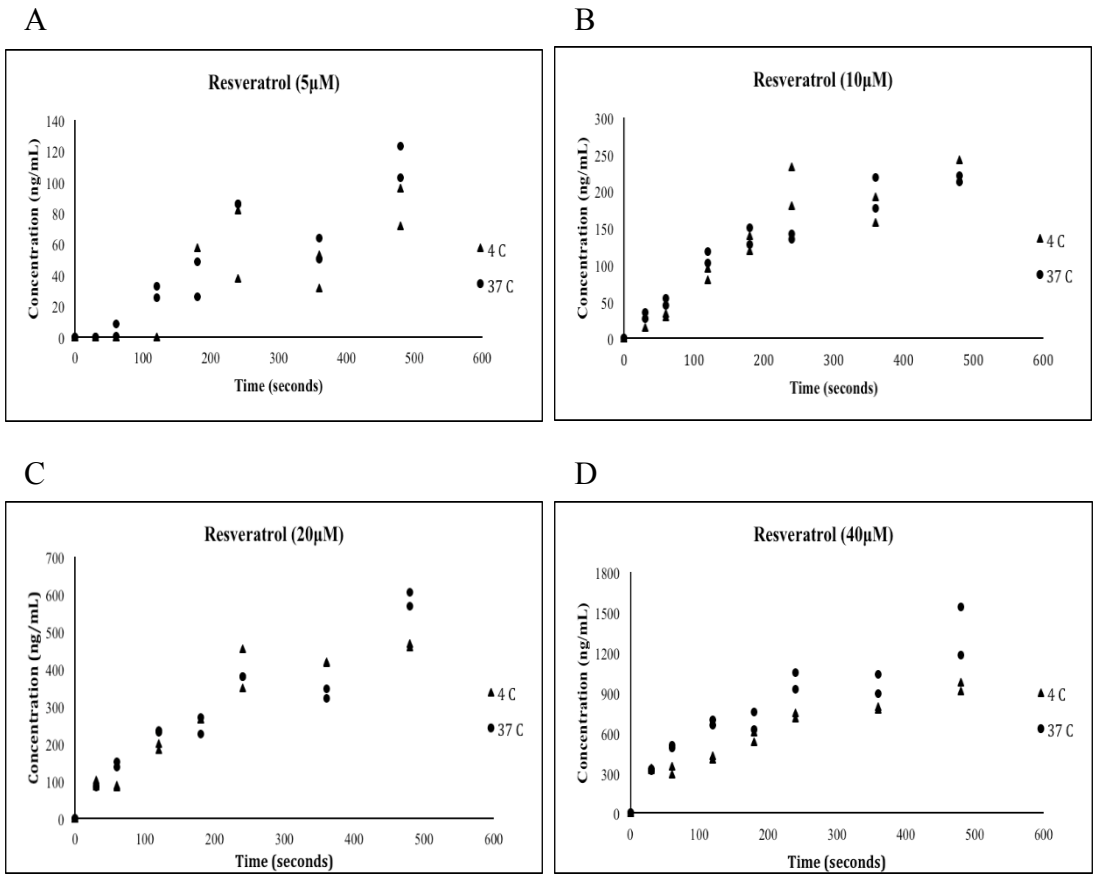

Fig 3.15 Resveratrol uptake in Caco-2 cells (A) resveratrol (5μM), (B) resveratrol (10μM), (C) resveratrol (20μM), (D) resveratrol (40μM). All experiments were performed at 37^0C and 4^0C. Data represented as duplicates.

A B

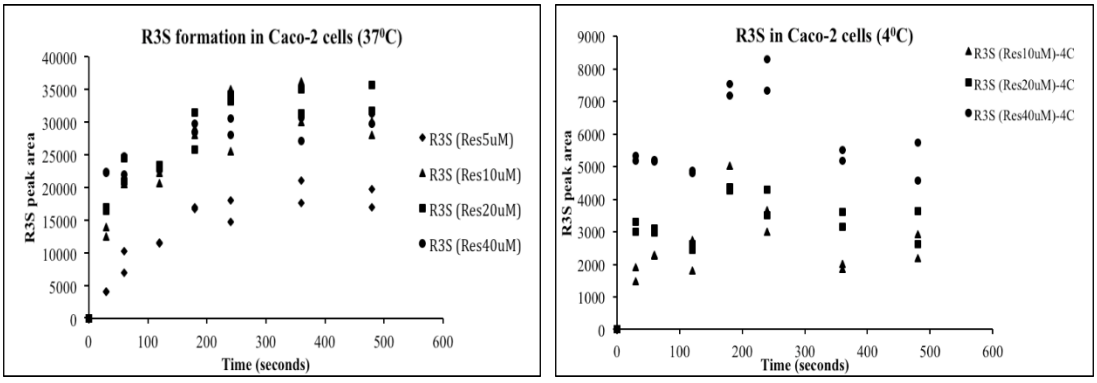

Fig. 3.16. R3S concentrations for resveratrol uptake assay performed at (A) 37^0C and (B) 4^0C. Data represented as duplicates (n=2).

3.5 Discussion:

The expression and transport of OATP transporters was studied in this chapter using human cancer cell lines in order to study the role of uptake transporters in the disposition of resveratrol and R3G.

3.5.1 Inside-out vesicle assay:

The CDCF transport experiment suggested that CDCF was a substrate of hMRP2 with a V_{max} and K_m of 263.6 ± 42.75 pmol/min/mg and 28.57 ± 14.86 µM respectively. The literature reported V_{max} and K_m values range from 64 pmol/min/mg to 245 pmol/min/mg and 13µM to 23.4µM respectively (Pratt et al., 2006; Heredi-Szabo et al., 2008a). One of the limitations of using inside-out vesicles is the inability of this assay to distinguish between passive diffusion and active transport for highly permeable compounds. The predominant mechanism of transport of resveratrol has been proposed to

be passive diffusion. Hence, the transport experiments for resveratrol using hMRP2 inside-out vesicles did not show any transport.

3.5.2 Western blot:

Western blots were performed on HT-29 cells before performing uptake assays in HT-29 cell line. The western blot analysis to detect OATP1B in HT-29 cells was inconclusive with a light but consistent band at 60kDa. OATP1B bands in the positive control have been reported at 77kDa (77.2kDa) (Novus biologicals Inc.). An OATP1B1 western blot performed on hepatocytes and OATP1B1 overexpressed HEK, MDCK cells was reported to show OATP1B1 bands between 58 and116kDa (Konig et al., 2000; Cui et al., 2003). Konig et.al. (Konig et al., 2000) also performed unglycosylation experiments, which produced a band at 58kDa. Variable bands of OATP1B1 and OATP1B3 have also been detected (Ho et al., 2006). OATP1B bands in this case occurred from 75kDa to 100kDa (Ho et al., 2006). Hence, the band observed at 60kDa in this western blot may be the unglycosylated OATP1B protein.

3.5.3 Uptake assay in HT-29 and Caco-2 cells:

The uptake experiments with HT-29 and Caco-2 cell lines using atorvastatin as a probe substrate for OATP1B (Lau et al., 2007) did not provide adequate insight into the transport mechanisms involved in the flux of resveratrol. Our preliminary experiments in Caco-2 cells were performed using atorvastatin as a probe substrate for OATP (Lau et al., 2007) and pretreatments with sodium butyrate (Kalgutkar et al., 2007a) and dexamethasone. These treatments were performed with an intention to induce the

expression of OATP transporters. The next set of experiments included OATP uptake experiments with OATP and Pgp inhibitors. All the experiments were performed at 37^0C and 4^0C. The active processes are inactive at 4^0C and only passive diffusion is prevalent, hence the experiments performed at 4^0C served as a control. Our uptake experiments involving resveratrol showed uptake of resveratrol via passive diffusion (Kaldas et al., 2003). These experiments did show the metabolism of resveratrol to R3S as has been previously reported (Kaldas et al., 2003). The contribution of uptake transporters seemed to be negligible. This corroborates with literature reports, which propose passive diffusion as the predominant mechanism of resveratrol transport (Kaldas et al., 2003; Maier-Salamon et al., 2006). The uptake experiments showed passive diffusion and the difference between total cell concentrations at 37^0C and 4^0C was indistinguishable. This may be attributed to the low levels/lack of uptake proteins in Caco-2 cells. In the uptake experiment performed for R3G, the total cell concentration of R3G was below the limit of quantitation. Hence, passive diffusion or active transport was not observed for R3G in Caco-2 cells.

There are a few possibilities due to which delineation of active transport from total transport would be challenging when using human cancer cell lines. 1. One of the possibilities is that the contribution of uptake by saturable processes is only a small fraction of the total flux for resveratrol. 2. Human cancer cell lines selected here may not be an ideal system to study uptake as Caco-2 and HT-29 cells express transporters other than OATPs as well. These may interfere with the uptake assay. 3. In addition to that there may be a significant difference in the expression level of transporters in cancer cell

lines depending on the passage number and cell culture conditions (Behrens and Kissel, 2003; Sambuy et al., 2005).

3.6 Conclusions:

The study of transport of chemical entities as well as metabolites is becoming a vital step in preclinical development and the contribution of all major transporters should be taken into account. In case of polar metabolites, passive diffusion may be unlikely and the role of uptake transporters assumes importance. The role of uptake transporters may be important for chemical entities such as resveratrol that are metabolized extensively into polar conjugated metabolites. In this chapter, an effort was made to study the uptake kinetics using human cancer cell lines. Human cancer cell lines have been reported to express mRNA for OATP1B1, 1B3 (Seithel et al., 2006; Muto et al., 2007; Ichihara et al., 2010; Imai et al., 2013), OATP2B1 (Englund et al., 2006; Maubon et al., 2007; Hayeshi et al., 2008; Annaert et al., 2010) but the active protein expression has not been studied. So, western blots were used to assess the expression of OATPs. The western blots performed to detect OATP1B1/1B3 proved to be inconclusive. The uptake assays using Caco-2 cells confirmed passive diffusion of resveratrol but the active uptake of resveratrol and R3G could not be delineated.

3.7 Future directions:

A finer way to delineate the uptake processes is the use of a transwell type assay. Such an assay has been previously used for resveratrol (Maier-Salamon et al., 2006). The transporter overexpressed MDCK cells would be useful tool to study the transport of

resveratrol and its major metabolites. This will provide an excellent way to study the transport of glucuronide and sulfate metabolites in presence of a single transporter. Thus, this assay could be used to study uptake of polar metabolites like R3G and R3S by OATP1B1/1B3, 2A1 and 2B1.

ACKNOWLEDGMENTS

I would like to acknowledge the work of Ms. Min Ye and Ms. Priyanka Kulkarni in developing HPLC-MS/MS method for atorvastatin. This assay was used extensively for evaluating atorvastatin uptake in cell lines.

REFERENCES

Alfaras I, Perez M, Juan ME, Merino G, Prieto JG, Planas JM, and Alvarez AI (2010) Involvement of breast cancer resistance protein (BCRP1/ABCG2) in the bioavailability and tissue distribution of trans-resveratrol in knockout mice. J Agric Food Chem 58:4523-4528.

Annaert P, Ye ZW, Stieger B, and Augustijns P (2010) Interaction of HIV protease inhibitors with OATP1B1, 1B3, and 2B1. Xenobiotica 40:163-176.

Aronica E, Gorter JA, Redeker S, van Vliet EA, Ramkema M, Scheffer GL, Scheper RJ, van der Valk P, Leenstra S, Baayen JC, Spliet WG, and Troost D (2005) Localization of breast cancer resistance protein (BCRP) in microvessel endothelium of human control and epileptic brain. Epilepsia 46:849-857.

Behrens I and Kissel T (2003) Do cell culture conditions influence the carrier-mediated transport of peptides in Caco-2 cell monolayers? Eur J Pharm Sci 19:433-442.

Colombo F, Poirier H, Rioux N, Montecillo MA, Duan J, and Ribadeneira MD (2013) A membrane vesicle-based assay to enable prediction of human biliary excretion. Xenobiotica 43:915-919.

Cui Y, Konig J, Nies AT, Pfannschmidt M, Hergt M, Franke WW, Alt W, Moll R, and Keppler D (2003) Detection of the human organic anion transporters SLC21A6 (OATP2) and SLC21A8 (OATP8) in liver and hepatocellular carcinoma. Lab Invest 83:527-538.

Englund G, Rorsman F, Ronnblom A, Karlbom U, Lazorova L, Grasjo J, Kindmark A, and Artursson P (2006) Regional levels of drug transporters along the human intestinal tract: co-expression of ABC and SLC transporters and comparison with Caco-2 cells. Eur J Pharm Sci 29:269-277.

Fox E and Bates SE (2007) Tariquidar (XR9576): a P-glycoprotein drug efflux pump inhibitor. Expert Rev Anticancer Ther 7:447-459.

Hagenbuch B and Meier PJ (2003) The superfamily of organic anion transporting polypeptides. Biochimica Et Biophysica Acta-Biomembranes 1609:1-18.

Hagenbuch B and Meier PJ (2004) Organic anion transporting polypeptides of the OATP/SLC21 family: phylogenetic classification as OATP/SLCO superfamily, new nomenclature and molecular/functional properties. Pflugers Archiv-European Journal of Physiology 447:653-665.

Hayeshi R, Hilgendorf C, Artursson P, Augustijns P, Brodin B, Dehertogh P, Fisher K, Fossati L, Hovenkamp E, Korjamo T, Masungi C, Maubon N, Mols R, Mullertz A, Monkkonen J, O'Driscoll C, Oppers-Tiemissen HM, Ragnarsson EG, Rooseboom M, and Ungell AL (2008) Comparison of drug transporter gene expression and functionality in Caco-2 cells from 10 different laboratories. Eur J Pharm Sci 35:383-396.

Hegedus C, Szakacs G, Homolya L, Orban TI, Telbisz A, Jani M, and Sarkadi B (2009) Ins and outs of the ABCG2 multidrug transporter: an update on in vitro functional assays. Adv Drug Deliv Rev 61:47-56.

Heredi-Szabo K, Kis E, and Krajcsi P (2012) The vesicular transport assay: validated in vitro methods to study drug-mediated inhibition of canalicular efflux transporters ABCB11/BSEP and ABCC2/MRP2. Curr Protoc Toxicol Chapter 23:Unit 23 24.

Heredi-Szabo K, Kis E, Molnar E, Gyorfi A, and Krajcsi P (2008a) Characterization of 5 (6)-Carboxy-2,'7'-Dichlorofluorescein Transport by MRP2 and Utilization of this Substrate as a Fluorescent Surrogate for LTC4. Journal of biomolecular screening.

Heredi-Szabo K, Kis E, Molnar E, Gyorfi A, and Krajcsi P (2008b) Characterization of 5(6)-carboxy-2,'7'-dichlorofluorescein transport by MRP2 and utilization of this substrate as a fluorescent surrogate for LTC4. J Biomol Screen 13:295-301.

Hillgren KM, Keppler D, Zur AA, Giacomini KM, Stieger B, Cass CE, Zhang L, and International Transporter C (2013) Emerging transporters of clinical importance: an update from the International Transporter Consortium. Clin Pharmacol Ther 94:52-63.

Ho RH, Tirona RG, Leake BF, Glaeser H, Lee W, Lemke CJ, Wang Y, and Kim RB (2006) Drug and bile acid transporters in rosuvastatin hepatic uptake: function, expression, and pharmacogenetics. Gastroenterology 130:1793-1806.

Ichihara S, Kikuchi R, Kusuhara H, Imai S, Maeda K, and Sugiyama Y (2010) DNA methylation profiles of organic anion transporting polypeptide 1B3 in cancer cell lines. Pharm Res 27:510-516.

Imai S, Kikuchi R, Tsuruya Y, Naoi S, Nishida S, Kusuhara H, and Sugiyama Y (2013) Epigenetic regulation of organic anion transporting polypeptide 1B3 in cancer cell lines. Pharm Res 30:2880-2890.

Iwuchukwu OF, Sharan S, Canney DJ, and Nagar S (2012) Analytical method development for synthesized conjugated metabolites of trans-resveratrol, and application to pharmacokinetic studies. J Pharm Biomed Anal 63:1-8.

Juan ME, Gonzalez-Pons E, and Planas JM (2010) Multidrug resistance proteins restrain the intestinal absorption of trans-resveratrol in rats. J Nutr 140:489-495.

Kaldas MI, Walle UK, and Walle T (2003) Resveratrol transport and metabolism by human intestinal Caco-2 cells. J Pharm Pharmacol 55:307-312.

Kalgutkar AS, Feng B, Nguyen HT, Frederick KS, Campbell SD, Hatch HL, Bi YA, Kazolias DC, Davidson RE, Mireles RJ, Duignan DB, Choo EF, and Zhao SX (2007) Role of transporters in the disposition of the selective phosphodiesterase-4 inhibitor (+)- 2-[4-({[2-(benzo[1,3]dioxol-5-yloxy)-pyridine-3-carbonyl]-amino}-methyl)-3-fl uoro- phenoxy]-propionic acid in rat and human. Drug Metab Dispos 35:2111-2118.

Kalliokoski A and Niemi M (2009) Impact of OATP transporters on pharmacokinetics. British Journal of Pharmacology 158:693-705.

Kannan P, Telu S, Shukla S, Ambudkar SV, Pike VW, Halldin C, Gottesman MM, Innis RB, and Hall MD (2011) The "specific" P-glycoprotein inhibitor Tariquidar is also a substrate and an inhibitor for breast cancer resistance protein (BCRP/ABCG2). ACS Chem Neurosci 2:82-89.

Kobayashi D, Ieiri I, Hirota T, Takane H, Maegawa S, Kigawa J, Suzuki H, Nanba E, Oshimura M, Terakawa N, Otsubo K, Mine K, and Sugiyama Y (2005) Functional assessment of ABCG2 (BCRP) gene polymorphisms to protein expression in human placenta. Drug Metab Dispos 33:94-101.

Konig J, Cui Y, Nies AT, and Keppler D (2000) A novel human organic anion transporting polypeptide localized to the basolateral hepatocyte membrane. Am J Physiol Gastrointest Liver Physiol 278:G156-164.

Konig J, Muller F, and Fromm MF (2013) Transporters and drug-drug interactions: important determinants of drug disposition and effects. Pharmacol Rev 65:944-966.

Lau YY, Huang Y, Frassetto L, and Benet LZ (2007) effect of OATP1B transporter inhibition on the pharmacokinetics of atorvastatin in healthy volunteers. Clin Pharmacol Ther 81:194-204.

Lee W, Belkhiri A, Lockhart AC, Merchant N, Glaeser H, Harris EI, Washington MK, Brunt EM, Zaika A, Kim RB, and El-Rifai W (2008) Overexpression of OATP1B3 Confers Apoptotic Resistance in Colon Cancer. Cancer Res 68:10315-10323.

Li L, Lee TK, Meier PJ, and Ballatori N (1998) Identification of glutathione as a driving force and leukotriene C4 as a substrate for oatp1, the hepatic sinusoidal organic solute transporter. Journal of Biological Chemistry 273:16184-16191.

Maier-Salamon A, Hagenauer B, Reznicek G, Szekeres T, Thalhammer T, and Jager W (2008) Metabolism and disposition of resveratrol in the isolated perfused rat liver: Role of Mrp2 in the biliary excretion of glucuronides. Journal of Pharmaceutical Sciences 97:1615-1628.

Maier-Salamon A, Hagenauer B, Wirth M, Gabor F, Szekeres T, and Jager W (2006) Increased transport of resveratrol across monolayers of the human intestinal Caco-2 cells is mediated by inhibition and saturation of metabolites. Pharm Res 23:2107-2115.

Maubon N, Le Vee M, Fossati L, Audry M, Le Ferrec E, Bolze S, and Fardel O (2007) Analysis of drug transporter expression in human intestinal Caco-2 cells by real-time PCR. Fundam Clin Pharmacol 21:659-663.

Mistry P, Stewart AJ, Dangerfield W, Okiji S, Liddle C, Bootle D, Plumb JA, Templeton D, and Charlton P (2001) In vitro and in vivo reversal of P-glycoprotein-mediated multidrug resistance by a novel potent modulator, XR9576. Cancer Res 61:749-758.

Muto M, Onogawa T, Suzuki T, Ishida T, Rikiyama T, Katayose Y, Ohuchi N, Sasano H, Abe T, and Unno M (2007) Human liver-specific organic anion transporter-2 is a potent prognostic factor for human breast carcinoma. Cancer Sci 98:1570-1576.

Niemi M, Pasanen MK, and Neuvonen PJ (2011) Organic anion transporting polypeptide 1B1: a genetically polymorphic transporter of major importance for hepatic drug uptake. Pharmacol Rev 63:157-181.

Patel KR, Andreadi C, Britton RG, Horner-Glister E, Karmokar A, Sale S, Brown VA, Brenner DE, Singh R, Steward WP, Gescher AJ, and Brown K (2013) Sulfate metabolites provide an intracellular pool for resveratrol generation and induce autophagy with senescence. Sci Transl Med 5:205ra133.

Planas JM, Alfaras I, Colom H, and Juan ME (2012) The bioavailability and distribution of trans-resveratrol are constrained by ABC transporters. Arch Biochem Biophys 527:67- 73.

Pratt S, Chen V, Perry III WI, Starling JJ, and Dantzig AH (2006) Kinetic validation of the use of carboxydichlorofluorescein as a drug surrogate for MRP5-mediated transport. European journal of pharmaceutical sciences 27:524-532.

Roth M, Obaidat A, and Hagenbuch B (2012) OATPs, OATs and OCTs: the organic anion and cation transporters of the SLCO and SLC22A gene superfamilies. Br J Pharmacol 165:1260-1287.

Sambuy Y, De Angelis I, Ranaldi G, Scarino ML, Stammati A, and Zucco F (2005) The Caco-2 cell line as a model of the intestinal barrier: influence of cell and culture-related factors on Caco-2 cell functional characteristics. Cell Biol Toxicol 21:1-26.

Seithel A, Karlsson J, Hilgendorf C, Bjorquist A, and Ungell AL (2006) Variability in mRNA expression of ABC- and SLC-transporters in human intestinal cells: comparison between human segments and Caco-2 cells. Eur J Pharm Sci 28:291-299.

Sharan S, Iwuchukwu OF, Canney DJ, Zimmerman CL, and Nagar S (2012) In vivo-formed versus preformed metabolite kinetics of trans-resveratrol-3-sulfate and trans- resveratrol-3-glucuronide. Drug Metab Dispos 40:1993-2001.
Suzuki M, Suzuki H, Sugimoto Y and Sugiyama Y (2003) ABCG2 transports sulfated conjugates of steroids and xenobiotics. J Biol Chem 278:22644-9.

van de Wetering K, Burkon A, Feddema W, Bot A, de Jonge H, Somoza V, and Borst P (2009) Intestinal breast cancer resistance protein (BCRP)/Bcrp1 and multidrug resistance protein 3 (MRP3)/Mrp3 are involved in the pharmacokinetics of resveratrol. Mol Pharmacol 75:876-885.

van Staden CJ, Morgan RE, Ramachandran B, Chen Y, Lee PH, and Hamadeh HK (2012) Membrane vesicle ABC transporter assays for drug safety assessment. Curr Protoc Toxicol Chapter 23:Unit 23 25.

Vander Borght S, Libbrecht L, Katoonizadeh A, van Pelt J, Cassiman D, Nevens F, Van Lommel A, Petersen BE, Fevery J, and Jansen PL (2006) Breast cancer resistance protein (BCRP/ABCG2) is expressed by progenitor cells/reactive ductules and hepatocytes and its expression pattern is influenced by disease etiology and species type: possible functional consequences. Journal of Histochemistry & Cytochemistry 54:1051-1059.

CHAPTER 4

EVALUATION OF THE DISPOSITION OF RESVERATROL AND ITS METABOLITES IN THE PRESENCE OF BCRP AND/OR MRP2 INHIBITORS

4.1. Background:

ABC (ATP binding cassette) transporters are a family of transmembrane proteins, which consume energy in the form of ATP. The binding and hydrolysis of ATP at nucleotide binding domain (NBD) generates the energy required to transport substrates (Albermann et.al. 2005). ABC transporters are expressed in major eliminating organs and reduce the bioavailability by limiting the absorption and facilitating excretion (Albermann et.al. 2005). ABC transporters efflux a wide variety of compounds including xenobiotics and endogenous compounds such as bile acids and steroids (Klein et.al. 1999, Leslie et.al. 2005). ABC transporters are classified into seven subfamilies (A-G). The roles of some ABC transporters like MRP (ABCC), P-gp (ABCB1) and BCRP (ABCG2) are well defined (Schinkel and Jonker, 2003). Figure 3.1 (chapter 3, section 3.1) shows the expression of prominent ABC transports in polarized cells (Hilgren et.al. 2013).

The human subfamily of ABCC (MRP family of proteins) consists of twelve members. These proteins are involved in the efflux of xenobiotics and several endogenous compounds. The amino acid sequence for the human MRPs ranges from 1325-1545 amino acids (Protein database: www.ncbi.mm.nih.gov (website visited on 04/2014), (Nies et al., 2006; Takano et al., 2006). MRPs are predominantly located on the apical membrane of polarized epithelial cells (MRP4 being an exception) in kidneys

(MRP2/ABCC2), intestine (MRP2) and hepatocyte (MRP2 on apical membrane and MRP3/ABCC3, MRP4/ABCC4, MRP1/ABCC1, MRP/ABCC5 on basolateral membrane).

A few orthologs have been identified for MRPs. MRP orthologs in mouse (8 orthologs) have been identified, prominent among them being MRP1 and MRP5 (König et al., 1999). Phylogenetic analyses show a high degree of homology between the human and rodent MRPs. Full length sequences for MRPs have been elucidated in humans, rodents, dogs, rhesus monkey, chicken and zebrafish (Nies et al., 2006).

4.1.1 ABC transporters: Structure and mechanism:

ABC transporters commonly have 2 nucleotide binding domains (NBDs) and 2 membrane spanning domains (MSDs). Each MSD consists of six transmembrane alpha helices (Higgins and Linton, 2004, Davidson and Maloney, 2007). Some transporters such as ABCG2 (BCRP) are monomers, which couple to form a functional dimer. Transporters of ABCC (MRP) subfamily may have two or three MSDs. The binding and hydrolysis of ATP at NBDs causes a conformational change in MSDs, facilitating the transport of substrates (Higgins and Linton, 2004, Daidson and Maloney 2007, Linton and Higgins 2007). As compared with MSDs, which are located across the lipid bilayer, NBDs are located in cytoplasm. NBDs also contain Walker A, Walker B and ABC signature motifs (Walker et.al. 1982, Higgins and Linton, 2004).

An ATP switch model has been developed through extensive studies to describe the mechanism of transport by P-glycoprotein (Higgins and Linton, 2004). The ATP switch model is primarily based on the coordination of MSDs and NBDs resulting in two

major conformations, 1. Closed dimer and 2. Open dimer. The transporter protein switches between these configurations to transport a substrate across a lipid bilayer. The first step of the process is the binding of the substrate to the high affinity binding site on the transporter (Higgins and Linton, 2004). This high affinity site of the transporter facilitates the binding of ATP at the NBDs (Higgins and Linton, 2004).

Next, the ATP binding facilitates the formation of the closed dimer configuration of the transporter. The high affinity binding site is converted to a low affinity binding site which faces the extracellular side in case of an efflux transporter (Higgins and Linton, 2004). The binding affinity of transporter towards the substrate decreases, which leads to the substrate leaving the transport site. Step 3 involves the hydrolysis of ATP to ADP+ Pi. This transition state has low affinity towards the substrate. Step 4 involves the release of Pi and ADP respectively. It has been speculated that the transporter resets and shows high affinity towards the substrate even when ADP is bound to the NBD. The ADP is released only when a new substrate molecule binds to the transporter (Higgins and Linton, 2004).

4.1.2 ABCC transporters:

The C-subfamily of ABC transporters (also known as MRPs) contain nine members. Out of the nine members, four members (ABCC4, -5,-11,-12) have four domains-2 membrane spanning domains and 2 nucleotide binding domains. ABCC1,-2,-6,-10 contain an additional membrane spanning domain (Chen and Tiwari, 2011). MRP2 (ABCC2) is a 1545 amino acid protein that separates as a 190kDa band upon protein electrophoresis (Cole et al., 1992).

4.1.3 MRP2/ABCC2 function and localization:

MRP2 plays an important role in ADME of drugs. MRP2 is localized on the apical membrane of polarized cells in liver, intestine and kidneys (Chen and Tiwari 2011). MRP2 is localized in renal proximal tubules, hepatocytes, gall bladder, placenta, bronchi and colorectal cancer cell lines (Chen and Tiwari 2011, Narasaki et.al., 1997). It is responsible for biliary excretion and limits the absorption of orally administered drugs. The primary role of this efflux transporter is decreasing the exposure of toxins or xenobiotics (Leslie et al., 2005). MRP2 has broad substrate specificity. MRP2 substrates comprise of leukotriene C_4, bilirubin glucuronides and sulfates, bromosulfothalein, polycyclic aromatic hydrocarbons, methotrexate, estradiol glucuronide and estrone sulfate. Inhibitors of MRP2 include cyclosporine, MK571, benzbromarone, probenecid (Bodo et al., 2003; Nies and Keppler, 2007; Vlaming et al., 2008; Heredi-Szabo et al., 2009; Karlsson et al., 2010).

4.1.4 ABCG transporters:

Breast cancer resistance protein (BCRP/ABCG2) was identified first in MCF-7 cell line, which displayed drug resistance. The ABCG subfamily consists of six half transporters. Each polypeptide consists of one transmembrane domain (6 helices) and one ATP binding domain. BCRP consists of 655 amino acids and exhibits a 72kDa band on a western blot (Mao, 2005). There have been mixed reports of BCRP functioning as a homodimer or a heterodimer (Kage et al., 2002; Doyle and Ross, 2003; Nakanishi et al., 2003; Robey et al., 2006). The number of binding sites of BCRP has yet to be determined. Giri et.al. (2009) showed that in murine bcrp the binding sites of prazocin or

imatinib were different from those of zidovudine or abacavir, which may further explain multiple binding sites for substrates and inhibitors (Giri et al., 2009).

4.1.5 BCRP/ABCG2 function and localization:

BCRP was identified in cancer cell lines and hence cancer chemotherapeutic compounds were among the first identified substrates of BCRP. It transports a wide range of compounds such as anthracyclines, etoposide, mitoxanthrone, methotrexate, topotecan, gefitinib, flavopiridol, rifampicin, sulfasalazine, and SN-38 (Kawabata et al., 2001; Allen et al., 2003; Volk and Schneider, 2003; Mao, 2005; Li et al., 2008; Zamek-Gliszczynski et al., 2008; Mennone et al., 2010). BCRP has been known to transport drug conjugates such as estrone sulfates, 17-β-estradiol conjugates, benzopyrene sulfates and glucuronides, 4-methylumbelliferone sulfates and glucuronides (Suzuki M et.al., 2003). The known inhibitors of BCRP include FTC, Ko143, eracridar, reserpine etc. (Rabindran et al., 2000; Allen et al., 2002; Doyle and Ross, 2003). Among the naturally occurring compounds, compounds such as chrysin, hesperitin, silymarin, resveratrol etc. have been proposed to be inhibitors of BCRP (Zhang et al., 2005).

BCRP is a membrane transporter located on the apical side of polarized epithelial cells. Using immunohistochemistry, BCRP appeared to be highly expressed in colon, small intestine, biliary canaliculi, placenta, breast tissue, venous endothelium and blood capillaries. Further, correlation of results using RT-PCR showed BCRP expression in these tissues (Maliepaard et al., 1999). BCRP is also expressed in apical membrane of enterocytes, hepatocytes and blood brain barrier (Giacomini et al., 2010).

The biological effects of resveratrol are better known than its disposition.

Resveratrol (3, 4', 5-trihydroxy stilbene) is a phytochemical which is being extensively studied for its role as a cancer chemopreventive (Jang et al., 1997), anti-oxidant (Leonard et al., 2003) and cardio protective (Kopp, 1998) compound. Unfortunately, the transport of resveratrol and its metabolites is not well established. Upon oral dosing, trans-resveratrol is highly absorbed (>70%) but shows very low bioavailability (Walle et al., 2004). This low exposure is due to its extensive metabolism mainly by conjugation, yielding metabolites, which may not be active. MRP2 and BCRP are abundantly expressed in intestine and liver, which are the main sites for resveratrol metabolism and excretion.

Resveratrol is primarily metabolized to glucuronide and sulfate conjugates, which may also be substrates of MRP2 and BCRP. Recent research suggests the transport of resveratrol conjugates by BCRP and MRP2, hence these transporters may be the missing link to fully explain the disposition of resveratrol and its metabolites (Maier-Salamon et al., 2008; Alfaras et al., 2010; Maier-Salamon et al., 2013). Any change in expression and activity of these transporters may lead to corresponding changes in resveratrol exposure. Also, the contribution of each transporter towards the disposition of resveratrol and its metabolites needs to be further investigated.

4.2 Experimental section:

4.2.1 Materials:

Resveratrol, resveratrol-3-glucuronide (R3G) and resveratrol-3-sulfate (R3S) were purchased from Toronto Research Chemicals Inc. (Toronto, Canada).

Hydroxylpropyl-β-cyclodextrin and 4-acetamidophenol (APAP) was purchased from Sigma-Aldrich (St. Louis, MO). Ko143 was purchased from Cayman Chemicals (Michigan, USA). MK571 was purchased from Santa Cruz Biotechnology (Dallas, TX, USA). Corn oil was purchased from Fisher Science Education (Nazareth, PA). Sterile saline solution (0.9%) was purchased from Teknova (Hollister, CA). Ammonium acetate was purchased from Fisher Scientific (Fair Lawn, NJ). Methanol was purchased from two vendors: Honeywell B & J (Muskegon, MI), EMD Chemicals (Gibbstown, NJ). Mouse (Balb/C) plasma was purchased from GeneTex. Inc (Irvine, CA, USA). Male C57BL/6 mice weighing between 20-25gm were obtained from Charles River Laboratories (Wilmington, MA) and maintained in American Association for the Accreditation of Laboratory Animal Care-accredited University Laboratory Animal Resources of Temple University.

4.2.2 Experimental design:

Male C57BL/6 mice were used for these experiments. The animals were divided into 2 groups of 3 animals each (Group 1-No inhibitor, Group 2-either bcrp inhibitor Ko143 or mrp2 inhibitor MK571, each intraperitoneally (i.p.) administered). Animals were fed normal diet and a standard 12hour dark/light cycle was maintained. The animals were fasted 10hour prior to administration of resveratrol to rule out variability of gall bladder emptying due to food. Resveratrol was solubilized in 20% 2-hydroxypropyl-β-cyclodextrin in sterile saline (Juan et al., 2010). Blood was collected by cardiac puncture at 5, 10, 15, 30, 60, 90, 120 and 180 minutes. The blood samples thus collected were centrifuged and the plasma fraction was collected and analyzed using LC-MS/MS.

4.2.3 Blood collection:

The blood collection was performed by cardiac puncture. The procedure was performed under anesthesia. The ventral chest area of injection was disinfected with 70% ethanol. A needle was inserted at the base of the sternum, injected upwards into the thoracic cavity at a $250\text{-}300^0$ angle and slightly leftwards. The blood was withdrawn slowly until the required volume was collected (Morton DB et.al., 1993; Diehl et al., 2001).

4.2.4 In vivo administration of mrp2 inhibitor:

The mrp2 inhibitor [(3-(((3-(2-(7-chloro-2-quinolinyl)-(E)-ethenyl) phenyl) ((3-(dimethylamino-3-oxopropyl) thio) methyl)-thio) propanoic acid] (MK571) was administered as a intraperitoneal injection (10mg/kg). MK571 was dissolved in sterile saline and was administered i.p. 30 minutes before administration of 60mg/kg resveratrol.

4.2.5 In vivo administration of bcrp inhibitor:

The bcrp inhibitor [(3S, 6S, 12aS)-1,2,3,4,6,7,12,12a-octahydro-9-methoxy-6-(2-methylpropyl)-1,4-dioxo-pyrazino[1',2':1,6]pyrido[3,4-b]indole-3-propanoic acid 1,1-dimethyl ester] (Ko143) was administered i.p. using corn oil as the vehicle. Ko143 stock was prepared in DMSO. The inhibitor solution was administered i.p. 30 minutes before administration of 60mg/kg resveratrol.

4.2.6 Analytical method validation for Resveratrol, R3S and R3G:

An LC-MS/MS method was previously developed for resveratrol, R3S and R3G (Iwuchukwu et.al., 2012). The stock solutions for calibration and quality control standards were prepared in DMSO. The standards were prepared by spiking stock solutions in mouse plasma. A set of eight calibration standards was prepared within the concentration range of 0.02µg/ml to 200µg/ml.

4.2.7 LC-MS/MS conditions:

Liquid chromatography-triple quadrapole mass spectrometer (LC-MS/MS) analysis was performed on an Agilent liquid chromatography system (HPLC-1100) equipped with a degasser, binary pump system, autosampler and a thermostat coupled to a ABSciex API-4000 tandem mass spectrometer. Analyst (Ver: 6.1) software was used for acquisition and processing of LC-MS/MS data. An Agilent Zorbax SB-C18 (5µm, 4.6mm x 15mm) column with an Agilent SB-C18 (5µm, 4.6mm x 12.5mm) guard column was used for analytical separation. Acetoamidophenol (APAP) 80ng/ml was used as an internal standard (IS). A gradient mobile phase of A: 5mM ammonium acetate and B: methanol was used. The elution started at 90% A at 0 minute to 80% at 2 minutes, 65% at 10 minutes, 40% at 12 minutes to 17 minutes and 90% at 19 minutes. A flow rate of 1 ml/min was used and the flow from the column was split 1:3 into the mass spectrometer equipped with a turboionspray source operating at 450^0C (Iwuchukwu et al., 2012). The column temperature was maintained at 35^0C. The MS parameters (table 4.1) for resveratrol, R3S and R3G were used as mentioned in Iwuchukwu et.al. (Iwuchukwu et al., 2012). Nitrogen was used as the curtain, collision and ion source gas (Iwuchukwu

et al., 2012). (See appendix D for representative chromatograms of resveratrol, R3S and R3G).

4.2.8 LC-MS/MS assay validation:

Calibration curves were constructed using peak area ratios of the analyte and internal standard (IS). The calibration curve was constructed using the linear least squares method and a weighting of $1/x^2$ was applied. The MS/MS parameters used for resveratrol, R3G and R3S are summarized in table 4.1. Interday (table 4.2) and intraday (table 4.3) accuracy was determined using n=3 replicates. Accuracy was calculated by the following equation:

% accuracy = ((observed mean concentration-nominal concentration)/nominal concentration)* 100. (Eq. 4.1)

Table 4.1. ESI tandem MS parameters for resveratrol, R3S and R3G (Iwuchukwu et al., 2012).

Operating parameters	Settings			
Collision gas (CAD) (psi)	6			
Curtain gas (CUR) (psi)	40			
Ion source gas (GS1) (psi)	55			
Ion source gas (GSI) (psi)	55			
IonSpray voltage (IS) (V)	-3900			
Temperature (TEM) (^{0}C)	450			
Entrance potential (EP) (V)	-10			
Operating parameters	Resveratrol	R3G	R3S	APAP
Precursor ion (m/z)	227	403	307	150
Product ion (m/z)	185	113	227	107
Dwell time (ms)	400	400	400	400
DP (V)	-70	-65	-40	-40
CE (V)	-26	-24	-32	-24
CXP (V)	-11	-5	-5	-5

The retention time for APAP was ~5 min, ~7.9 min for R3G, ~11.2 min for R3S and ~14.2 min for resveratrol.

Table 4.2. Interday precision and accuracy for resveratrol, R3S and R3G

Res concentration (µg/ml)	Average observed concentration (µg/ml)			Mean (µg/ml)	SD	% CV	% RE
	Day 1	Day 2	Day 3				
0.005	0.006	0.008	0.006	0.006	1.2	18.8	15.7
0.5	0.464	0.733	0.454	0.550	158	19.5	10.1
3.0	2.030	3.010	2.730	2.590	504	28.8	-13.7
7.5	4.610	6.290	4.600	5.167	972	17.1	-31.1
R3S concentration (µg/ml)	Average observed concentration (µg/ml)			Mean (µg/ml)	SD	% CV	% RE
	Day 1	Day 2	Day 3				
0.0166	0.013	0.016	0.017	0.015	0.2	13.6	-5.2
0.166	0.151	0.183	0.168	0.167	16	9.6	0.8
1	0.960	0.938	1.150	1.016	116	11.5	1.6
2.5	2.550	2.220	2.550	2.440	190	7.8	-2.4
R3G concentration (µg/ml)	Average observed concentration (µg/ml)			Mean (µg/ml)	SD	% CV	% RE
	Day 1	Day 2	Day 3				
0.033	0.030	0.036	0.022	0.029	7.2	24.5	-11.4
0.333	0.355	0.357	0.326	0.346	17.3	5	3.9
2	1.990	2.160	2.120	2.090	88	4.3	4.5
5	4.930	4.840	4.240	4.670	375	8	-6.6

SD: standard deviation, CV: coefficient of variation, RE: mean bias, Res: resveratrol

Table 4.3. Intraday validation for resveratrol, R3S and R3G

Res concentration (µg/ml)	Average observed concentration (µg/ml)			Mean (µg/ml)	SD	% CV	% RE
	1	2	3				
0.05	0.05	0.05	0.05	25.83	3.47	13.43	-13.89
0.5	0.6	0.48	0.55	62.63	7.68	12.27	4.39
5	4.1	4.72	5	111.1	18.3	16.53	-7.42
12.5	11.4	11.9	11.7	251.33	12.1	4.81	4.72
R3S concentration (µg/ml)	Average observed concentration (µg/ml)			Mean (µg/ml)	SD	% CV	% RE
	1	2	3				
0.016	0.016	0.016	0.016	0.016	0	0	0
0.166	0.164	0.14	0.18	0.2	0.02	12.5	-2.8
1.660	1.31	1.48	1.64	1.5	0.2	11.2	-11
4.165	3.8	3.81	3.98	3.9	0.1	2.6	-7.2
8.330	10.3	9.130	8.140	9.2	1.1	11.8	10.3
R3G concentration (µg/ml)	Average observed concentration (µg/ml)			Mean (µg/ml)	SD	% CV	% RE
	1	2	3				
3.33	3	3.47	2.81	3.1	0.3	11	-7.1
8.33	7.74	7.3	9.6	8.2	1.2	14.9	-1.4
16.66	16.3	17.6	16.3	18.4	2.7	14.4	10.6
33.3	46.5	41.3	--	43.9	--	--	--
50	56.3	44.7	--	50.5	--	--	--

SD: standard deviation, CV: coefficient of variation, RE: mean bias,(--): not measured/calculated, Res: resveratrol

4.3 Pharmacokinetic analysis of Resveratrol, R3G and R3S:

The area under the curve ($AUC_{0-\infty}$) was calculated based on the plasma concentrations of resveratrol, R3S and R3G using the trapezoidal method. Apparent clearance (Cl/F) was calculated as Dose/$AUC_{0-\infty}$. Apparent volume of distribution (Vd_{β}/F) was calculated by $D/(\lambda \times AUC_{0-\infty})$, where λ is the elimination rate constant. λ was

calculated from the slope of the terminal part of the concentration time profile. The terminal half-life was calculated as $\lambda/0.693$. C_{max} and T_{max} were reported based on the pharmacokinetic profiles. The values of AUC_{0-t} and $AUC_{t-\infty}$ were calculated by the linear trapezoidal method. Percent AUC extrapolated was calculated as follows: $(AUC_{0-t}/ AUC_{t-\infty})*100$. Microsoft excel (licensed to Temple University, Microsoft Office 2013, Redmond, WA) and Kinetica software (ThermoFisher Scientific Inc., PA) were used to calculate pharmacokinetic parameters.

4.4 Results:

The pharmacokinetic profiles of resveratrol, R3G and R3S in control mice and in the presence of mrp2 and bcrp inhibitors are shown in fig. 4.1 through fig. 4.3 respectively (see appendix E 1 through E 3 for concentration time profiles for resveratrol, R3G and R3S in the presence of mrp2 and bcrp inhibitors where data is represented as replicates).

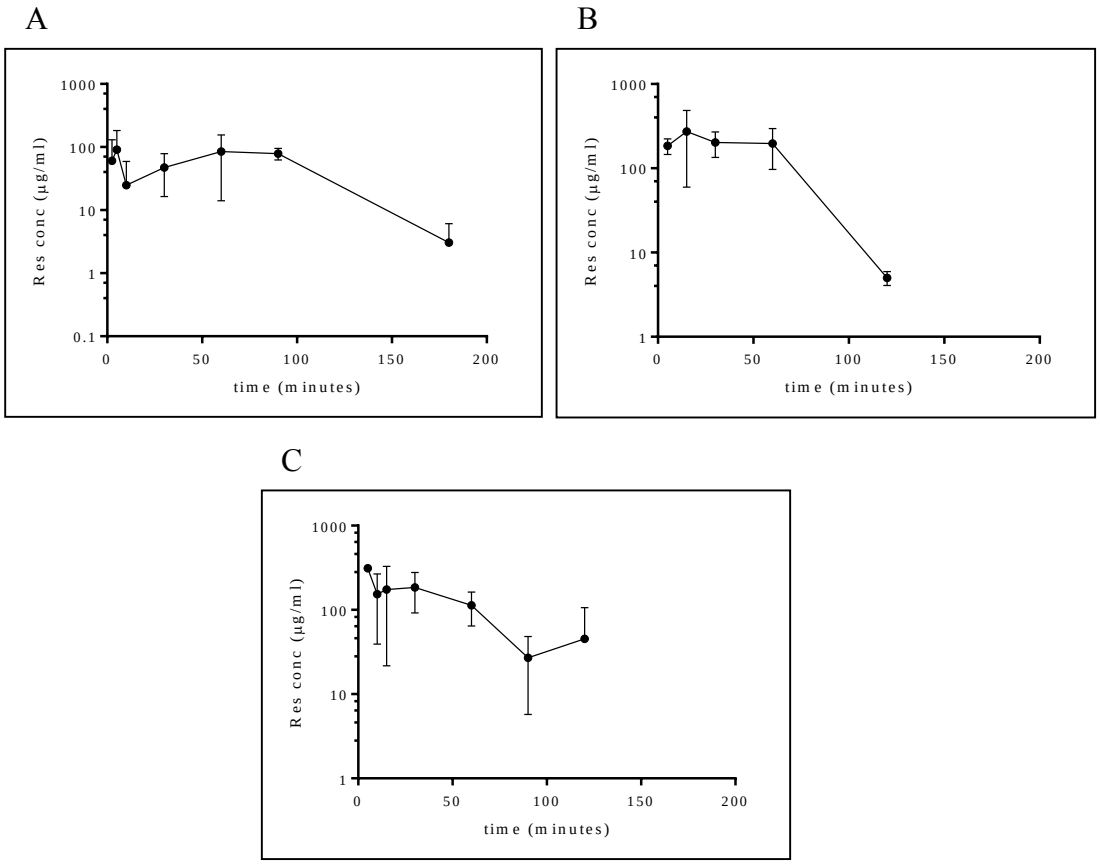

Figure 4.1. Concentration-time profile of (A) resveratrol (60mg/kg) in control group, (B) in presence of mrp2 inhibitor, (C) in presence of bcrp inhibitor (n=3). Data represented as mean values ± standard deviation.

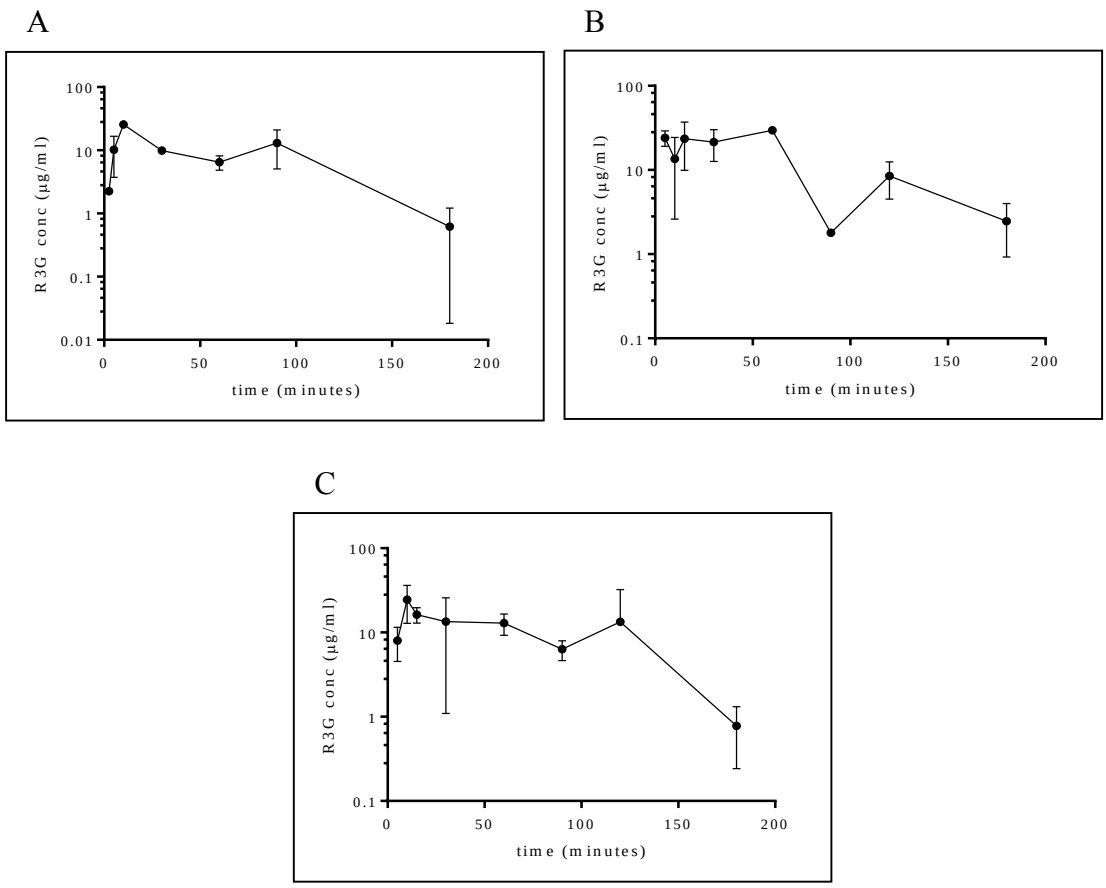

Figure 4.2. Concentration-time profile of R3G (A) in control group, (B) in the presence of mrp2 inhibitor, (C) in the presence of bcrp inhibitor (when resveratrol (60mg/kg) administered i.p., n=3). Data represented as mean values ± standard deviation.

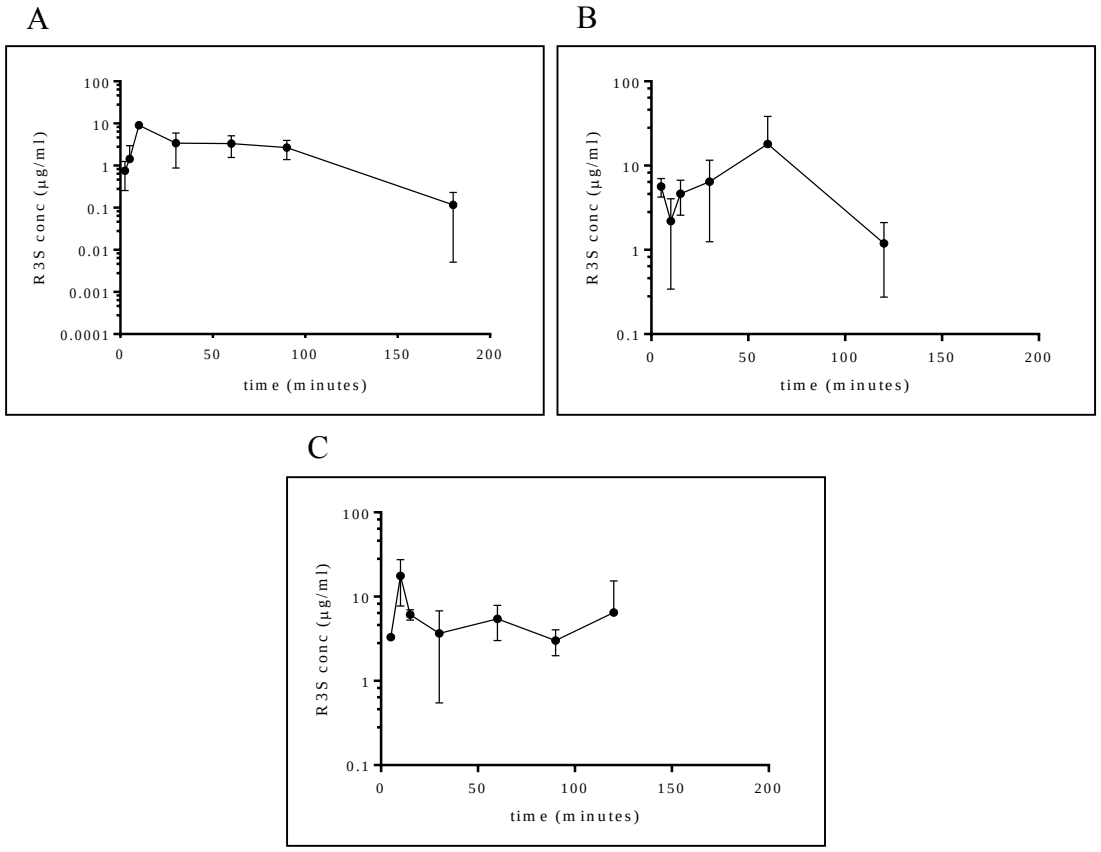

Figure 4.3. Concentration-time profile of R3S (A) in control group, (B) in the presence of mrp2 inhibitor, (C) in the presence of bcrp inhibitor (when resveratrol (60mg/kg) administered i.p., n=3). Data represented as mean values ± standard deviation.

The pharmacokinetic parameters in presence of mrp2 and bcrp inhibitors obtained by noncompartmental analysis are summarized in table 4.4 and table 4.5 respectively. Due to the variability in data, C_{max} values were not selected as a key parameter to evaluate the effect of transporter inhibitors. In the presence of mrp2 inhibitor, the $AUC_{0-\infty}$ of both the metabolites increased marginally with the $AUC_{0-\infty}$ of R3S increasing 2 fold.

The percent AUC extrapolated in presence of mrp2 inhibitor was <20% for all 3 compounds. The statistical tests usually performed on such data would be a two sided independent samples t test. In this test, the control vs mrp2 treated group and control vs bcrp treated group would be compared to verify if the two sets are significantly different. The experimental design used here is serial sacrifice (where each time point is an independent animal). Hence, the standard error in $AUC_{0-\infty}$ is not easily obtained.

In the presence of bcrp inhibitor, the $AUC_{0-\infty}$ of R3S increased >2 fold. The percent AUC extrapolated was calculated for each compound. The percent extrapolated AUC for R3S was ~ 48% of the total AUC which may suggest that the calculated AUC for R3S may be unreliable and hence, was treated with caution (Marzo et al., 1999). The AUC_{0-t} for R3S did not increase by 2 fold. The percent extrapolated AUC for resveratrol and R3G was less than 20% of the calculated total AUC.

Table 4.4 Noncompartmental pharmacokinetic analysis of resveratrol, R3S and R3G upon 60mg/kg i.p. administration of resveratrol in presence of mrp2 inhibitor (10mg/kg)

	Resveratrol		R3G		R3S	
Parameter	- Mrp2 inhibitor	+Mrp2 inhibitor	- Mrp2 inhibitor	+Mrp2 inhibitor	- Mrp2 inhibitor	+Mrp2 inhibitor
C_{max} (μM)	90.87	1197	12.06	73.4	3.38	58
T_{max} (min)	5	15	5	60	30	60
Cl/F ml/min/kg	5.71	3.44	--	--	--	--
Vd_{β}/F ml/kg	167.9	51	--	--	--	--
$AUC_{0-\infty}$ min.mM	46.036	76.43	4.58	5.93	1.6	3.81
AUC_{0-t} min.mM	46.035	76.28	4.57	5.7	1.56	3.49
$AUC_{tlast-\infty}$ min.mM	0.001	0.15	0.01	0.23	0.04	0.32
$M_{AUC0-\infty}/D_{AUC0-\infty}$	--	--	0.099	0.074	0.034	0.049
% extrapolated	0.002	0.22	0.218	3.87	2.5	8.4
λ (min^{-1})	0.034	0.068	0.018	0.026	0.018	0.012
$t_{1/2}$ (min)	20.4	10.2	37.2	26.7	38.5	57.8

(--): parameter not calculated, $M_{AUC0-\infty}/D_{AUC0-\infty}$: ratio of $AUC_{0-\infty}$ of metabolite to $AUC_{0-\infty}$ of resveratrol

Table 4.5 Noncompartmental pharmacokinetic analysis of resveratrol, R3S and R3G upon 60mg/kg i.p. administration of resveratrol in presence of bcrp inhibitor (10mg/kg)

	Resveratrol		R3G		R3S	
Parameter	-Bcrp inhibitor	+Bcrp inhibitor	-Bcrp inhibitor	+Bcrp inhibitor	-Bcrp inhibitor	+Bcrp inhibitor
C_{max} (μM)	398	1367	63.5	60.6	29.5	57
T_{max} (min)	5	5	5	10	30	10
Cl/F ml/min/kg	5.71	3.9	--	--	--	--
Vd_{β}/F ml/kg	167.9	195	--	--	--	--
$AUC_{0-\infty}$ min.mM	46.036	67.46	4.58	6.12	1.6	3.97
AUC_{0-t} min.mM	46.035	57.54	4.57	5.63	1.56	2.05
$AUC_{tlast-\infty}$ min.mM	0.001	9.92	0.01	0.49	0.04	1.92
$M_{AUC0-\infty}/D_{AUC0-\infty}$	--	--	0.099	0.09	0.034	0.058
% extrapolated	0.002	14.7	0.218	8	2.5	48.36
λ (min^{-1})	0.034	0.020	0.018	0.013	0.018	0.011
$t_{1/2}$ (min)	20.4	34.65	37.2	53.3	38.5	58

4.5. Discussion:

Resveratrol is a phytochemical and a naturally occurring compound. On oral administration, it is rapidly absorbed and is extensively metabolized to resveratrol conjugates, which, are observed in plasma. The role of certain ABC transporters such as BCRP and MRP3 has been demonstrated using knockout mice with an oral dose of 50 or 60mg/kg (van de Wetering et al., 2009; Alfaras et al., 2010). The results obtained confirmed the role of some ABC transporters but not Pgp. Mrp2 inhibitor (MK571) has been reported to impact the disposition of R3G and R3S without affecting resveratrol concentrations (Maier-Salamon et al., 2008; Juan et al., 2010). The role of bcrp in the disposition of R3G and R3S has also been reported (Maier-Salamon et al., 2008; van de Wetering et al., 2009; Alfaras et al., 2010; Juan et al., 2010).

AUCs observed in the control group and transporter inhibited group were used to assess the effect of efflux transporter inhibition. Due to large variability in resveratrol, R3S and R3G plasma concentrations at each time point, C_{max} and T_{max} were not considered as reliable pharmacokinetic paramters. Based on recent reports we hypothesized that inhibition of mrp2 and bcrp would affect the disposition of resveratrol and/or its metabolites. Hence, in this study, we attempted to inhibit mrp2 and bcrp using MK571 and Ko143 respectively. Inhibition of Mrp2 by MK571 increased $AUC_{0-\infty}$ of R3S by 2.38 fold, which may indicate a role of Mrp2 transporter in R3S disposition. For example, the inhibition of Mrp2 at the basolateral membrane of liver may decrease the excretion of R3S thus decreasing biliary elimination. In the presence of MK571, $AUC_{0-\infty}$ of R3G increased 1.33 fold. In the presence of Ko143, the $AUC_{0-\infty}$ of R3S increased 2.48 fold while the $AUC_{0-\infty}$ of R3G increased 1.33 fold. A minor change in $AUC_{0-\infty}$ of

resveratrol was observed. The $AUC_{0-\infty}$ of resveratrol changed by 1.7 fold and 1.4 fold in the presence of mrp2 and bcrp inhibitor. This may indicate a minor role of mrp2 and bcrp in the overall disposition of resveratrol. Another reason for the change in resveratrol exposure may be due to the change in disposition of its metabolites. Decreased elimination of R3S and R3G may result in the conversion of these metabolies into parent due the the presence of β-glucuronidase and sulfatases. The change observed in AUCs may also be due to the variability in the plasma concentration data. Hence, such changes in AUCs should be treated with caution.

The percent AUC extrapolated for R3S in presence of Ko143 was 48%, which is much higher than the acceptable limit. No more than 20% should be added to AUC_{0-t} (Marzo et.al.1999). Hence, the $AUC_{0-\infty}$ calculated for R3S (in the presence of bcrp inhibitor) by using the trapezoidal rule may not be reliable. Future pharmacokinetic studies with resveratrol in the presence of transporter or enzyme inhibition should be performed using survival blood collection techniques or increased number of animals should be alloted to each group in order to provide more data points. This would provide a more reliable AUC prediction. MK571 and Ko143 are considered to be specific MRP and BCRP inhibitors but their effects on enzymes have not been investigated. Hence, the effects of MK571 and Ko143 on UGTs, SULTs and Pgp should also be investigated.

4.6. Conclusions:

The current in vivo study was performed to shed light on the impact of efflux transporter inhibition on the disposition of resveratrol, R3S and R3G. The in vivo disposition of resveratrol, R3S and R3G was monitered in the presence of mrp2 and bcrp

inhibitor. Both inhibitors showed an effect on the total exposure of resveratrol, R3S and R3G. R3S seemed to be affected more by MK571 and Ko143 with 2.38 fold and 2.48 fold increase in $AUC_{0-\infty}$. Thus inhibition of efflux transporters may not only affect the disposition of R3S and R3G but also resveratrol.

4.7 Future directions:

We investigated the role of efflux transporters by inhibiting mrp2 and bcrp in vivo in mice. For future studies, the use of transporter knock-out mice should be preferred. This mouse model would provide a clearer picture of transporter involvment. Future studies could focus on 1. tissue specific transporter-metabolite kinetics, 2. effect of polymorphism of transporters or 3. transporter-metabolite kinetics in disease states such as cholestasis. It would be fasinating to study the effect cholestasis on glucuronide and sulfate metabolite pkarmacokinetics.

REFERENCES

Alfaras I, Perez M, Juan ME, Merino G, Prieto JG, Planas JM, and Alvarez AI (2010) Involvement of breast cancer resistance protein (BCRP1/ABCG2) in the bioavailability and tissue distribution of trans-resveratrol in knockout mice. J Agric Food Chem 58:4523-4528.

Allen JD, van Dort SC, Buitelaar M, van Tellingen O, and Schinkel AH (2003) Mouse breast cancer resistance protein (Bcrp1/Abcg2) mediates etoposide resistance and transport, but etoposide oral availability is limited primarily by P-glycoprotein. Cancer Res 63:1339-1344.

Allen JD, van Loevezijn A, Lakhai JM, van der Valk M, van Tellingen O, Reid G, Schellens JHM, Koomen GJ, and Schinkel AH (2002) Potent and specific inhibition of the breast cancer resistance protein multidrug transporter in vitro and in mouse intestine by a novel analogue of fumitremorgin C. Molecular Cancer Therapeutics 1:417-425.

Bodo A, Bakos E, Szeri F, Varadi A, and Sarkadi B (2003) Differential modulation of the human liver conjugate transporters MRP2 and MRP3 by bile acids and organic anions. J Biol Chem 278:23529-23537.

Chen ZS and Tiwari AK (2011) Multidrug resistance proteins (MRPs/ABCCs) in cancer chemotherapy and genetic diseases. FEBS journal 278:3226-3245.

Cole SP, Bhardwaj G, Gerlach JH, Mackie JE, Grant CE, Almquist KC, Stewart AJ, Kurz EU, Duncan AM, and Deeley RG (1992) Overexpression of a transporter gene in a multidrug-resistant human lung cancer cell line. Science 258:1650-1654.

Diehl KH, Hull R, Morton D, Pfister R, Rabemampianina Y, Smith D, Vidal JM, van de Vorstenbosch C, European Federation of Pharmaceutical Industries A, and European Centre for the Validation of Alternative M (2001) A good practice

guide to the administration of substances and removal of blood, including routes and volumes. J Appl Toxicol 21:15-23.

Doyle LA and Ross DD (2003) Multidrug resistance mediated by the breast cancer resistance protein BCRP (ABCG2). Oncogene 22:7340-7358.

Giri N, Agarwal S, Shaik N, Pan G, Chen Y, and Elmquist WF (2009) Substrate-dependent breast cancer resistance protein (Bcrp1/Abcg2)-mediated interactions: consideration of multiple binding sites in in vitro assay design. Drug metabolism and Disposition 37:560-570.

Heredi-Szabo K, Jemnitz K, Kis E, Ioja E, Janossy J, Vereczkey L, and Krajcsi P (2009) Potentiation of MRP2/Mrp2-mediated estradiol-17beta-glucuronide transport by drugs--a concise review. Chem Biodivers 6:1970-1974.

Giacomini KM, Huang SM, Tweedie DJ, Benet LZ, Brouwer KL, Chu X, Dahlin A, Evers R, Fischer V, Hillgren KM, Hoffmaster KA, Ishikawa T, Keppler D, Kim RB, Lee CA, Niemi M, Polli JW, Sugiyama Y, Swaan PW, Ware JA, Wright SH, Yee SW, Zamek-Gliszczynski MJ, and Zhang L (2010) Membrane transporters in drug development. Nat Rev Drug Discov 9:215-236.

Iwuchukwu OF, Sharan S, Canney DJ, and Nagar S (2012) Analytical method development for synthesized conjugated metabolites of trans-resveratrol, and application to pharmacokinetic studies. J Pharm Biomed Anal 63:1-8.

Jang M, Cai L, Udeani GO, Slowing KV, Thomas CF, Beecher CW, Fong HH, Farnsworth NR, Kinghorn AD, Mehta RG, Moon RC, and Pezzuto JM (1997) Cancer chemopreventive activity of resveratrol, a natural product derived from grapes. Science 275:218-220.

Juan ME, Gonzalez-Pons E, and Planas JM (2010) Multidrug resistance proteins restrain the intestinal absorption of trans-resveratrol in rats. J Nutr 140:489-495.

Kage K, Tsukahara S, Sugiyama T, Asada S, Ishikawa E, Tsuruo T, and Sugimoto Y (2002) Dominant-negative inhibition of breast cancer resistance protein as drug efflux pump through the inhibition of S-S dependent homodimerization. International journal of cancer 97:626-630.

Karlsson JE, Heddle C, Rozkov A, Rotticci-Mulder J, Tuvesson O, Hilgendorf C, and Andersson TB (2010) High-activity p-glycoprotein, multidrug resistance protein 2, and breast cancer resistance protein membrane vesicles prepared from transiently transfected human embryonic kidney 293-epstein-barr virus nuclear antigen cells. Drug Metab Dispos 38:705-714.

Kawabata S, Oka M, Shiozawa K, Tsukamoto K, Nakatomi K, Soda H, Fukuda M, Ikegami Y, Sugahara K, Yamada Y, Kamihira S, Doyle LA, Ross DD, and Kohno S (2001) Breast cancer resistance protein directly confers SN-38 resistance of lung cancer cells. Biochem Biophys Res Commun 280:1216-1223.

König J, Nies AT, Cui Y, Leier I, and Keppler D (1999) Conjugate export pumps of the multidrug resistance protein (MRP) family: localization, substrate specificity, and MRP2- mediated drug resistance. Biochimica et Biophysica Acta (BBA)-Biomembranes 1461:377-394.

Kopp P (1998) Resveratrol, a phytoestrogen found in red wine. A possible explanation for the conundrum of the 'French paradox'? European Journal of Endocrinology 138:619- 620.

Leonard SS, Xia C, Jiang BH, Stinefelt B, Klandorf H, Harris GK, and Shi X (2003) Resveratrol scavenges reactive oxygen species and effects radical-induced cellular responses. Biochem Biophys Res Commun 309:1017-1026.

Leslie EM, Deeley RG, and Cole SPC (2005) Multidrug resistance proteins: role of P-glycoprotein, MRP1, MRP2, and BCRP (ABCG2) in tissue defense. Toxicology and Applied Pharmacology 204:216-237.

Li H, Jin HE, Kim W, Han YH, Kim DD, Chung SJ, and Shim CK (2008) Involvement of P-glycoprotein, multidrug resistance protein 2 and breast cancer resistance protein in the transport of belotecan and topotecan in Caco-2 and MDCKII cells. Pharmaceutical Research 25:2601-2612.

Maier-Salamon A, Bohmdorfer M, Riha J, Thalhammer T, Szekeres T, and Jaeger W (2013) Interplay between metabolism and transport of resveratrol. Ann N Y Acad Sci 1290:98-106.

Maier-Salamon A, Hagenauer B, Reznicek G, Szekeres T, Thalhammer T, and Jager W (2008) Metabolism and disposition of resveratrol in the isolated perfused rat liver: Role of Mrp2 in the biliary excretion of glucuronides. Journal of Pharmaceutical Sciences 97:1615-1628.

Maliepaard M, van Gastelen MA, de Jong LA, Pluim D, van Waardenburg RC, Ruevekamp-Helmers MC, Floot BG, and Schellens JH (1999) Overexpression of the BCRP/MXR/ABCP gene in a topotecan-selected ovarian tumor cell line. Cancer Res 59:4559-4563.

Mao Q (2005) Role of the breast cancer resistance protein (ABCG2) in drug transport. The AAPS journal 7:E118-E133.

Marzo A, Monti NC, and Vuksic D (1999) Experimental, extrapolated and truncated areas under the concentration-time curve in bioequivalence trials. Eur J Clin Pharmacol 55:627-631.

Mennone A, Soroka CJ, Harry KM, and Boyer JL (2010) Role of Breast Cancer Resistance Protein in the Adaptive Response to Cholestasis. Drug metabolism and Disposition 38:1673-1678.

Morton DB, Abbot D, Barclay R, Close BS, Ewbank R, Gask D, Heath M, Mattic S, Poole T, Seamer J, Southee J, Thompson A, Trussell B, West C and Jennings M (1993) Removal of blood from laboratory mammals and birds. First report of the BVA/FRAME/RSPCA/UFAW Joint Working Group on Refinement. Lab Anim 27:1-22.

Nakanishi T, Doyle LA, Hassel B, Wei Y, Bauer KS, Wu S, Pumplin DW, Fang H-B, and Ross DD (2003) Functional characterization of human breast cancer resistance protein (BCRP, ABCG2) expressed in the oocytes of Xenopus laevis. Mol Pharmacol 64:1452-1462.

Nies AT and Keppler D (2007) The apical conjugate efflux pump ABCC2 (MRP2). Pflugers Arch 453:643-659.

Nies AT, Rius M, and Keppler D (2006) Multidrug Resistance Proteins of the ABCC Subfamily, in: Drug Transporters, pp 263-318, John Wiley & Sons, Inc.

Rabindran SK, Ross DD, Doyle LA, Yang W, and Greenberger LM (2000) Fumitremorgin C reverses multidrug resistance in cells transfected with the breast cancer resistance protein. Cancer Res 60:47-50.

Robey RW, Polgar O, Deeken J, To KKW, and Bates SE (2006) Breast Cancer Resistance Protein, in: Drug Transporters, pp 319-358, John Wiley & Sons, Inc.

Sharan S, Iwuchukwu OF, Canney DJ, Zimmerman CL, and Nagar S (2012) In vivo-formed versus preformed metabolite kinetics of trans-resveratrol-3-sulfate and trans- resveratrol-3-glucuronide. Drug Metab Dispos 40:1993-2001.

Takano M, Yumoto R, and Murakami T (2006) Expression and function of efflux drug transporters in the intestine. Pharmacol Ther 109:137-161.

van de Wetering K, Burkon A, Feddema W, Bot A, de Jonge H, Somoza V, and Borst P (2009) Intestinal breast cancer resistance protein (BCRP)/Bcrp1 and multidrug resistance protein 3 (MRP3)/Mrp3 are involved in the pharmacokinetics of resveratrol. Mol Pharmacol 75:876-885.

Vlaming ML, Pala Z, van Esch A, Wagenaar E, van Tellingen O, de Waart DR, Oude Elferink RP, van de Wetering K, and Schinkel AH (2008) Impact of Abcc2 (Mrp2) and Abcc3 (Mrp3) on the in vivo elimination of methotrexate and its main toxic metabolite 7- hydroxymethotrexate. Clin Cancer Res 14:8152-8160.

Volk EL and Schneider E (2003) Wild-type breast cancer resistance protein (BCRP/ABCG2) is a methotrexate polyglutamate transporter. Cancer Res 63:5538-5543.

Walle T, Hsieh F, DeLegge MH, Oatis JE, Jr., and Walle UK (2004) High absorption but very low bioavailability of oral resveratrol in humans. Drug Metab Dispos 32:1377-1382.

Zamek-Gliszczynski MJ, Hoffmaster KA, Nezasa KI, and Brouwer KLR (2008) Apparent Differences in Mechanisms of Harmol Sulfate Biliary Excretion in Mice and Rats. Drug metabolism and Disposition 36:2156-2158.

Zhang S, Wang X, Sagawa K, and Morris ME (2005) Flavonoids chrysin and benzoflavone, potent breast cancer resistance protein inhibitors, have no significant effect on topotecan pharmacokinetics in rats or mdr1a/1b (–/–) mice. Drug metabolism and Disposition 33:341-348.

CHAPTER 5

EVALUATING THE EFFECT OF ANTIBIOTICS ON RESVERATROL, R3S AND R3G DISPOSITION

5.1 Background:

5.1.1 Enterohepatic circulation (EHC):

Endogenous and exogenous compounds undergo EHC (Tvrdonova et al., 2009). Endogenous compounds such as bile acids, which are synthesized from cholesterol in liver, are conjugated to a polar group such as glucuronic acid, sulfate, glycine, taurine and glutathione to form bile salts. Bile salts are a major component of bile. The bile is excreted by the hepatobiliary system and stored in the gall bladder. The bile is released into the small intestine upon ingestion of food. The bile, being an aqueous solution, serves in reabsorption of water-soluble compounds. The bile acids facilitate the formation of micelles, which help in the absorption of dietary fats and fat-soluble compounds. These bile acids, also known as secondary conjugated bile acids, are actively reabsorbed into portal blood. Some bile acids may undergo deconjugation to lipid soluble form, which is reabsorbed.

Most of the bile acids secreted into small intestine are thus reabsorbed and are the main constituents of EHC. Orally ingested nutrients, drugs or toxins are reabsorbed by enterocytes and enter portal blood. The liver is responsible for the metabolism of drugs and toxins. These metabolized compounds may be secreted by bile into intestine and are

eliminated via feces. The liver efficiently reabsorbs bile acids, which are absorbed into the systemic circulation from the intestine. (Roberts MS, 2002).

5.1.2 Production of bile:

The bile is secreted by the liver normally at a rate of 600ml to 1000ml per day (E.Hall, 2016). Bile serves to emulsify fat particles, thus aiding in absorption of digested fat products, and it serves as a means of excretion of cholesterol and bilirubin. The bile is secreted by hepatocytes into bile canaliculi. The bile canaliculi empty into terminal bile ducts, which join into the larger hepatic bile duct. Hepatic bile duct merges with the cystic duct to form the common bile duct. The secreted bile is either emptied into duodenum or is stored in gall bladder. A secondary secretion (called initial bile), containing sodium and bicarbonate ions helps to neutralize gastric acid in the duodenum (Walle et al., 2004; E.Hall, 2016).

5.1.3 Composition of bile:

The most abundant substance in the bile acid is bile salts. The composition of bile changes if it undergoes a concentrating process in gall bladder. A more detailed composition of bile is provided in the table below (table 5.1) (E.Hall, 2016).

Table 5.1 Composition of human bile.

Composition	Liver bile
Water	97.5 g/dl
Bile salts	1.1 g/dl
Bilirubin	0.04 g/dl
Cholesterol	0.1 g/dl
Fatty acids	0.12 g/dl
Lecithin	0.04 g/dl
Na^{+}	145.04 mEq/l
K^{+}	5 mEq/l
Ca^{++}	5 mEq/l
Cl^{-}	100 mEq/l
$HCO3^{-}$	28 mEq/l

5.1.4. Bile salts:

The primary bile acids (cholic acid and chenodeoxycholic acid) are synthesized in the liver using cholesterol. Bile acids are steroid acids, which are conjugated with taurine or glycine to form bile salts. Bile salts and lecithin are responsible for emulsification of fats, which aid in their absorption.

5.1.5. EHC of resveratrol:

Resveratrol is conjugated to sulfate and glucuronide, its 3-glucuronide metabolite being the abundant metabolite. Resveratrol pharmacokinetic profile in rodents showed a secondary peak between 3-8 hours (Marier et al., 2002; Sharan et al., 2012). This peak is hypothesized to be due to the regeneration of resveratrol from its glucuronide metabolite.

Resveratrol glucuronides effluxed from the liver into the bile are metabolized in the intestine by β-glucuronidase to form the parent compound and hence the parent is absorbed back into the blood stream. This is hypothesized to result in a second peak which occurs between 3- 8 hours after dosing resveratrol. If β-glucuronidase is inhibited by antibiotics, the conversion of glucuronides to parent form will be prevented, potentially resulting in a decrease in resveratrol and R3G exposure.

Drug glucuronides are hydrolyzed by β-glucuronidase, an enzyme, which is expressed in human tissues and body fluids. As will be discussed below, the bacterial β-glucuronidase activity may result in the deconjugation reactions in the intestine (Roberts et al., 2002). The extent of contribution of β-glucuronidase on disposition of resveratrol and its glucuronide has not been established as yet but this enzyme may enable the release of resveratrol from its glucuronide locally or systemically. There are few examples where β-glucuronidase mediated drug deconjugation is significant (e.g. SN-38 and glucuronide) (Sperker et al., 1997; Roberts et al., 2002; Naz et al., 2013).

5.1.6 Intestinal flora:

Gut flora is a complex of microorganisms that live in intestinal tracts of animals and maintain a symbiotic relationship with the host animal. The gut microbes also help in the synthesis of vitamin B and K, and metabolism of sterols, bile acids and xenobiotics. Gut microbes consist of 300-500 species of bacteria (Guarner and Malagelada, 2003), mainly anaerobic, (Guarner and Malagelada, 2003; Vedantam and Hecht, 2003; Beaugerie and Petit, 2004; Sears, 2005). In human beings, the most prominent genera are *Bacteroides, Bifidobacterium, Eubacterium, Clostridium, Peptococcus,*

Peptostreptococcus, Ruminococcus, Escherichia, Enterobacter, Enterococcus, Klebsiella, Lactobacillus, Proteus, etc (Guarner and Malagelada, 2003). When the gastric content enters the small intestine, it is mixed with bile and pancreatic secretions. The transit time in the small intestine slows down to increase the digestion processes.

The disposition of xenobiotics may be affected by the presence of gut flora. The action of gut flora may have beneficial or toxic effects. An example of toxic effect could be seen in the poisoning due to amygdalin in normal rats versus germ free rats. The production of cyanide due to β-glucuronidase activity resulted in toxicity and convulsions indicating a role of intestinal flora in this toxicity (Gustafsson and Lanke, 1960; Carter et al., 1980; Coates, 2005; Hill, 2005). The intestinal flora plays a role in protection of gut and metabolism. For example, the intestinal flora provides a barrier against the colonization of exogenous bacteria thus preventing invasion of pathogenic bacteria (Guarner and Malagelada, 2003). The intestinal flora also plays a role in the metabolism of bilirubin to urobilinogen, which is subsequently absorbed and excreted by kidneys (Gustafsson and Lanke, 1960; Coates, 2005; Hill, 2005; Donald Voet, 2012). A wide range of xenobiotics and endogenous compounds are glucuronidated and sulfated in liver. These compounds are excreted in bile and pass into small intestine and colon. Enzymes produced by the intestinal bacteria such as β-glucuronidase, sulfatase and glycosidase deconjugate the metabolites and release the parent compound, which is absorbed across the intestinal wall (Gorbach, 1996). This may result in an increased exposure of parent compound (figure 5.1).

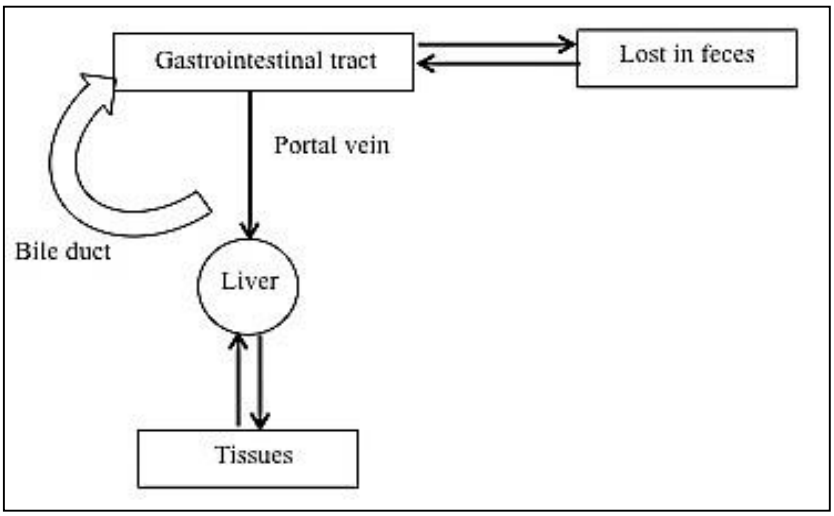

Figure 5.1. Enterohepatic circulation. The intestinal contents are absorbed into the portal vein. These contents pass go to the liver where they are metabolized and excreted into intestine through bile duct.

5.1.7 β-glucuronidase:

Human β-glucuronidase is a tetrameric glycoprotein expressed in tissues and fluids and shows dual localization in lysosomes and endoplasmic reticulum (Naz et al., 2013). The cleavage of glucuronide metabolites in vivo is of significance especially when the glucuronides act as a depot for the parent compound. This enzyme is present in blood cells, liver, lungs, kidneys, intestine and intestinal juice but has a large inter-individual variability in its activity and expression. Increased β-glucuronidase activity has been observed in disease states such as cancer, AIDS, and inflammatory joint disease. The main role is thought to be the degradation of glycosaminoglycan in lysosomes by removing β-glucuronosyl residues from oligosaccharides. Deficiency of β-glucuronidase leads to Sly syndrome. Various point mutations have also been identified (Sperker et al.,

1997). Although significant information is available for human β-glucuronidase, information on mouse β-glucuronidase is scarce.

Drug glucuronides are susceptible to enterohepatic circulation because many glucuronides are secreted in bile. In the intestine, glucuronides may be hydrolyzed by enteric and bacterial β-glucuronidase and subsequently reabsorbed (Roberts et al., 2002). Several factors should be considered before assessing the possible role of human β-glucuronidase in the cleavage of glucuronide metabolites. At physiological pH, the activity of β-glucuronidase is low. The primary localization of β-glucuronidase is in the endoplasmic reticulum (Naz et al., 2013).

5.1.8 Intestinal sulfatases:

The sulfatase family of enzymes catalyzes the hydrolysis of sulfate ester bonds of substrates such as steroids, carbohydrates and glycolipids (Ghosh, 2005; Sardiello et al., 2005). Most of the sulfatases such as human estrone sulfatase, arylsulfatases A, B, D, E and F are located in lysosomes or golgi compartments (Parenti et al., 1997; Ghosh, 2005). Other members of human sulfatase family include iduronate-2-sulfatase, galactose-6-sulfatase and glucosamine sulfatase, all of which are located in lysosomes (Ghosh, 2005).

Up until 2005, 17 human sulfatase genes have been identified while 14 rodent sulfatase genes have been explored. In humans, minute amounts of major bile acids are excreted as sulfate conjugates. Lithocholic acid is an example of bile acid, which is excreted as a sulfate conjugate (Eyssen et al., 1976). Only a few bacterial sulfatases have been characterized. The *Bacteroides* species (gram negative, anerobic bacteria), which colonize the intestinal mucosal layer in humans, have been known to metabolize sulfated

glycans such as mucin and glycoaminoglycans (Ulmer et al., 2014). Steroid sulfatases exist in human intestine. *Peptococcus species* (gram positive bacteria) have been found to produce steroid sulfatases to metabolize steroid-3-sulfate esters such as estradiol-3-sulfate and estrone-3-sulfate (Van Eldere et al., 1987). Some non-steroid arylsulfate compounds such as paranitrophenyl sulfate, paranitrocatechol sulfate and phenolphthanein disulfate were found to be desulfated by this strain (Van Eldere et al., 1987). The knowledge on the activity of bactetial sulfatases on xenobiotics is still lacking.

5.1.9 β-glucuronidase inhibitors:

Neomycin is an aminoglycoside with broad-spectrum antibiotic activity, and displays low incidence of toxic and hypersensitivity reactions. It is slightly absorbed from intestinal tract hence it is less likely to produce systemic effects. It is used against gram negative bacilli (Beale, 2004). Bacitracin is a polypeptide type of antibiotic (Beale, 2010). It interferes with bacterial cell wall synthesis and is effective against gram-positive bacteria. It is not orally absorbed hence, oral administration does not cause a systemic antibiotic effect (Beale, 2004).

The treatment with Neo/Bac has shown to inhibit β-glucuronidase in male Wistar rats. This inhibition ameliorated CPT-11 (the active metabolite of irinotecan) induced diarrhea and reduced intestinal toxicity without decreasing the anti-tumor activity of CPT-11 (Takasuna et al., 2006). Kehrer et.al reported the use of neomycin to ameliorate diarrhea in CPT-11 treated patients (Kehrer et al., 2001). Almonti et.al (2004) utilized neomycin and bacitracin in combination (25,000 IU and 2500 IU respectively) given at a

single oral dose three times a day to patients (Alimonti et al., 2004). The incidence and severity of diarrhea was decreased significantly (Alimonti et al., 2003; Alimonti et al., 2004). Thus, a combination of neomycin and bacitracin would eliminate gram negative bacteria such as *Bacteroides, Peptococcus, Enterococcus* species as well as gram positive bacteria such as *Peptostreptococcus, Lactobacillus* that produce intestinal β-glucuronidase and sulfatase (Gadelle et al., 1985).

The study was aimed to eliminate intestinal microbiota thus completely inhibiting the bacterial β-glucuronidase activity in the intestine and interrupting the enterohepatic circulation of resveratrol and R3G. The plasma concentrations of resveratrol, R3G and R3S were monitored to assess the impact of inhibition of enterohepatic circulation. The experiments were conducted in vivo in C57BL/6 mice. Oral antibiotics were dosed, with the intent to inhibit the bacterial deconjugating enzymes in the rodent intestine, for four days prior to resveratrol administration and during the experiment. Blood samples were collected from both groups and the concentration of resveratrol, R3G and R3S were evaluated by using LC- MS/MS. Noncompartmental analysis was performed using the measured plasma concentrations of resveratrol, R3S and R3G.

5.2 Experimental section:

5.2.1 Materials:

Resveratrol, R3Gand R3S were purchased from Toronoto Research Chemicals Inc. (Toronto, Canada). Hydroxylpropyl-β-cyclodextrin and neomycin were purchased from Sigma-Aldrich (St.Louis, MO, USA). Bacitracin and 4-acetamidophenol (APAP)

was purchased from Sigma-Aldrich (St.Louis, MO, USA). Mouse (Balb/C) plasma was purchased from GeneTex. Inc. (Irvine, CA, USA). Sterile saline solution (0.9%) was purchased from Teknova (Hollister, CA, USA). Male C57BL/6 mice weighing between 20- 25g were obtained from Charles River Laboratories (Wilmington, MA) and maintained according to American Association for the Accredition of Laboratory Animal Care-accredited University Laboratory Animal Resources of Temple University standards.

5.2.2 Experimental design:

Male C57BL/6 mice were used for this experiment. The animals were divided into 2 groups, each with 7 time points. Three mice were sacrificed at every time point. Animals were fed a normal diet and a standard 12 hour dark/light cycle was maintained. During the procedure, the animals were fasted 10 hours prior to dosing resveratrol to rule out variability of gall bladder emptying due to food. Blood was withdrawn by cardiac puncture. Resveratrol (60mg/kg) was solubilized in 20% 2-hydroxypropyl-β-cyclodextrin in sterile saline (Juan et.al. 2010). Resveratrol was dosed intraperitoneally (i.p.). Heparinized tubes (40µl) for blood collection were prepared prior to the start of the experiment. Blood was collected at 2.5, 5, 30, 180, 360, 780, 1440 minutes. The blood samples thus collected were centrifuged at 15000 rpm for 15 minutes and the plasma fraction was collected and analyzed using LC-MS/MS. The LC-MS/MS method validation for resveratrol, R3G and R3S is detailed in chapter 4 (section 4.3.1 through 4.3.3).

5.2.3. In vivo administration of resveratrol with and without antibiotic:

Antibiotics were administered orally in the form of 2mg neomycin per ml of drinking water from 4 days before the administration of resveratrol and throughout the experiment in order to achieve full antibiotic efficiency. Also, neomycin 20mg/kg and bacitracin 10mg/kg were administered orally twice daily starting 2 days before, and continued during, the administration of resveratrol (Takasuna et al., 2006). The control group of mice did not receive oral antibiotics and were administered resveratrol intraperitoneally.

5.3. Pharmacokinetic analysis of resveratrol, R3G and R3S:

The area under the curve ($AUC_{0-\infty}$) was calculated based on the measured plasma concentrations of resveratrol, R3S and R3G using the linear trapezoidal method. Apparent clearance (CL/F) was calculated as Dose/$AUC_{0-\infty}$. Apparent volume of distribution (Vd_{β}/F) was calculated as $D/(\lambda \times AUC_{0-\infty})$. The terminal half-life was calculated as $\lambda /0.693$, where λ is the elimination rate constant. C_{max} and T_{max} were obtained from the pharmacokinetic profiles. AUC_{0-t} was the area calculated between 0 to 180 minutes. % AUC extrapolated was calculated using the following formula:

$$\% \text{ AUC extrapolated} = (AUC_{t-\infty} / AUC_{0-\infty})*100 \qquad \text{(Eq. 5.1)}$$

where,

$AUC_{t-\infty}$: area under the curve from the last time point to infinity, $AUC_{0-\infty}$: area under the curve from time 0 to infinity.

5.4. Results:

The concentration time profiles of resveratrol (fig. 5.2 (A), (B) and (C)), R3G (fig. 5.3 (A) and (B)) and R3S (fig.5.4 (A), (B) and (C)) with and without antibiotic treatment were constructed from the concentrations obtained from the plasma samples. The concentration time profiles of resveratrol (fig. 5.2(C)) and R3S (fig. 5.4(C)-both with antibiotics) both depict profiles for initial time points (t=0 to 180 minutes). (See appendix F 1 through F 3 for concentration time profiles for resveratrol, R3G and R3S where data is represented as replicates).

The kinetic parameters obtained are summarized in table 5.2. The apparent clearance obtained for resveratrol with and without antibiotics was 5.71ml/min/kg and 4.65ml/min/kg. Apparent volume of distribution for resveratrol with and without antibiotic was calculated to be 0.17l and 48.5l. The pharmacokinetic parameters calculated are summarized in table 5.2.

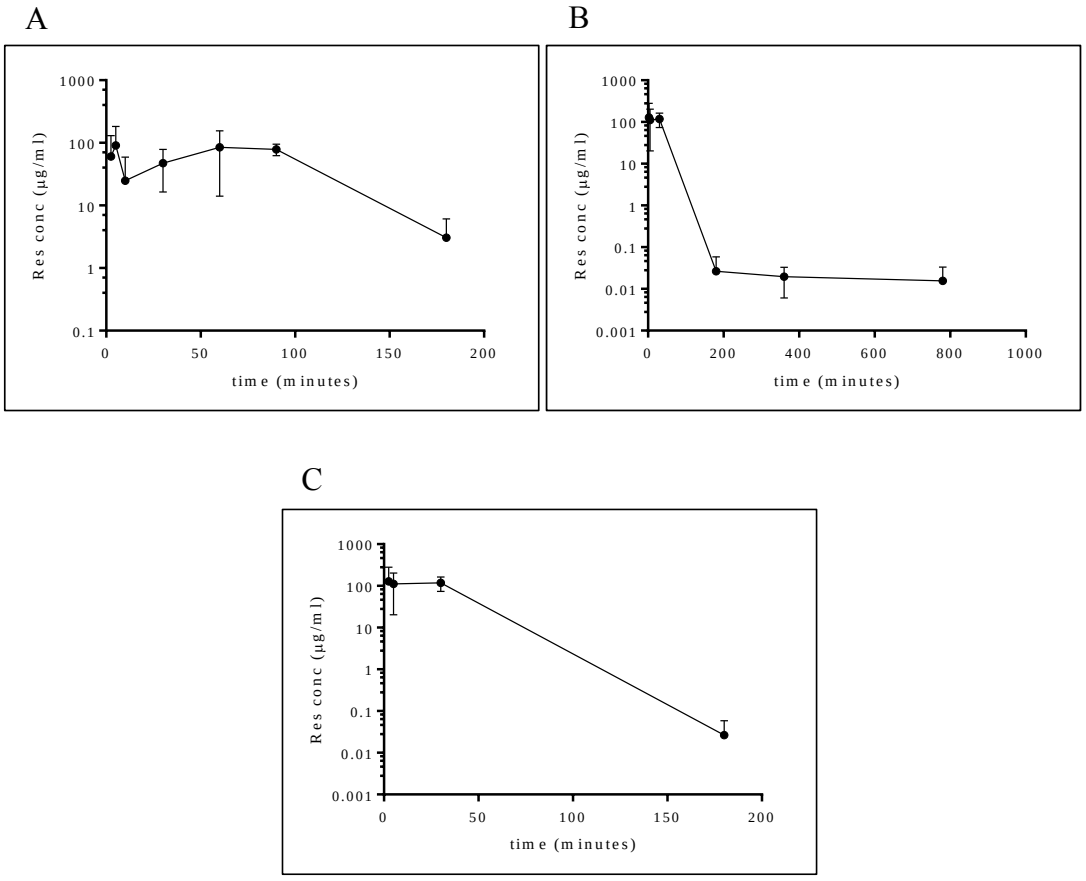

Figure 5.2. Concentration time profile of resveratrol (60mg/kg) (A) without Neo/Bac and (B) with Neo/Bac (20mg/kg and 10mg/kg) treatment (n=3, except for t=360, 780 minutes, where n=2, (C) with Neo/Bac treatment (fig. 5.2(C) depicts the initial time points (t=0-180 minutes) of fig. 5.2(B)).

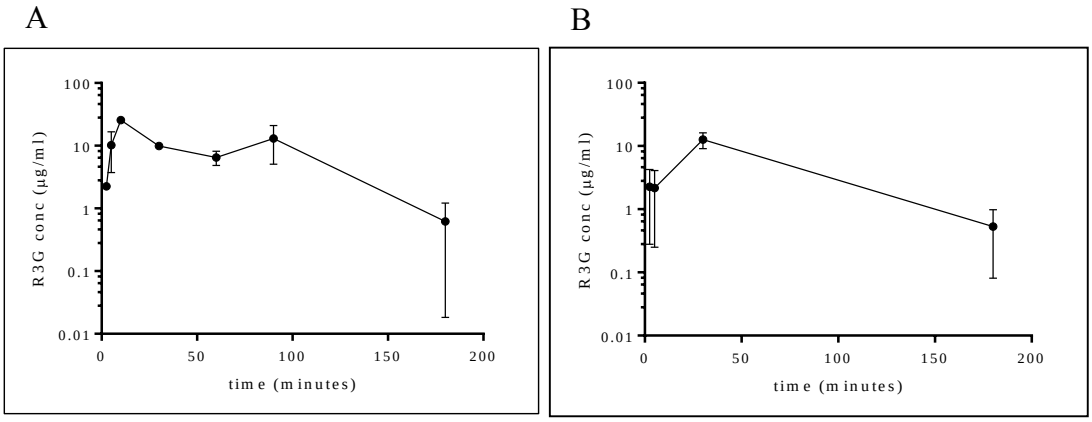

Figure 5.3. Concentration time profile of R3G (when resveratrol 60mg/kg-administered intraperitoneally) (A) without Neo/Bac and (B) with oral Neo/Bac (20mg/kg and 10mg/kg) treatment (n=3) except for t=360min, 780 minutes where n=2).

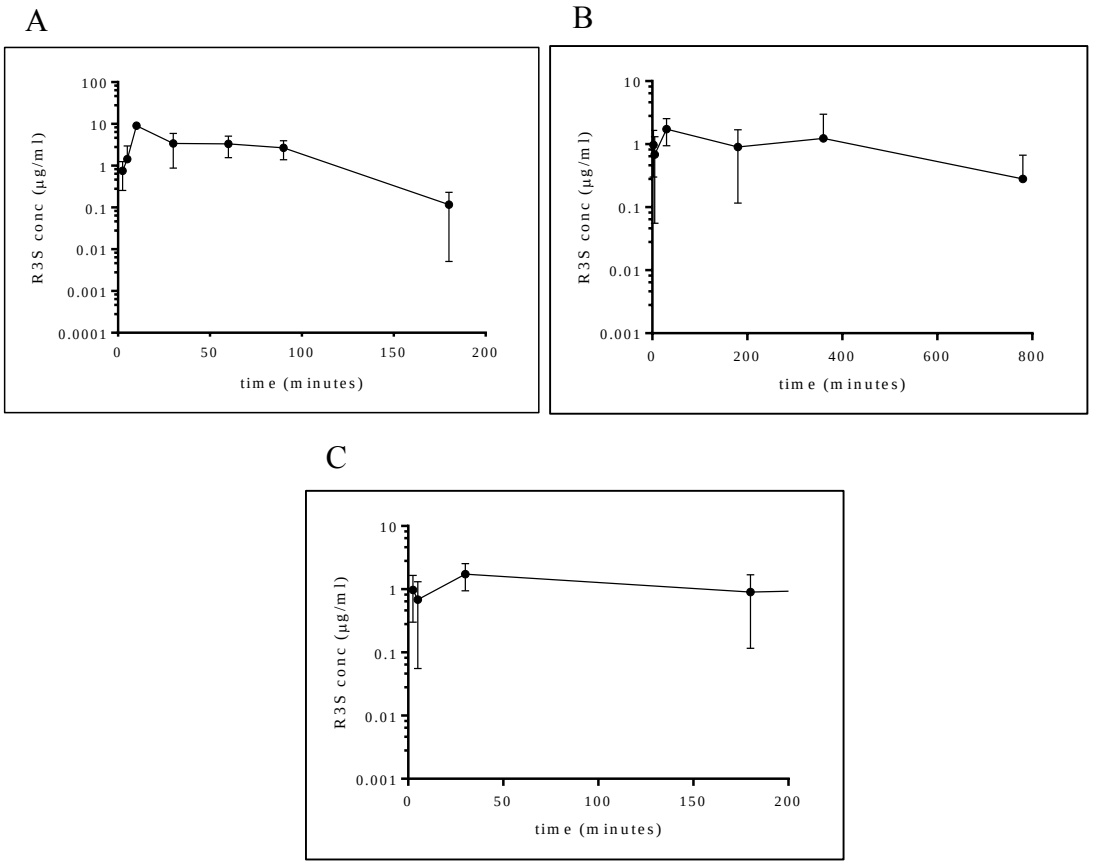

Figure 5.4. Concentration time profile of R3S (when resveratrol 60mg/kg-administered intraperitoneally) (A) without Neo/Bac (B) with Neo/Bac (20mg/kg and 10mg/kg) treatment (n=3, except for t=360, 780 minutes, where n=2, (C) with Neo/Bac treatment (fig. 5.4(C) depicts the initial time points (t=0-180 minutes) of fig. 5.4(B)).

Table 5.2 Noncompartmental pharmacokinetic analysis of resveratrol, R3G and R3S upon 60mg/kg i.p. of resveratrol, with and without antibiotic treatment.

	Resveratrol		R3G		R3S	
Parameter	No antibiotic	With antibiotic	No antibiotic	With antibiotic	No antibiotic	With antibiotic
C_{max} (μM)	398	561	63.5	31.3	29.5	5.64
T_{max} (min)	5	2.5	10	30	10	30
Cl/F ml/min/kg	5.71	4.85	--	--	--	--
Vd_{β}/F l/kg	0.168	48.5	--	--	--	--
$AUC_{0-\infty}$ mM.min	46.036	54.18	4.586	4.84	1.62	2.07
$M_{AUC0-\infty}$ $/D_{AUC0-\infty}$	--	--	0.099	0.089	0.035	0.038
AUC_{0-t} mM.min	46.035	53.5	4.57	4.54	1.55	1.83
$AUC_{t-\infty}$ mM.min	0.001	0.68	0.017	0.3	0.07	0.24
%AUC extrapolated	0.002	1.25	0.17	6.2	4.32	0.4
λ (min^{-1})	0.034	0.0001	0.019	0.02	0.018	0.003
$t_{1/2}$ (min)	20.38	6930	37.25	34.65	38.5	231

(--): parameter not calculated, $M_{AUC0-\infty}/D_{AUC0-\infty}$: ratio of $AUC_{0-\infty}$ of metabolite to $AUC_{0-\infty}$ of resveratrol

5.5 Discussion:

Resveratrol undergoes extensive metabolism to glucuronide and sulfate conjugates (Walle et al., 2004; Iwuchukwu et al., 2012). Resveratrol and R3G are known to undergo enterohepatic circulation in which R3G is converted back into the parent due to the action of intestinal β-glucuronidase and thus, is reabsorbed (Sharan et al., 2012). Enterohepatic recycling results in a distributional route rather than an elimination pathway. Inhibition of intestinal β-glucuronidase may thus alter the exposure of resveratrol and R3G. The exposure of resveratrol in the presence of β-glucuronidase inhibitor was assessed. Neomycin and bacitracin were selected because they have low systemic availability. Hence, the probability of systemic effects would be minimal. Resveratrol was rapidly absorbed on intraperitoneal administration. Although no second peaks were observed due to enterohepatic circulation, it has been confirmed in previous reports (Marier et al., 2002; Sharan et al., 2012). Similarly, gut sulfatases would be expected to deconjugate R3S leading to absorption of resveratrol back into systemic circulation. The plasma concentrations of resveratrol, R3G and R3S were monitored. The $AUC_{0-\infty}$ of resveratrol and R3G were expected to be affected due to interruption of enterohepatic circulation. Lower plasma concentrations for resveratrol, R3G and R3S were expected due increased fecal elimination of R3G and R3S.

An increased apparent volume of distribution of resveratrol and no change in $AUC_{0-\infty}$ of R3S and R3G on antibiotic treatment were not expected. The above data also shows an increase in $t_{1/2}$ of resveratrol and R3S in the antibiotic treated group. The change in resveratrol $t_{1/2}$ may be due to increase in apparent volume of distribution

(Vd_{β}/F) of resveratrol (increased from 0.17l to 48.5l). This change in apparent volume of distribution may be a reflection of pharmacokinetic analysis of a dataset with high variability in plasma concentrations. Hence, it may be useful to collect data using a serial sampling technique instead of serial sacrifice technique.

The $AUC_{0-\infty}$ of the metabolites remained unchanged (4.5mM.min to 4.84mM.min for R3G and 1.62mM.min to 2.07mM.min for R3S). This was opposed to the expected result, as inhibition of enterohepatic circulation would lead to a decrease in exposure of the metabolites. One of the possibilities for the mnimal change in $AUC_{0-\infty}$ of the metabolites is that the antibiotic treatment was ineffective in curbing the bacterial β-glucuronidase and sulfatase activity, thus not resulting in EHC inhibition. Another possibility is that the gut bacteria were able to recuperate during the antibiotic treatment. This might have resulted in the deconjugation of resveratrol metabolites and absorption of the parent.

Simulations performed using the pharmacokinetic model (chapter 6) will help to explain the extent of inhibition of enterohepatic circulation on antibiotic treatment (Sharan et al., 2012). This is further discussed in Chapter 6.

5.6 Conclusions:

The antibiotic treatment did not show a marked effect on the disposition of both, the resveratrol metabolites and resveratrol itself. The changes observed in the pharmacokinetic parameters such as apparent volume of distribution after antibiotic treatment were not expected and may be a reflection of variability in data. Simulations using the comprehensive pharmacokinetic model (discussed in chapter 6) may be able

to explain if the antibiotic treatment was effective in inhibiting enterohepatic circulation (Sharan et al., 2012).

5.7 Future directions:

Further studies could be performed in germ free animals. Germ free animals do not have gut microorganisms. The use of germ free mice and normal mice in a similar experimental design would provide a clearer picture of whether the antibiotics were effective in eliminating gut microbiota. Additionally, R3G and R3S could be dosed i.p. in antibiotic treated and germ free mice in order to obtain estimates of apparent volume of distribution and clearance of the metabolites. The combination of antibiotics used in this experiments could be changed or the antibiotics could be administered more frequently. Another way to study the impact of EHC is to perform a similar experiment in bile cannulated mice. Future experiments could involve 1. EHC in disease states such as Crohn's disease and ulcers or 2. effect of probiotics on EHC.

REFERENCES

Alimonti A, Gelibter A, Pavese I, Satta F, Cognetti F, Ferretti G, Rasio D, Vecchione A, and Di Palma M (2004) New approaches to prevent intestinal toxicity of irinotecan-based regimens. Cancer Treat Rev 30:555-562.

Alimonti A, Satta F, Pavese I, Burattini E, Zoffoli V, and Vecchione A (2003) Prevention of irinotecan plus 5-fluorouracil/leucovorin-induced diarrhoea by oral administration of neomycin plus bacitracin in first-line treatment of advanced colorectal cancer. Ann Oncol 14:805-806.

Beale J (2010) Wilson and Gisvold's Textbook of Organic Medicinal and Pharmaceutical Chemistry. LWW.

Beale JMJ (2004) Anti bacterial antibiotics, in: Wilson and Gisvold's Textbook of Organic Medicinal and Pharmaceutical Chemistry (John M. Beale JB, John M. Beale Jr. ed).

Beaugerie L and Petit JC (2004) Microbial-gut interactions in health and disease. Antibiotic-associated diarrhoea. Best Pract Res Clin Gastroenterol 18:337-352.

Carter JH, Mclafferty MA, and Goldman P (1980) Role of the Gastrointestinal Microflora in Amygdalin (Laetrile)-Induced Cyanide Toxicity. Biochem Pharmacol 29:301-304.

Coates ME (2005) The use of gnotobiotic animals in studies of toxicology, in: Role of gut bacteria in human toxicology and pharmacology.

Donald Voet JGV, Charlotte W. Pratt (2012) Principles of Biochemistry. E.Hall J (2016) Guyton and Hall Textbook of Medical physiology.Saunders.

Eyssen HJ, Parmentier GG, and Mertens JA (1976) Sulfate bile acids in germ-free and conventional mice. Eur J Biochem 66:507-514.

Gadelle D, Raibaud P, and Sacquet E (1985) beta-Glucuronidase activities of intestinal bacteria determined both in vitro and in vivo in gnotobiotic rats. Appl Environ Microbiol 49:682-685.

Ghosh D (2005) Three-dimensional structures of sulfatases. Methods Enzymol 400:273-293.

Gorbach S (1996) Medical Microbiology.

Guarner F and Malagelada JR (2003) Gut flora in health and disease. Lancet 361:512-519.

Gustafsson BE and Lanke LS (1960) Bilirubin and urobilins in germfree, ex-germfree, and conventional rats. J Exp Med 112:975-981.

Hill MJ (2005) The metabolic activity of gut bacteria, in: Role of gut bacteria in human toxicology and pharmacology.

Iwuchukwu OF, Sharan S, Canney DJ, and Nagar S (2012) Analytical method development for synthesized conjugated metabolites of trans-resveratrol, and application to pharmacokinetic studies. J Pharm Biomed Anal 63:1-8.

Kehrer DF, Sparreboom A, Verweij J, de Bruijn P, Nierop CA, van de Schraaf J, Ruijgrok EJ, and de Jonge MJ (2001) Modulation of irinotecan-induced diarrhea by cotreatment with neomycin in cancer patients. Clin Cancer Res 7:1136-1141.

Marier JF, Vachon P, Gritsas A, Zhang J, Moreau JP, and Ducharme MP (2002) Metabolism and disposition of resveratrol in rats: extent of absorption,

glucuronidation, and enterohepatic recirculation evidenced by a linked-rat model. J Pharmacol Exp Ther 302:369-373.

Marill J, Capron CC, Idres N, and Chabot GG (2002) Human cytochrome P450s involved in the metabolism of 9-cis- and 13-cis-retinoic acids. Biochem Pharmacol 63:933-943.

Marzo A, Monti NC, and Vuksic D (1999) Experimental, extrapolated and truncated areas under the concentration-time curve in bioequivalence trials. Eur J Clin Pharmacol 55:627-631.

Morton DB, Abbot D, Barclay R, Close BS, Ewbank R, Gask D, Heath M, Mattic S, Poole T, Seamer J, Southee J, Thompson A, Trussell B, West C and Jennings M (1993) Removal of blood from laboratory mammals and birds. First report of the BVA/FRAME/RSPCA/UFAW Joint Working Group on Refinement. Lab Anim 27:1-22.

Naz H, Islam A, Waheed A, Sly WS, Ahmad F, and Hassan I (2013) Human beta-glucuronidase: structure, function, and application in enzyme replacement therapy. Rejuvenation Res 16:352-363.

Parenti G, Meroni G, and Ballabio A (1997) The sulfatase gene family. Curr Opin Genet Dev 7:386-391.

Periti P, Mazzei T, Mini E, and Novelli A (1992) Pharmacokinetic drug interactions of macrolides. Clinical Pharmacokinetics 23:106-131.

Roberts MS, Magnusson BM, Burczynski FJ, and Weiss M (2002) Enterohepatic circulation - Physiological, pharmacokinetic and clinical implications. Clinical Pharmacokinetics 41:751-790.

Sardiello M, Annunziata I, Roma G, and Ballabio A (2005) Sulfatases and sulfatase modifying factors: an exclusive and promiscuous relationship. Hum Mol Genet 14:3203- 3217.

Sears CL (2005) A dynamic partnership: celebrating our gut flora. Anaerobe 11:247-251.

Sharan S, Iwuchukwu OF, Canney DJ, Zimmerman CL, and Nagar S (2012) In vivo-formed versus preformed metabolite kinetics of trans-resveratrol-3-sulfate and trans- resveratrol-3-glucuronide. Drug Metab Dispos 40:1993-2001.

Sperker B, Backman JT, and Kroemer HK (1997) The role of beta-glucuronidase in drug disposition and drug targeting in humans. Clinical Pharmacokinetics 33:18-31.

Takasuna K, Hagiwara T, Watanabe K, Onose S, Yoshida S, Kumazawa E, Nagai E, and Kamataki T (2006) Optimal antidiarrhea treatment for antitumor agent irinotecan hydrochloride (CPT-11)-induced delayed diarrhea. Cancer Chemother Pharmacol 58:494-503.

Tvrdonova M, Dedik L, Mircioiu C, Miklovicova D, and Durisova M (2009) Physiologically motivated time-delay model to account for mechanisms underlying enterohepatic circulation of piroxicam in human beings. Basic Clin Pharmacol Toxicol 104:35-42.

Ulmer JE, Vilen EM, Namburi RB, Benjdia A, Beneteau J, Malleron A, Bonnaffe D, Driguez PA, Descroix K, Lassalle G, Le Narvor C, Sandstrom C, Spillmann D, and Berteau O (2014) Characterization of glycosaminoglycan (GAG) sulfatases from the human gut symbiont Bacteroides thetaiotaomicron reveals the first GAG-specific bacterial endosulfatase. J Biol Chem 289:24289-24303.

Van Eldere JR, De Pauw G, and Eyssen HJ (1987) Steroid sulfatase activity in a Peptococcus niger strain from the human intestinal microflora. Appl Environ Microbiol 53:1655-1660.

Vedantam G and Hecht DW (2003) Antibiotics and anaerobes of gut origin. Curr Opin Microbiol 6:457-461.

Walle T, Hsieh F, DeLegge MH, Oatis JE, Jr., and Walle UK (2004) High absorption but very low bioavailability of oral resveratrol in humans. Drug Metab Dispos 32:1377-1382.

Zweier JL (1988) Measurement of superoxide-derived free radicals in the reperfused heart. Evidence for a free radical mechanism of reperfusion injury. J Biol Chem 263:1353-1357.

CHAPTER 6

SIMULATING THE IMPACT OF TRANSPORTER AND ENTEROHEPATIC CIRCULATION INHIBITION ON THE DISPOSITION OF RESVERATROL AND ITS MAJOR METABOLITES

6.1. Background:

A comprehensive model had been previously developed in our laboratory to study the disposition of resveratrol, resveratrol-3-glucuronide (R3G) and resveratrol-3-sulfate (R3S) (Sharan et al., 2012). In the present study, this model was used to simulate transporter and enterohepatic circulation (EHC) inhibition scenarios. Using the simulated data generated by the comprehensive pharmacokinetic model, possible explanations for observed changes in AUCs (area under the curve) of resveratrol and its metabolites observed in the experimental data (Chapters 4 and 5) were sought. Resveratrol is metabolized extensively in vivo (Walle et.al. 2004). Resveratrol and R3G undergo enterohepatic circulation. β-glucuronidase in intestine is responsible for converting R3G into resveratrol, which may be reabsorbed by the enterocytes. The role of transporters in the disposition of resveratrol, R3G and R3S is increasingly being recognized. Modulation of β- glucuronidase and transporters may change the pharmacokinetic profiles of resveratrol and R3G.

6.1.1 Simulation:

Simulation is a recognized and effective tool to predict drug concentrations in plasma and tissues (Chien et al., 2005). The impact of modeling and simulation on decision-making and drug development is dependent on questions being asked and the

quality and availability of data. Modeling and simulation thus help explain the uncertainty in data and use the data to decide the plausible range of dose and predict the concentrations which may be achieved (Chien et al., 2005). Advances in predicting human pharmacokinetics served to reduce the rate of drug failure in clinical trials (Schuck et al., 2015). PK/PD (pharmacokinetic/pharmacodynamic) modeling can thus provide a better understanding of drug efficacy at the preclinical stage of drug development (Chien et al., 2005; Schuck et al., 2015).

6.1.2 Description of the comprehensive model:

The pharmacokinetic model (fig. 6.1) was built to characterize the pharmacokinetic profile of resveratrol, in vivo formed R3G and R3S (Sharan et al., 2012).

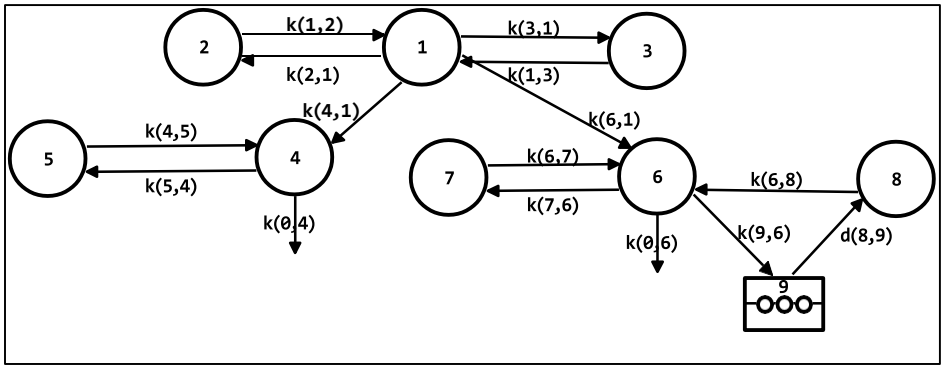

Figure 6.1. Compartmental model of intra arterially administered resveratrol (15mg/kg) and in vivo formed R3G and R3S.

The primary condition of this model was that the clearance of preformed metabolites is different than in vivo formed metabolites (Sharan et al., 2012). All the

parameters used in this model, except the formation rates of R3G [k(6,1)] and R3S [k(4,1)], and elimination rate of R3G [k(0,6)] and R3S [k(0,4)], were derived from three separate models for intra-arterial dosing of resveratrol (15mg/kg), R3G (3.5mg/kg) and R3S (5mg/kg) (Sharan et al., 2012).

The pharmacokinetics of resveratrol was explained by a three compartment open model, compartment 1 being the central compartment and compartments 2, 3 being the peripheral compartments (fig. 6.1) (Sharan et al., 2012). The model assumes that resveratrol is exclusively metabolized into R3S and R3G and no other pathways for elimination of resveratrol exist. The pharmacokinetics of i.a. administered R3S was explained by a two compartment open model with compartment 4 being the central compartment (for rapidly equilibrating tissues) and compartment 5 being the peripheral compartment (for slowly equilibrating tissues) (fig. 6.1) (Sharan et al., 2012). The pharmacokinetics of i.a. administered R3G was described using a three compartment open model. In this model, compartment 6 was the central compartment while compartments 7 and 8 were the peripheral compartments. To account for the enterohepatic circulation, which was characterized by the appearance of a second peak at about 180 minutes in the i.a. dosing studies, a delay compartment was added to the model. Hence, for R3G, compartment 6 comprised of rapid equilibrating tissues, compartment 7 comprised of slowly equilibrating tissues and compartment 8 represented the intestinal compartment from which R3G would be absorbed back into compartment 6. The rate constant [k(9,6)] may be thought of as a pooled rate constant which comprised of the rate of biliary excretion, transit through the intestine, deconjugation of R3G into resveratrol and the eventual uptake of R3G and resveratrol (Sharan et al., 2012).

6.2 Experimental section:

6.2.1 Methods:

Using the comprehensive model, we assessed the possible mechanistic reason for the change in disposition of resveratrol, R3G and R3S in presence of mrp2, bcrp and EHC inhibitors. The observed data for mrp2 and bcrp inhibition was obtained by i.p. administration of mrp2 and bcrp inhibitors in mice. MK571 and Ko143 were used as mrp2 and bcrp inhibitors respectively. The inhibitors were administered 30 min prior to i.p. administration of resveratrol. The plasma concentrations of resveratrol, R3S and R3G were monitored using LC-MS/MS (for experimental and analytical details see chapter 4, sections 4.2 through 4.7). A combination of antibiotics (neomycin and bacitracin) was given orally from 4 days prior to i.p. administration of resveratrol for the study involving EHC inhibition. The plasma concentrations of resveratrol, R3S and R3G were monitored using LC-MS/MS (for experimental details see section 5.2.2 and 5.2.3). For the control group mice, resveratrol was administered i.p. without any prior treatment. The plasma concentration data obtained from the above experiments was used to perform simulations. The simulations were performed by varying one parameter at a time in order to match resveratrol, R3S and R3G AUCs. All the simulations were performed using SAAM 2 software (version 6.2, Charlottesville, VA).

6.2.1.1 Simulation for control group mice:

Simulation for control group (i.p. administration of resveratrol without any treatment) was performed using observed pharmacokinetic data for resveratrol, R3S and

R3G (see section 5.4, fig. 5.2(A), 5.3(A), 5.4(A), table 5.2). The parameters used in this simulation are listed in table 6.1.

Table 6.1 List of parameters used for simulation for control group

Table 6.1	
Parameter	Value
V_R3G (l/kg)	100.6
V_R3S (l/kg)	501.86
k(0,4) (min^{-1})	0.2
k(0,6) (min^{-1})	0.2
k(1,2) (min^{-1})	0.6
k(1,3) (min^{-1})	0.014
k(2,1) (min^{-1})	0.147
k(3,1) (min^{-1})	0.009
k(4,1) (min^{-1})	0.014
k(4,5) (min^{-1})	0.012
k(5,4) (min^{-1})	0.15
k(6,1) (min^{-1})	0.015
k(6,7) (min^{-1})	0.030
k(6,8) (min^{-1})	0.002
k(7,6) (min^{-1})	0.040
k(9,6) (min^{-1})	0.072
Vc (l/kg)	201.57

6.2.1.2 Simulation for mrp2 inhibition in mice:

Simulations were performed using observed plasma concentrations of resveratrol, R3S and R3G in presence of mrp2 inhibitor (MK571) in mice (see section 4.4, fig 4.1(B) 4.2(B), 4.3(B), table 4.4). Decrease in biliary excretion of resveratrol-disulfate, R3S and R3G has been reported in mrp2 knockout mice (Maier-Salamon et al., 2013). The simulations were performed with an understanding that the elimination rate constant of

R3G and R3S will be altered in presence of mrp2 inhibitor (fig. 6.2). Hence, the elimination rate constant for R3S [k(0,4)] and R3G [k(0,6)] were varied.

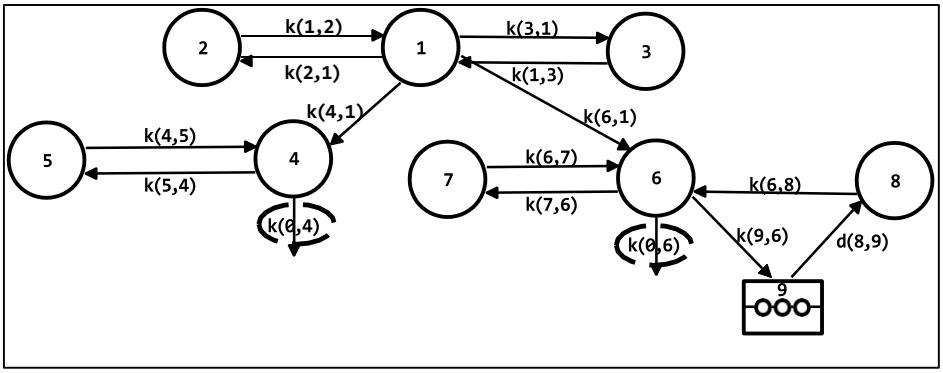

Figure 6.2. Compartmental model used to perform simulations for i.p. administered resveratrol and in vivo formed R3S and R3G in presence of mrp2 inhibitor. The dashed circled rate constants [k(0,4)] and [k(0,6)] were varied in this simulation.

The range tried for [k(0,4)] and [k(0,6)] was from 0.01-0.2. The simulated concentrations for resveratrol, R3S and R3G were obtained from SAAM 2 software. $AUC_{0-\infty}$ for observed as well as simulated concentrations was measured in Microsoft Excel® using the linear trapezoidal rule.

6.2.1.3 Simulation for bcrp inhibition in mice:

Simulations were performed using observed plasma concentrations of resveratrol, R3S and R3G in presence of bcrp2 inhibitor (Ko143) in mice (see section 4.4, fig 4.1(C) 4.2(C), 4.3(C), table 4.5). R3G, R3S and resveratrol-disulfate have been previously reported to be transported by BCRP in transport vesicle experiments (van de Wetering et al., 2009). The simulations were performed by decreasing the elimination rate constants

for R3S [k(0,4)] and R3G [k(0,6)], which would be due to inhibition of bcrp (fig. 6.3, table 6.3).

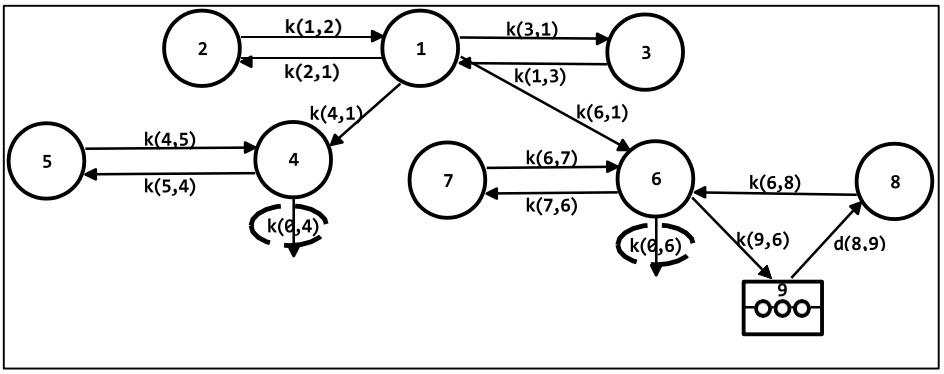

Figure 6.3. Compartmental model used to perform simulations for i.p. administered resveratrol and in vivo formed R3S and R3G in presence of bcrp inhibitor. The dashed circled rate constants [k(0,4)] and [k(0,6)] were varied in this simulation.

The range tried for [k(0,4)] and [k(0,6)] was from 0.01-0.2. The simulated concentrations for resveratrol, R3S and R3G were obtained from SAAM 2 software. $AUC_{0-\infty}$ for observed as well as simulated concentrations was measured in Microsoft Excel® using the trapezoidal rule.

6.2.1.4 Simulation for EHC inhibition in mice:

Simulations were performed using observed plasma concentrations of resveratrol, R3S and R3G in presence of antibiotics (Neo/Bac) in mice (see section 5.4, fig 5.2(B), 5.3(B), 5.4(B), table 5.2). Several parameters were changed in the PK model to simulate EHC inhibition. The simulated concentrations for resveratrol, R3S and R3G were obtained from SAAM 2 software. The $AUCs_{0-\infty}$ were calculated in Microsoft Excel®

using the trapezoidal rule. Four scenarios were considered by changing the rate constants in the pharmacokinetic model. The four scenarios were as follows:

1st scenario: EHC rate constant [k(9,6)] (rate constant for delay compartment) was decreased (from 0.073 to 0.0073), elimination rate constants for R3G and R3S were decreased and the formation rate constants of R3G and R3S were changed (fig. 6.4). The rate constant [k(9,6)] represents EHC and hence was decreased to simulate inhibition of EHC.

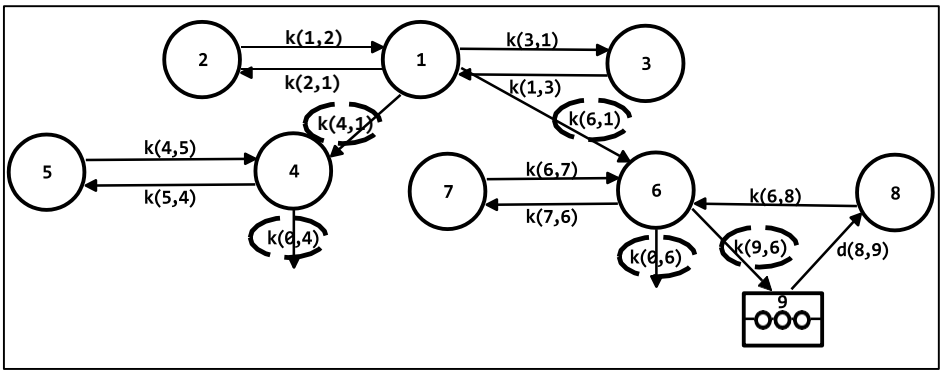

Figure 6.4. (Scenario 1) Compartmental model used to perform simulations for i.p. administered resveratrol and in vivo formed R3S and R3G in presence of antibiotics. The dashed circled rate constants [k(0,4)] and [k(0,6)], [k(6,1)], [k(4,1)] and [k(9,6)] were varied in this simulation.

Several parameters were varied in this simulation. The elimination rate constants [k(0,4)] and [k(0,6)] were varied from 0.01-0.2. The formation rate constants for R3S [k(4,1)] was varied from 0.0024-0.014 while the formation rate constant for [k(6,1)] was

varied from 0.0056-0.0086. The rate constant which depicts EHC [k(9,6)], was decreased 10 fold to 0.007.

2nd scenario: EHC rate constant was decreased (from 0.073 to 1.7x 10^{-6}), the formation rates for R3S [k(4,1)] and R3G [k(6,1)] were varied from 0.005-0.014 and 0.001-0.02 respectively. The elimination rate constants for R3G [k(0,6)] and R3S [k(0,4)] were varied from 0.1-0.2. The rate constant [k(9,6)] was decreased further to (1.7 x 10^{-6}) simulate complete inhibition of EHC (fig. 6.5).

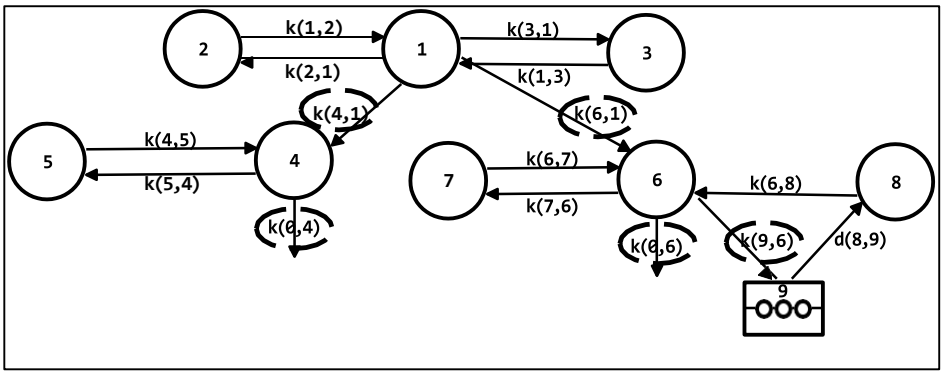

Figure 6.5. (Scenario 2) Compartmental model used to perform simulations for i.p. administered resveratrol and in vivo formed R3S and R3G in presence of antibiotics. The dashed circled rate constants [k(0,4)] and [k(0,6)], [k(6,1)], [k(4,1)] and [k(9,6)] were varied in this simulation.

3rd scenario: A rate constant was added to include reversible transfer [k(1,6)] for resveratrol and R3G from central compartments of each compounds (fig. 6.6). The rate constant for EHC was kept at (1.7x 10^{-6}). Additionally, a rate constant was added to represent the elimination of unchanged resveratrol [k(0,1)]. The distributional rate

constants (between the central compartment and the peripheral compartment) [k(1,3)], [k(3,1)] for resveratrol were changed, elimination rate constant for R3S [k(0,4)], R3G [k(0,6)] and the formation rate constants for R3S [k(4,1)], R3G [k(6,1)] were changed.

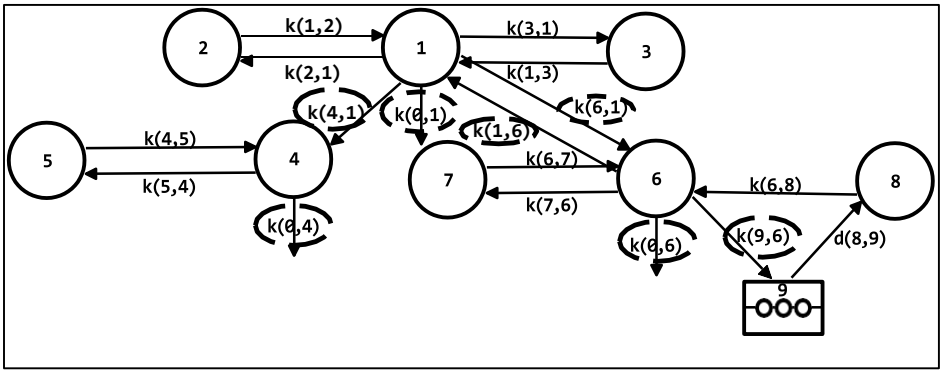

Figure 6.6. (Scenario 3) Compartmental model used to perform simulations for i.p. administered resveratrol and in vivo formed R3S and R3G in presence of antibiotics. The dashed circled rate constants [k(4,1)], [k(6,1)], [k(0,4)], [k(0,6)], [k(9,6)] were varied in this simulation. The rate constants [k(0,1)] and [k(6,1)] were added.

The rate constants [k(1,3)] and [k(3,1)] were varied from 0.1-0.2 and 0.05-0.2 respectively.

4th scenario: EHC rate constant was decreased (from 0.073 to 1.7x 10^{-6}), the distributional rate constants (between the central compartment and the peripheral compartment) [k(1,3)], [k(3,1)] for resveratrol were changed, elimination rate constant for R3S [k(0,4)], R3G [k(0,6)] and the formation rate constants for R3S [k(4,1)], R3G [k(6,1)] were changed. A rate constant for elimination for resveratrol was added to the resveratrol

central compartment to include the possibility of resveratrol excreted unchanged [k(0,1)] (fig. 6.7).

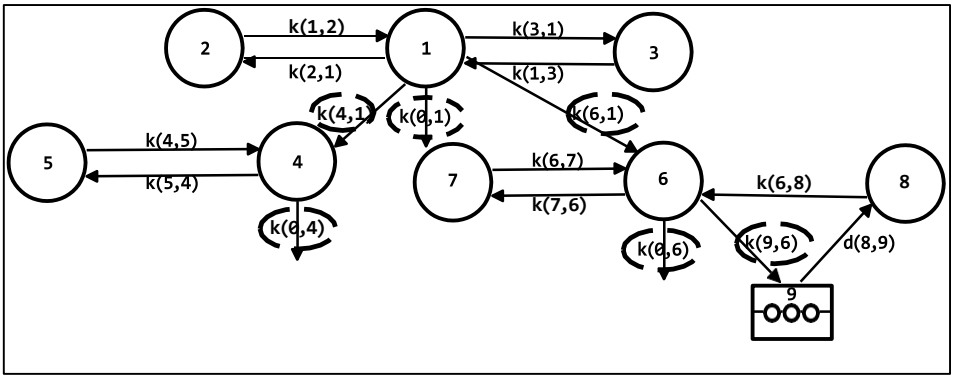

Figure 6.7. (Scenario 4) Compartmental model used to perform simulations for i.p. administered resveratrol and in vivo formed R3S and R3G. The dashed circled rate constants [k(0,4)], [k(0,6)], [k(6,1)], [k(4,1)], [k(9,6)], [k(3,1)], [k(1,3)] and [k(9,6)] were varied in this simulation. The rate constant for elimination of unchanged resveratrol marked by dotted circle was added [k(0,1)].

The elimination rate constant for unchanged resveratrol was varied from 0.07-0.1. The distribution rate constants [k(1,3)] was varied from 0.001-0.01 while [k(3,1)] was decreased by 10 fold (from 0.0094-0.00094).

6.3 Calculation of errors:

The sum of squared errors was computed by calculating the error sum of squares (SSE) of the difference between the observed and simulated concentrations. The following equation was used to calculate SSE:

$$SSE = \sum_{i=1}^{N} (x_o - x_e)^2 \qquad \text{(Eq.6.1)}$$

where,

Xo : observed plasma concentration, Xe : estimated plasma concentration (obtained from simulation).

6.4 Results:

6.4.1 Simulation for control group mice:

The simulations for control group mice (resveratrol dosing only) were performed using the observed plasma profiles of resveratrol, R3S and R3G (fig. 6.8). The parameters obtained from the simulation are listed in table 6.1.

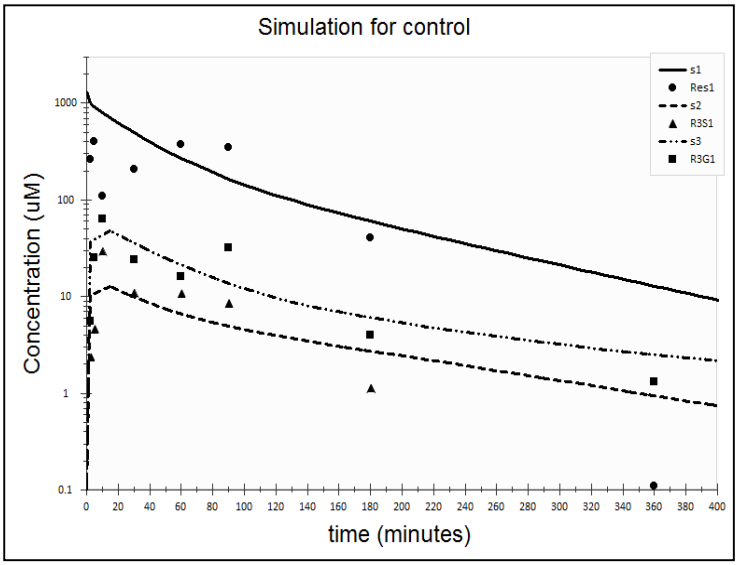

Figure 6.8. Observed and simulated plasma concentration time profiles for control group mice (resveratrol dosing only). Observed data represented as mean values.

6.4.2 Simulation for mrp2 inhibition:

The parameters varied to simulate resveratrol, R3S and R3G plasma concentration time profiles in presence of mrp2 inhibitor (fig. 6.9) are listed in table 6.2

Table 6.2 List of parameters varied to simulate resveratrol, R3S and R3G profile in the presence of mrp2 inhibitor.

Parameters changed	Control value (from table 6.1) (min^{-1})	Simulated value (for fig. 6.9) (min^{-1})	SSE for resveratrol
k(0,4)	0.2	0.1	$1x\ 10^6$
k(0,6)	0.2	0.1	

SSE: errors sum of squares

The elimination rate constants for both metabolites, R3S and R3G were varied. The simulated profiles for R3S and R3G overlaid the observed plasma profiles for R3S and R3G in presence of mrp2 inhibitor (fig. 6.9). Hence, it is likely that the inhibitors lacked systemic effects other than desired transporter inhibition.

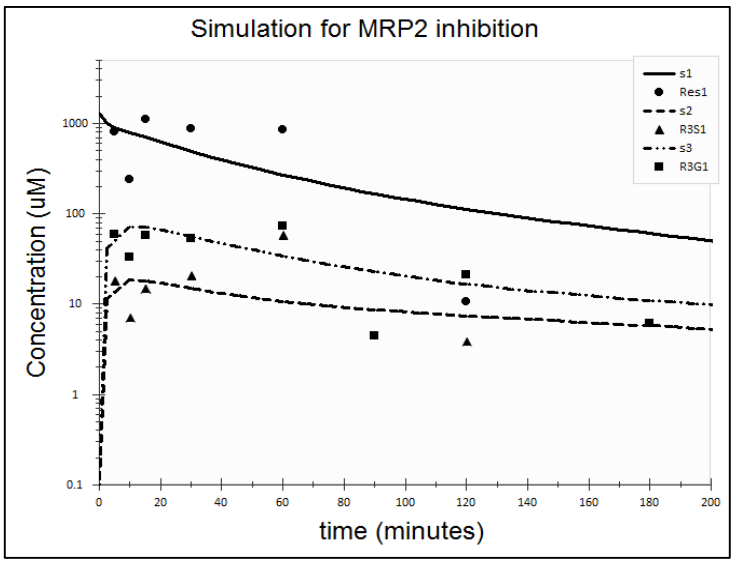

Figure 6.9. Observed and simulated plasma concentration time profiles for resveratrol, R3S and R3G in mice in the presence of mrp2 inhibitor. MK571 was used as mrp2 inhibitor. Observed data represented as mean values.

The observed plasma profile for resveratrol in the presence of mrp2 inhibitor did not agree with the initial part of the simulated profile.

6.4.3 Simulations for bcrp inhibition:

The parameters varied to simulate resveratrol, R3S and R3G plasma profile in presence of bcrp inhibitor (fig. 6.10) are listed in table 6.3.

Table 6.3 List of parameters varied to simulate resveratrol, R3S and R3G profile in the presence of bcrp inhibitor.

Parameters changed	Control value (from table 6.1) (min^{-1})	Simulated value (for fig. 6.10) (min^{-1})	SSE for resveratrol
k(0,4)	0.2	0.041	3×10^5
k(0,6)	0.2	0.093	

SSE: errors sum of squares

The elimination rate constants were varied for both metabolites, R3S and R3G. The final values of elimination rate constants for R3S and R3G obtained by simulations were lower than those obtained for mrp2 simulations. Although, this might indicate that bcrp inhibition has more impact on plasma concentrations of the three compounds, the variability in observed data should be considered.

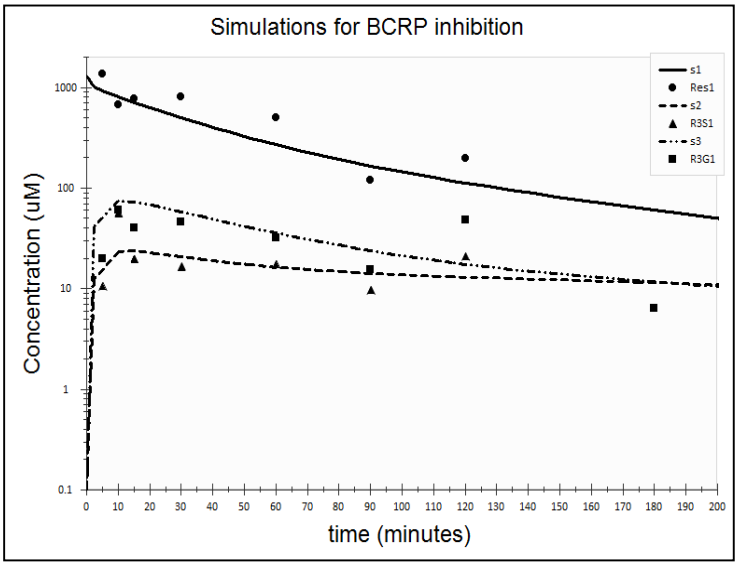

Figure 6.10. Observed and simulated plasma concentration time profiles for resveratrol, R3S and R3G in mice in the presence of bcrp inhibitor. Ko143 was used as bcrp inhibitor. Observed data represented as mean values.

The changes made in the elimination rate constants seemed to overlay the simulated profiles for R3S and R3G on the observed plasma profiles for R3S and R3G in presence of bcrp inhibitor and so, the model seemed to work for in vivo formed metabolites. Hence, it could be likely that the inhibitors lacked systemic effects other than the desired transporter inhibition effect. Here again, the simulated resveratrol profile did not help explain the initial part of the observed profile in presence of bcrp inhibitor.

6.4.4 Simulations for EHC inhibition:

As mentioned in section 6.2.1, orally administered combination of antibiotics (neomycin and bacitracin) were used to inhibit bacterial β-glucuronidase in the mouse intestine. The parameters varied to simulate resveratrol, R3S and R3G plasma profile in presence of antibiotics (fig. 6.11 through 6.14) are listed in tables 6.4 through 6.7. Four scenarios were considered while performing simulations for EHC inhibition and these scenarios are detailed below.

1st Scenario: The parameters varied in this simulation are detailed in table 6.4.

Table 6.4. List of parameters varied to simulate EHC inhibition (Scenario 1).

Parameters changed	Control value (from table 6.1) (min^{-1})	Simulated value(for fig. 6.11) (min^{-1})	SSE for resveratrol
k(0,4)	0.2	0.08	4.5×10^5
k(0,6)	0.2	0.295	
k(9,6)	0.07	0.0073	
k(4,1)	0.014	0.0054	
k(6,1)	0.0096	0.0086	

SSE: sum of squared errors

In this simulation, 5 parameters were varied. The rate constant for EHC [k(9,6)] was decreased 10 fold simulate incomplete inhibition of bacterial β-glucuronidase and EHC. The elimination rate constant for R3G was increased to portray EHC inhibition. Other parameters were varied in order to match AUCs of the three compounds. The plasma profiles for resveratrol, R3S and R3G obtained in this simulation was compared with the experimentally observed plasma profiles for resveratrol, R3S and R3G (fig. 6.11).

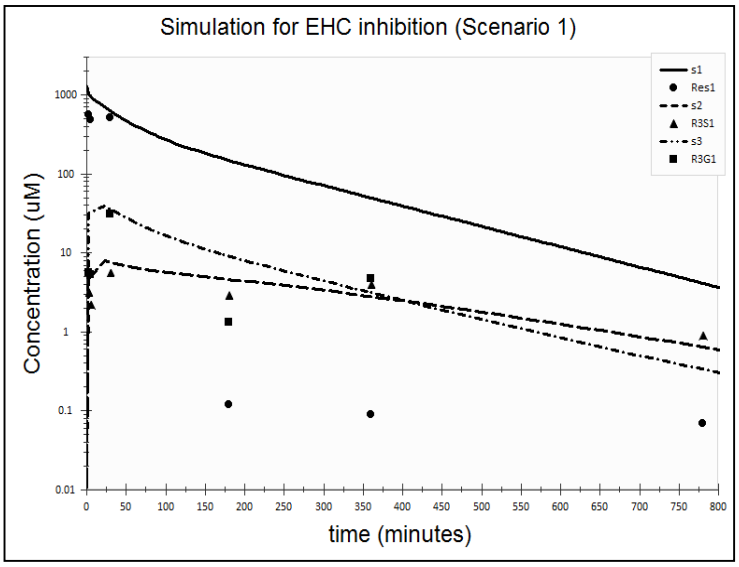

Figure 6.11. (Scenario 1) Observed and simulated plasma profiles for resveratrol, R3S and R3G in mice in the presence of antibiotics. A combination of Neo/bac was used for EHC inhibition. Observed data represented as mean values.

The simulated profile of R3S and R3G seemed to capture the observed data points, which was not the case for resveratrol. This may be due to either antibiotics having a greater impact on decreasing the resveratrol concentrations than predicted by this simulation, or due to the lack of rich data set for EHC inhibition. The AUCs for

resveratrol and R3G obtained from simulated concentrations were about 2 fold higher than those obtained from observed data (table 6.8).

2nd Scenario: The parameters varied in this simulation are detailed in table 6.5. In this simulation, the rate constant for EHC was lowered further to simulate complete inhibition of EHC. The simulated profiles for resveratrol, R3S and R3G were compared with the experimentally observed plasma profiles (fig. 6.12).

Table 6.5. List of parameters varied to simulate EHC inhibition (Scenario 2)

Parameters changed	Control value (from table 6.1) (min^{-1})	Simulated value (from fig. 6.12) (min^{-1})	SSE for resveratrol
k(0,6)	0.2	0.25	5.1×10^{5}
k(0,4)	0.2	0.15	
k(4,1)	0.014	0.0071	
k(6,1)	0.015	0.0043	
k(9,6)	0.07	1.7×10^{-6}	

SSE: sum of squared errors

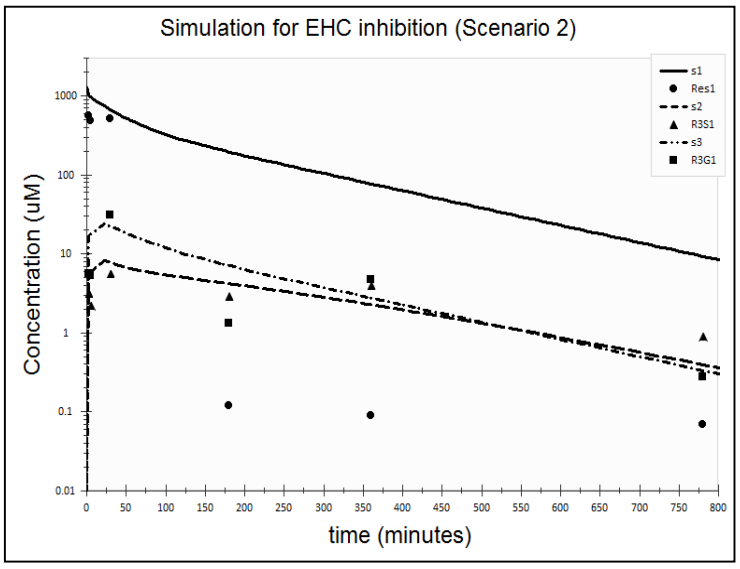

Figure 6.12. (Scenario 2) Observed and simulated plasma profiles for resveratrol, R3S and R3G in mice in the presence of antibiotics. A combination of Neo/bac was used for EHC inhibition. Observed data represented as mean values.

In this simulation, the simulated profile for R3S and R3G captured the observed data points. As for the simulation for resveratrol, it failed to capture the observed plasma profile. This may indicate that disruption of EHC has more effect on resveratrol concentrations than R3S and R3G but considering the lack of rich data, such conclusions must be made with caution. The $AUC_{0-\infty}$ for resveratrol and R3G obtained from simulated concentrations were about 2 fold higher than those obtained from the observed data (table 6.8).

3rd Scenario: The parameters varied in this simulation are detailed in table 6.6. In this simulation, an additional rate constant was added between the compartments 1 and 6.

This was done in order to simulate conversion of R3G into resveratrol and its return into systemic circulation.

Table 6.6 List of parameters varied to simulate EHC inhibition (Scenario 3).

Parameters changed	Control value (from table 6.1) (min^{-1})	Simulated value (for fig. 6.13) (min^{-1})	SSE for resveratrol
k(0,6)	0.2	0.093	1.66×10^{5}
k(0,4)	0.2	0.2	
k(0,1)	-	0.0001	
k(1,3)	0.014	0.144	
k(1,6)	-	0.001	
k(3,1)	0.009	0.094	
k(4,1)	0.014	0.044	
k(6,1)	0.015	0.0005	
k(9,6)	0.07	1.7×10^{-6}	

SSE: sum of squared errors

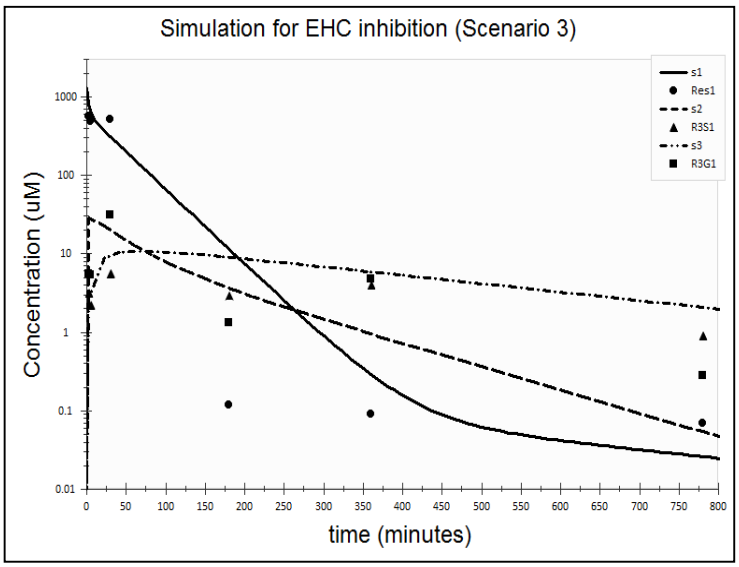

Figure 6.13. (Scenario 3) Observed and simulated plasma profiles for resveratrol, R3S and R3G in mice in the presence of antibiotics. A combination of Neo/bac was used for EHC inhibition. Observed data represented as mean values.

This simulation has two additional parameters, a rate constant for elimination of unchanged resveratrol [k(0,1)] and a rate constant for conversion of R3G into resveratrol. Although, the AUC calculated from simulated and observed concentrations was within 2 fold (table 6.8), the plasma profiles for resveratrol, R3S and R3G did not seem to capture the experimentally observed plasma profiles (fig. 6.13).

4th Scenario: The parameters varied in this simulation are detailed in table 6.7. In this simulation, apart from varying the elimination and formation rate constants of R3S and R3G, the distributional rate constants of resveratrol were varied. In addition to this, a rate constant for elimination of unchanged resveratrol was added to the model. The plasma

profiles obtained in this simulation were compared with the experimentally observed profiles for all the three compounds (fig. 6.14).

Table 6.7. List of parameters varied to simulate EHC inhibition (Scenario 4).

Parameters changed	Control value (from table 6.1) (min^{-1})	Simulated value (for fig. 6.14) (min^{-1})	SSE for resveratrol
k(0,1)	-	0.07	3×10^{5}
k(0,4)	0.2	0.015	
k(0,6)	0.2	0.019	
k(3,1)	0.0094	0.00094	
k(4,1)	0.014	0.0075	
k(6,1)	0.0156	0.0026	
k(1,3)	0.014	0.0034	
k(9,6)	0.07	1.7×10^{-6}	

SSE: sum of squared errors

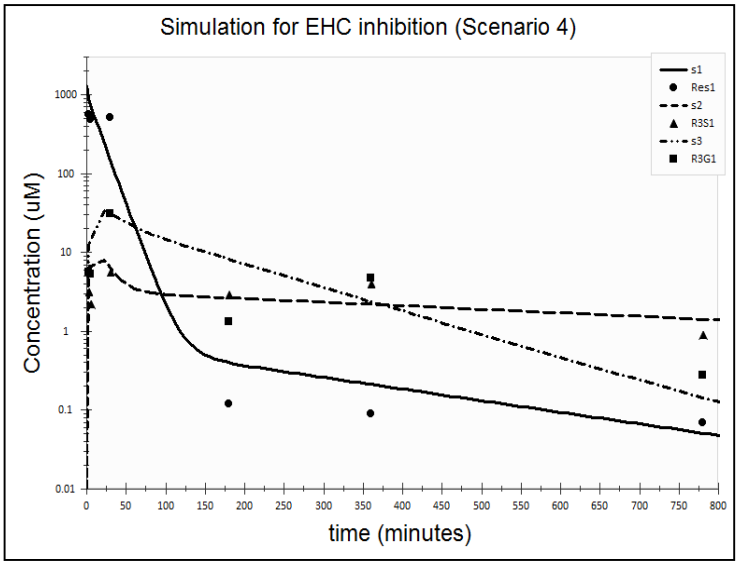

Figure 6.14. (Scenario 4) Observed and simulated plasma profiles for resveratrol, R3S and R3G in mice in the presence of antibiotics. A combination of Neo/bac was used for EHC inhibition. Observed data represented as mean values.

The distribution rate constants (between compartment 1 and 3) for resveratrol were changed in order to capture the observed plasma profile for resveratrol. This simulation seemed to perform better in terms of capturing the experimentally observed profile of resveratrol, R3S and R3G. But, a change in distribution rate constant might indicate that the orally administered antibiotics could have caused some unknown or undesired effects in vivo. The AUCs obtained from simulated concentrations were within 2 fold of the AUCs obtained from the observed data for R3G and R3S. For resveratrol, the $AUC_{0-\infty}$ obtained from simulation was 2 fold lower than the $AUC_{0-\infty}$ obtained from the observed data. This may be due to the addition of the rate constant for elimination of unchanged resveratrol [k(0,1)].

Table 6.8. List of observed and simulated AUCs obtained using the trapeziodal rule.

Control group			
	Resveratrol (mM.min)	R3S (mM.min)	R3G (mM.min)
Observed	46.03	1.62	4.58
Simulated	57.78	1.13	3.57
bcrp inhibition			
	Resveratrol (mM.min)	R3S (mM.min)	R3G (mM.min)
Observed	67.46	3.97	6.12
Simulated	49.6	2.34	5.77
mrp2 inhibition			
	Resveratrol (mM.min)	R3S (mM.min)	R3G (mM.min)
Observed	76.43	3.81	5.93
Simulated	50.34	1.47	5.65
EHC inhibition			
	Resveratrol (mM.min)	R3S (mM.min)	R3G (mM.min)
Observed	54.18	2.72	3.7
Simulated-Sce.1*	103.14	2.51	6.26
Simulated-Sce.2*	133.1	2.25	4.34
Simulated-Sce.3*	41.81	3.16	4.95
Simulated-Sce.4*	27.1	2.17	5.11

* Refer section 6.2.1.4 for details on EHC scenarios

6.5 Discussion:

MRPs and BCRP have been proposed to play a role in the transport of R3G and R3S (Breedveld et al., 2007; van de Wetering et al., 2009; Juan et al., 2010). A pharmacokinetic model, built to explain the pharmacokinetics of resveratrol and in vivo formed R3S and R3G, was used to perform simulation in order to explain experimentally observed data for mrp2, bcrp and EHC inhibition (chapter 4 and 5).

First, simulation was performed for control group of mice (resveratrol dosing only) to obtain parameters which are summarized in table 6.1. Next, simulations were performed for mrp2, bcrp and EHC inhibition. The simulations were performed in order to match the observed and simulated AUCs for resveratrol. The next step was to attempt and match the AUCs for R3S and R3G. Hence, each simulation involved multiple steps of varying a single parameter at a time in order to match the AUCs.

The simulations performed for mrp2 and bcrp inhibition indicated a decrease in elimination rate constants of R3S and R3G. The rate constants for simulations performed for bcrp inhibition were lower ([k(0,4) and [k(0,6)] were decreased to $0.041min^{-1}$ and $0.093min^{-1}$) than those in simulations performed for mrp2 inhibition ([k(0,4) and [k(0,6)] were decreased to $0.1min^{-1}$). The elimination rate constants for R3S [k(0,4] and R3G [k(0,6)] in simulation performed for control group mice (only resveratrol dosing) were $0.2min^{-1}$. Thus, the elimination rate constants were the only parameters to be varied for transporter inhibition simulations. The simulations seemed to explain the observed R3G and R3S plasma profiles for transporter inhibition.

For resveratrol plasma profiles, the simulations did not seem to explain the observed resveratrol plasma profiles. One of the reasons for this difference may be

because resveratrol was assumed to be administered i.a. instead of i.p. for ease of simulation. The major difference between i.a. and i.p. routes of administration is that after i.p. administration, the drug passes through liver as well as lungs while for i.a. administration, the drug by passes intestine, liver and lungs. Hence, the first pass metabolism by all the eliminating organs is avoided after i.a. administration and the bioavailability i.a. administration is considered to be 1. As, the drug may undergo metabolism in liver and lungs, the bioavailability after i.p. administration is not 1. Resveratrol undergoes metabolism in intestine, liver and lungs, hence after i.p. administration of resveratrol, it will only by pass the metabolism in intestine. Also, as i.p. administration is considered to be extravascular administration, there usually is a brief period of absorption, where the concentration of drug increases until it reaches Tmax. This absorption phase is not considered in the simulations performed for i.a. administered compounds. Hence, the initial part of simulations performed for resveratrol failed to agree with the observed data.

Although the extent of inhibition may not be fully known, this decrease in the rate may be due to the inhibition of transporters, for example at the apical side of hepatocytes or enterocytes.

For EHC inhibition, in addition to the above changes, the formation rate constants for R3G [k(6,1)] and R3S [k(4,1)] were varied. The rate constant for EHC [k(9,6)] was decreased to simulate EHC inhibition. The rate constant for EHC was decreased to a minimal value in 2nd scenario in order to simulate complete EHC inhibition. This simulation did capture R3G and R3S plasma profiles but lacked to capture the observed plasma profile of resveratrol.

Although the urinary excretion of resveratrol has been reported to be low (0.04% of dose) in patients (Boocock et al., 2007), a rate constant for elimination of unchanged resveratrol was added to include this route of elimination (in scenario 3 and 4). The 3rd scenario included the elimination rate constant for unchanged resveratrol and a rate constant for conversion of R3G to resveratrol. The distibution rate constants for resveratrol were also varied in this scenario. The AUCs obtained from this simulation were within 2 fold of the observed $AUC_{0-\infty}$ values for all the three compounds.
In the 4th scenario, the distribution rate constants for resveratrol (between compartment 1 and 3) were varied. Also, the elimination rate constant for unchanged resveratrol was included. This simulation seemed to capture the observed profiles of all the three compounds. The $AUC_{0-\infty}$ obtained from the simulated data was within 2 fold of the $AUC_{0-\infty}$ obtained from experimental data, except for resveratrol, which was 2 fold lower than the $AUC_{0-\infty}$ calculated from observed data. This may be due to the inclusion of [k(0,1)] in the model.

6.6 Conclusions:

Simulations using a comprehensive pharmacokinetic model were performed to assess the changes in AUCs of resveratrol and its metabolites. These simulations indicated a likely role of transporters in the disposition of R3G and R3S. In the presence of efflux transporter inhibitors, the elimination rate constants for R3G and R3S seemed to be decreased which may be due to inhibition of these transporters. The simulations for transporter inhibitor seemed to work by varying the elimination rate constants alone. In the case of EHC inhibition, the simulation, which included the rate constant for

elimination of unchanged resveratrol, seemed to agree with the observed plasma concentration time profiles of resveratrol, R3S and R3G.

ACKNOWLEDGMENTS

I would like to thank Dr. Nagar for her help with all the simulations performed in this chapter.

REFERENCES

Boocock DJ, Faust GE, Patel KR, Schinas AM, Brown VA, Ducharme MP, Booth TD, Crowell JA, Perloff M, Gescher AJ, Steward WP, and Brenner DE (2007) Phase I dose escalation pharmacokinetic study in healthy volunteers of resveratrol, a potential cancer chemopreventive agent. Cancer Epidemiol Biomarkers Prev 16:1246-1252.

Breedveld, P., D. Pluim, et al. (2007). "The effect of low pH on breast cancer resistance protein (ABCG2)-mediated transport of methotrexate, 7-hydroxymethotrexate, methotrexate diglutamate, folic acid, mitoxantrone, topotecan, and resveratrol in in vitro drug transport models." Mol Pharmacol 71(1): 240-249.

Chien, J. Y., S. Friedrich, et al. (2005). "Pharmacokinetics/Pharmacodynamics and the stages of drug development: role of modeling and simulation." AAPS J 7(3): E544-559.

Juan, M. E., E. Gonzalez-Pons, et al. (2010). "Multidrug resistance proteins restrain the intestinal absorption of trans-resveratrol in rats." J Nutr 140(3): 489-495.

Maier-Salamon A, Bohmdorfer M, Riha J, Thalhammer T, Szekeres T, and Jaeger W (2013) Interplay between metabolism and transport of resveratrol. Ann N Y Acad Sci 1290:98-106.

Patel, K. R., C. Andreadi, et al. (2013). "Sulfate metabolites provide an intracellular pool for resveratrol generation and induce autophagy with senescence." Sci Transl Med 5(205): 205ra133.

Schuck, E., T. Bohnert, et al. (2015). "Preclinical pharmacokinetic/pharmacodynamic modeling and simulation in the pharmaceutical industry: an IQ consortium survey examining the current landscape." AAPS J 17(2): 462-473.

Sharan, S., O. F. Iwuchukwu, et al. (2012). "In vivo-formed versus preformed metabolite kinetics of trans-resveratrol-3-sulfate and trans-resveratrol-3-glucuronide." Drug Metab
Dispos 40(10): 1993-2001.

van de Wetering, K., A. Burkon, et al. (2009). "Intestinal breast cancer resistance protein (BCRP)/Bcrp1 and multidrug resistance protein 3 (MRP3)/Mrp3 are involved in the pharmacokinetics of resveratrol." Mol Pharmacol 75(4): 876-885.

Walle T, Hsieh F, DeLegge MH, Oatis JE, Jr., and Walle UK (2004) High absorption but very low bioavailability of oral resveratrol in humans. Drug Metab Dispos 32:1377-1382.

APPENDIX A

A 1. Experimental plan for time dependent inhibition assay in sandwich cultured human hepatocytes

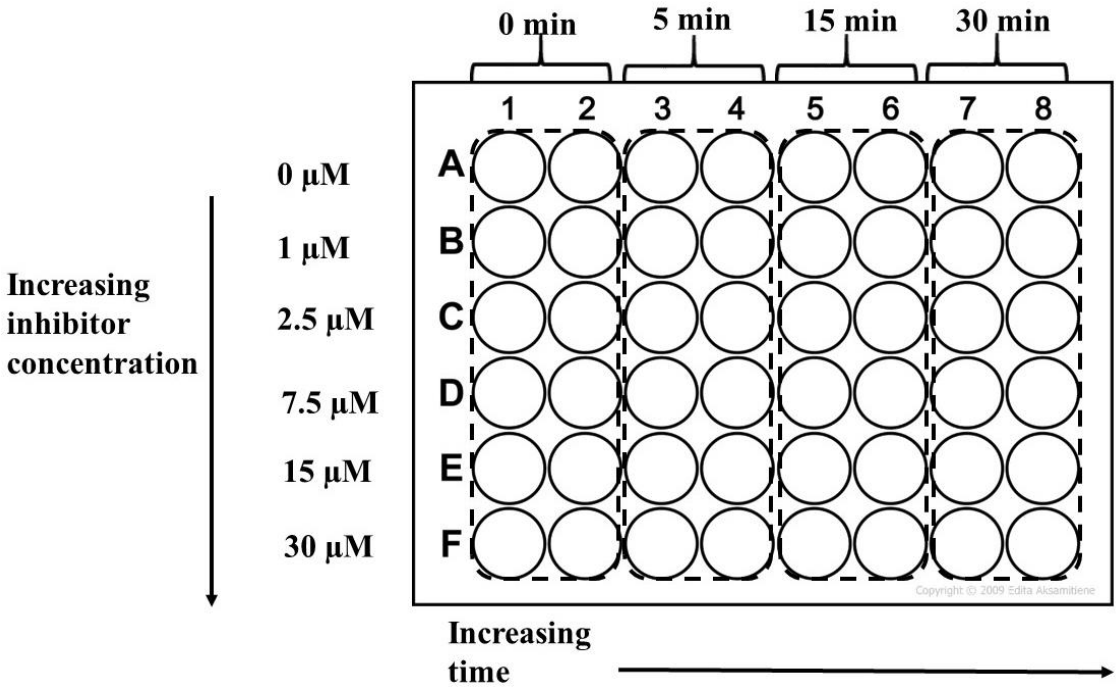

Figure A1. Experimental plan for time dependent inhibition assay in SCHH.

- Each dashed box indicates samples in duplicates
- Cells plated in 48 well format with matrix gel, incubated at 37^0C with 5% CO_2 for 24 hours
- Next day, each well was washed to remove dead cells before assay
- Primary incubation:
    - Different concentrations of inhibitors were incubated at different time points
    - After each time point, the inhibitor solution was removed and the cell layer washed
- Secondary incubation:
    - 20µM probe substrate (midazolam) incubated for 20 minutes
- Cold acetonitrile added to the cells, the cell layer scraped and collected

APPENDIX B

B 1. HPLC-MS/MS chromatogram for N-desethylamodiaquine

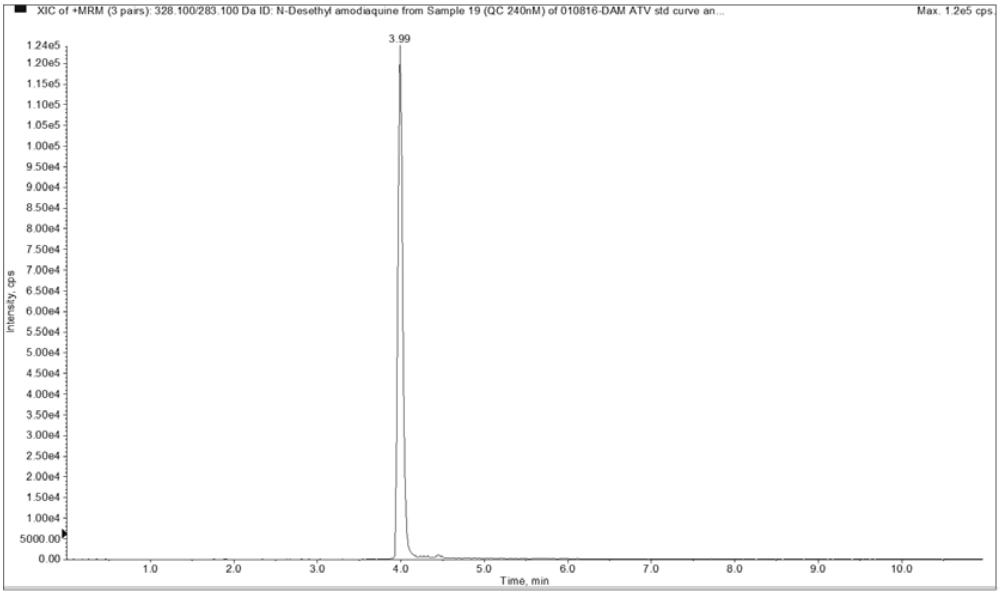

Figure B1. A representative chromatogram for N-desethylamodiaquine. Structure given in chapter 2.

B 2. N-desethylamodiaquine compound optimization

Infusion

Compound Optimization MS/MS Analysis, positive

Precursor ion: MW Ion Search Window: ± 1.000 (Da) Product ion: Auto Select, Criteria:

From the most intense: 10 peaks. Build final method using 7 most intense peaks. Exclude Product Ions within ± 10.000(Da) of Precursor Ion m/z.

Min. mass for product ion: 40.000(Da). Threshold for product ion > 1500.0(cps) Quad 1 Resolution: Unit resolution, Quad 3 Resolution: Unit resolution

Target Compound	MW(neutral, Da)	No. Charges
N-desethylamodiaquine	327.830	1

Initial Q1 Scan

Target Compound	Mass(Da)	Intensity(cps) (5 MCA Average)
N-desethylamodiaquine	328.146	1323080

Parameter: DP Start: 1.0 Stop: 400.0 Step: 5.0

Masses(Da)	Current Value	New Value	Intensity(cps)
328.146	20.0	61.0	2751249

Final Q1 Scan

Target Compound	Mass(Da)	Intensity(cps) (5 MCA Average)
N-desethylamodiaquine	328.133	9516760

Final Q1MI Method: N-desethylamodiaquine_QOpt_FinalQ1MI_Pos.dam Target Compound: N-desethylamodiaquine

Initial Product Mass	Initial Product Ion Intensity(cps) (26 MCA Sum)
283.048	4239000
285.032	646000

190.220 498000

218.161 493000

89.203 427000

255.009 402000

163.227 223000

216.222 203000

217.000 203000

217.400 203000

Parameter: CE Start: 5.0 Stop: 130.0 Step: 2.0

Masses(Da) Current Value New Value Intensity(cps)

Parameter: CXP Start: 0.0 Stop: 55.0

Step: 2.0

Masses(Da) Current Value New Value Intensity(cps)

328.133/89.203 15.0 16.0 8130

Parameter: CXP Start: 0.0 Stop: 55.0

Step: 2.0

Masses(Da) Current Value New Value Intensity(cps)

328.133/163.227 15.0 14.0 9532

Parameter: CXP Start: 0.0 Stop: 55.0

Step: 2.0

Masses(Da) Current Value New Value Intensity(cps)

328.133/190.220 15.0 12.0 3690

Parameter: CXP Start: 0.0 Stop: 55.0

Step: 2.0

Masses(Da) Current Value New Value Intensity(cps)

328.133/216.222 15.0 12.0 1208

Parameter: CXP Start: 0.0 Stop: 55.0

Step: 2.0

Masses(Da) Current Value New Value Intensity(cps)

328.133/217.000 15.0 36.0 6258

Parameter: CXP Start: 0.0 Stop: 55.0
Step: 2.0

Masses(Da)	Current Value	New Value	Intensity(cps)
328.133/217.400	15.0	14.0	10230

Parameter: CXP Start: 0.0 Stop: 55.0
Step: 2.0

Masses(Da)	Current Value	New Value	Intensity(cps)
328.133/218.161	15.0	38.0	42003

Parameter: CXP Start: 0.0 Stop: 55.0
Step: 2.0

Masses(Da)	Current Value	New Value	Intensity(cps)
328.133/255.009	15.0	6.0	51078

Parameter: CXP Start: 0.0 Stop: 55.0 Step: 2.0

Masses(Da)	Current Value	New Value	Intensity(cps)
328.133/283.048	15.0	6.0	170367

Parameter: CXP Start: 0.0 Stop: 55.0 Step: 2.0

Masses(Da)	Current Value	New Value	Intensity(cps)
328.133/285.032	15.0		

Final Product Ion Mass (Da) Average)

89.200 28.0 24478

Final Product Ion Intensity(cps) (10 MCA 7160)

163.400	4530
190.300	2950
216.600	2550
217.200	11610
217.300	12200
218.300	50390
255.100	67970
283.000	180150

285.000 28830

Optimal Product Ion Mass:	283.000	Optimal Product Ion Intensity:	180150
Optimal Product Ion Mass:	255.100	Optimal Product Ion Intensity:	67970
Optimal Product Ion Mass:	218.300	Optimal Product Ion Intensity:	50390
Optimal Product Ion Mass:	285.000	Optimal Product Ion Intensity:	28830
Optimal Product Ion Mass:	217.300	Optimal Product Ion Intensity:	12200
Optimal Product Ion Mass:	217.200	Optimal Product Ion Intensity:	11610
Optimal Product Ion Mass:	89.200	Optimal Product Ion Intensity:	7160

Final MRM Method: N-desethylamodiaquine_QOpt_FinalMRM_Pos.dam Compound optimization completed successfully.

APPENDIX C

C 1. Experimental plan for uptake assay in HT-29 and Caco-2 cell lines

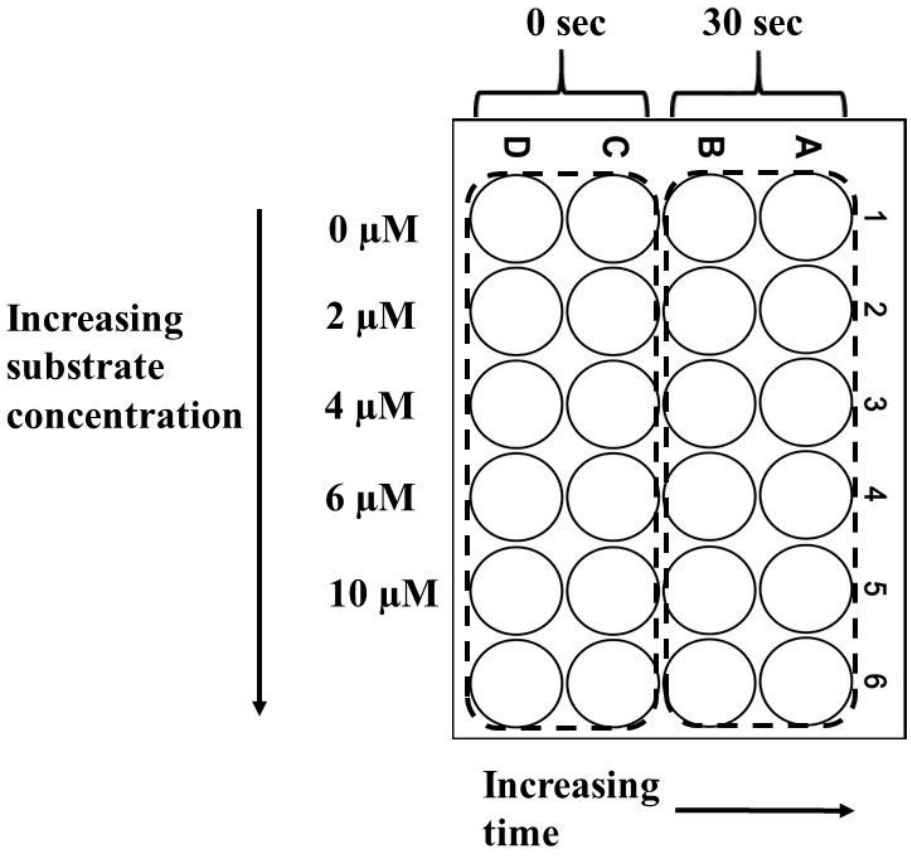

Figure C1. Experimental plan for uptake assays in HT-29 and Caco-2 cell lines.

- Each dashed box indicates samples in duplicates
- Cells plated at 100,000 cells/well, assay performed on 5th day for Caco-2 and 8th day for HT-29 cells
- Cells washed by HBSS buffer, solution of substrate in HBSS added to cell layer
- Different concentrations of substrate incubated for different time points
- After each time point, the substrate solution was removed and the cell layer washed
- Cold acetonitrile + water (80:20) added to the cell layer, cell layer scraped and collected

C 2. HPLC-MS/MS chromatogram of resveratrol uptake in Caco-2 cells

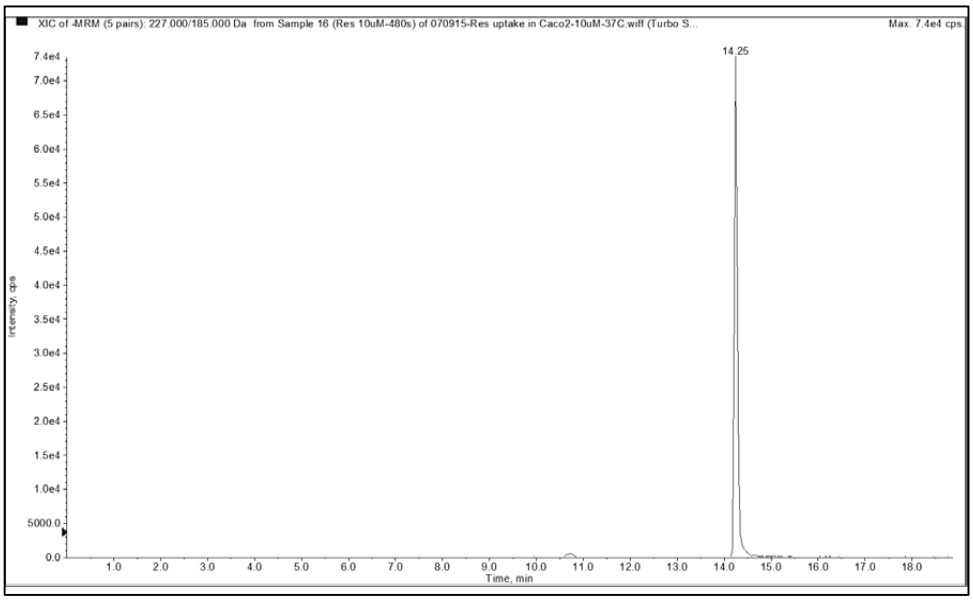

Figure C2. A representative chromatogram for resverative in Caco-2 uptake assays.

C 3. HPLC-MS/MS chromatogram of absence of R3G uptake in Caco-2 cells

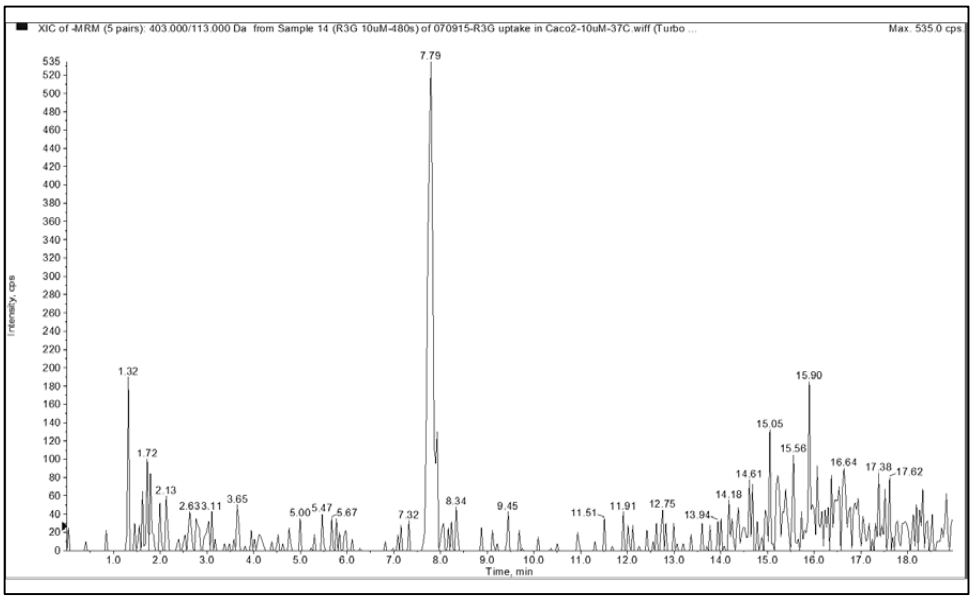

Figure C3. A representative chromatogram for the absence of R3G in Caco-2 uptake assays.

APPENDIX D

D 1. HPLC-MS/MS chromatogram of resveratrol

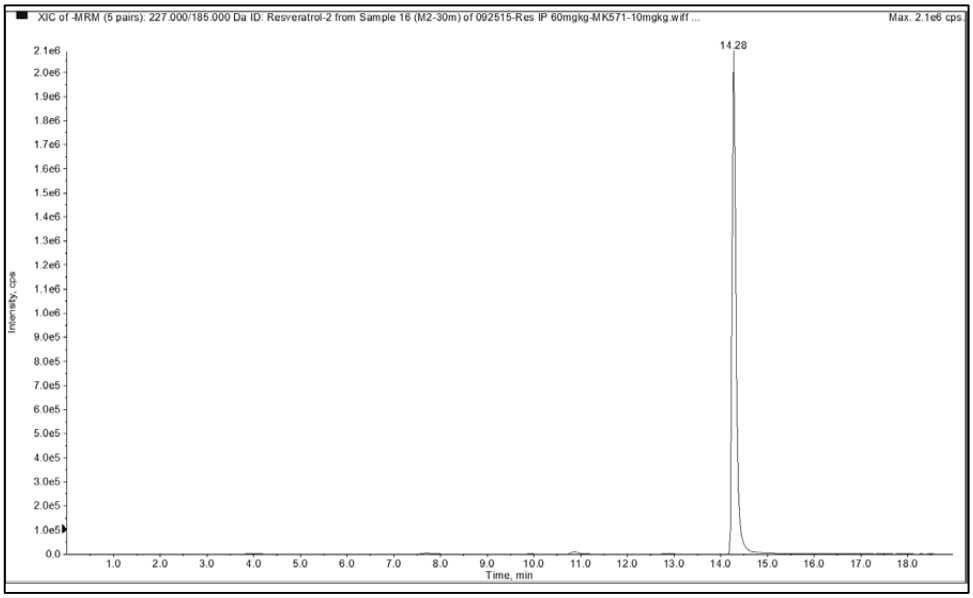

Figure D1. A representative chromatogram for resveratrol. Structure of resveratrol given in chapter 1

D 2. HPLC-MS/MS chromatogram for R3G

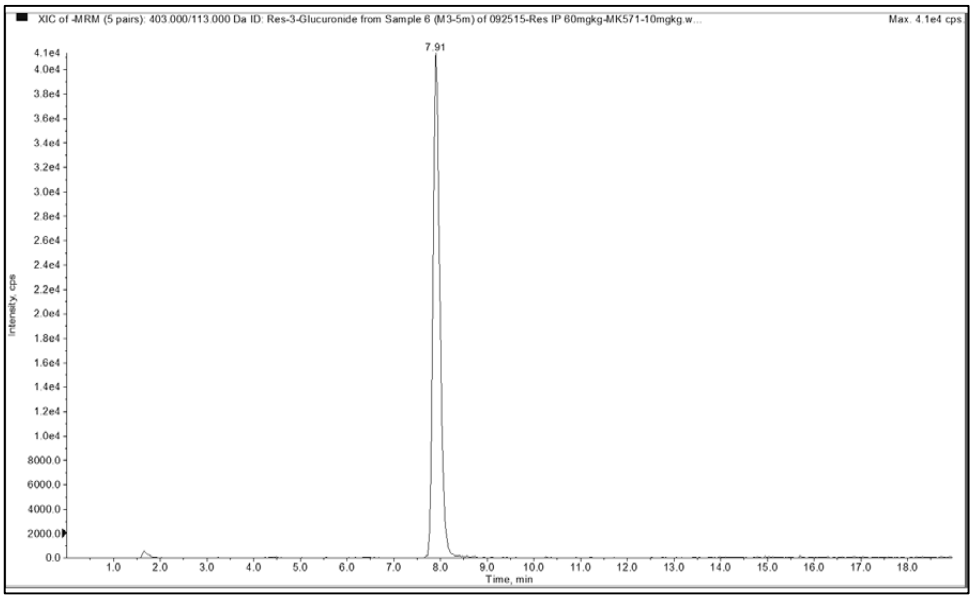

Figure D2. A representative chromatogram for R3G. Structure given in chapter 1.

D 3. HPLC-MS/MS chromatogram for R3S

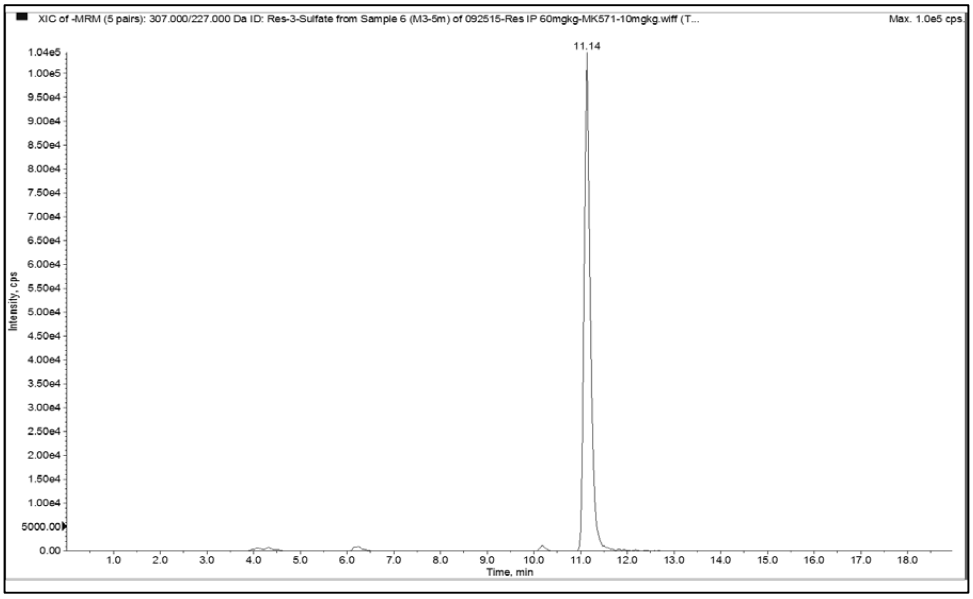

Figure D3. A representative chromatogram for R3S. Strucutre given chapter 1.

APPENDIX E

E 1. Concentration time profile of resverstrol with and without transporter inhibitors (resveratrol dosed i.p. 60mg/kg).

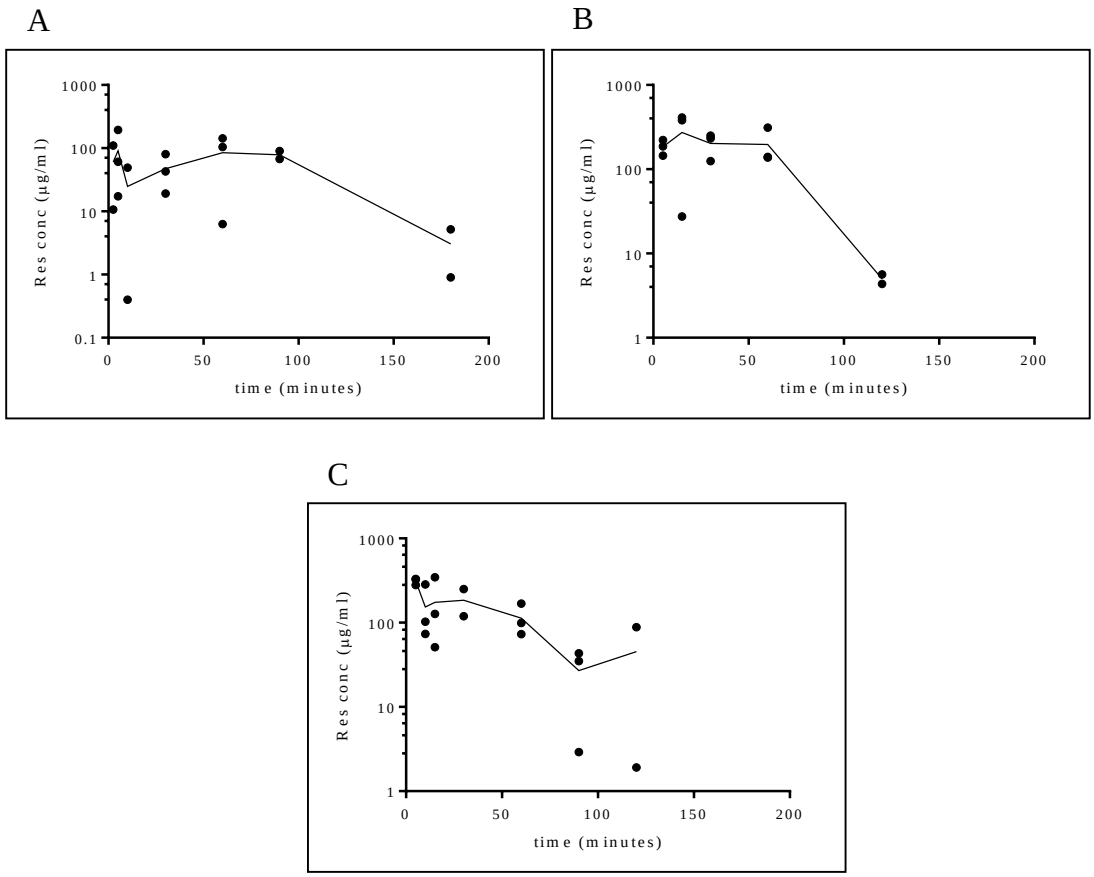

Figure E1. Concentration time profile of resverstrol (60mg/kg) in (A) control group, (B) in presence of mrp2 inhibitor, (C) in presence of bcrp inhibitor. Data represented as replicates. The solid line represents the mean data.

E 2. Concentration time profile of R3G with and without transporter inhibitors (resveratrol dosed i.p. 60mg/kg).

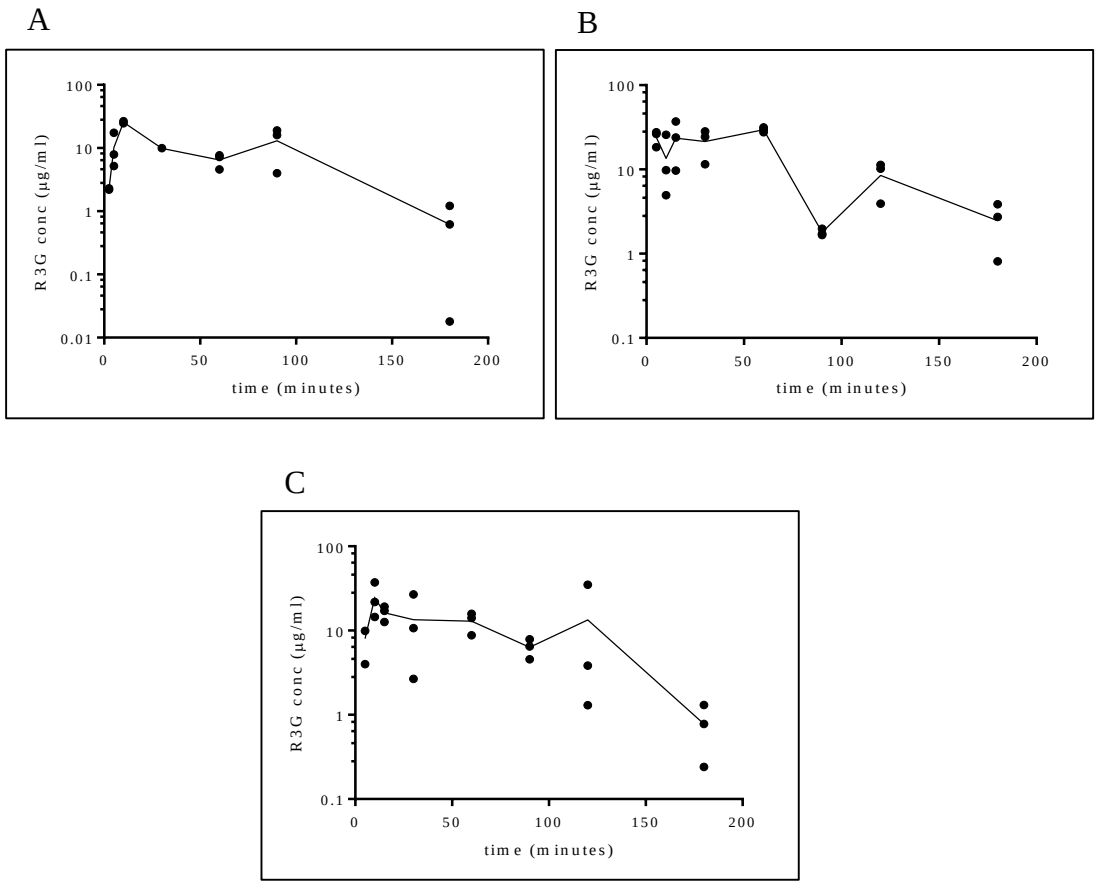

Figure E2. Concentration time profile of R3G (60mg/kg) in (A) control group, (B) in presence of mrp2 inhibitor, (C) in presence of bcrp inhibitor. Data represented as replicates. The solid line represents the mean data.

E 3. Concentration time profile of R3S with and without transporter inhibitors (resveratrol dosed i.p. 60mg/kg).

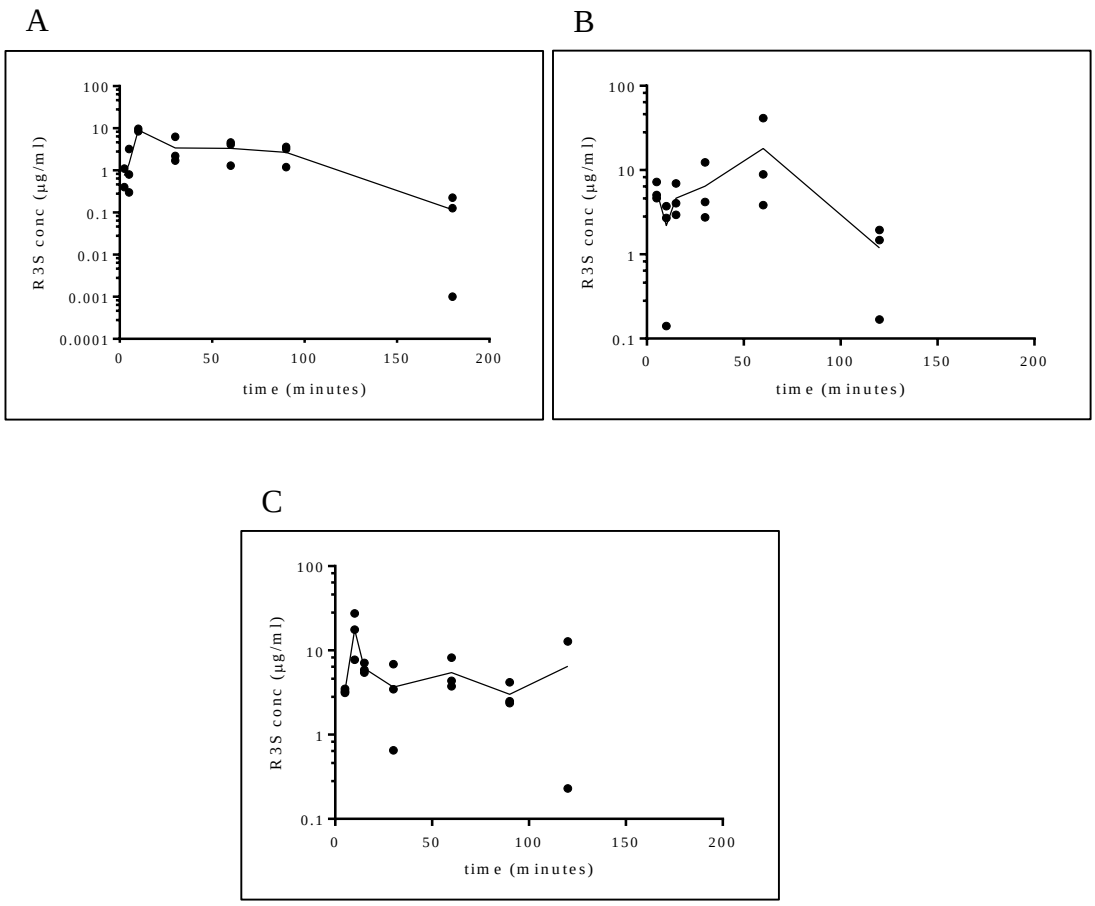

Figure E3. Concentration time profile of R3S in (A) control group, (B) in presence of mrp2 inhibitor, (C) in presence of bcrp inhibitor. Data represented as replicates. The solid line represents the mean data.

APPENDIX F

F 1. Concentration time profile of resverstrol with and without antibiotics (resveratrol dosed i.p. 60mg/kg).

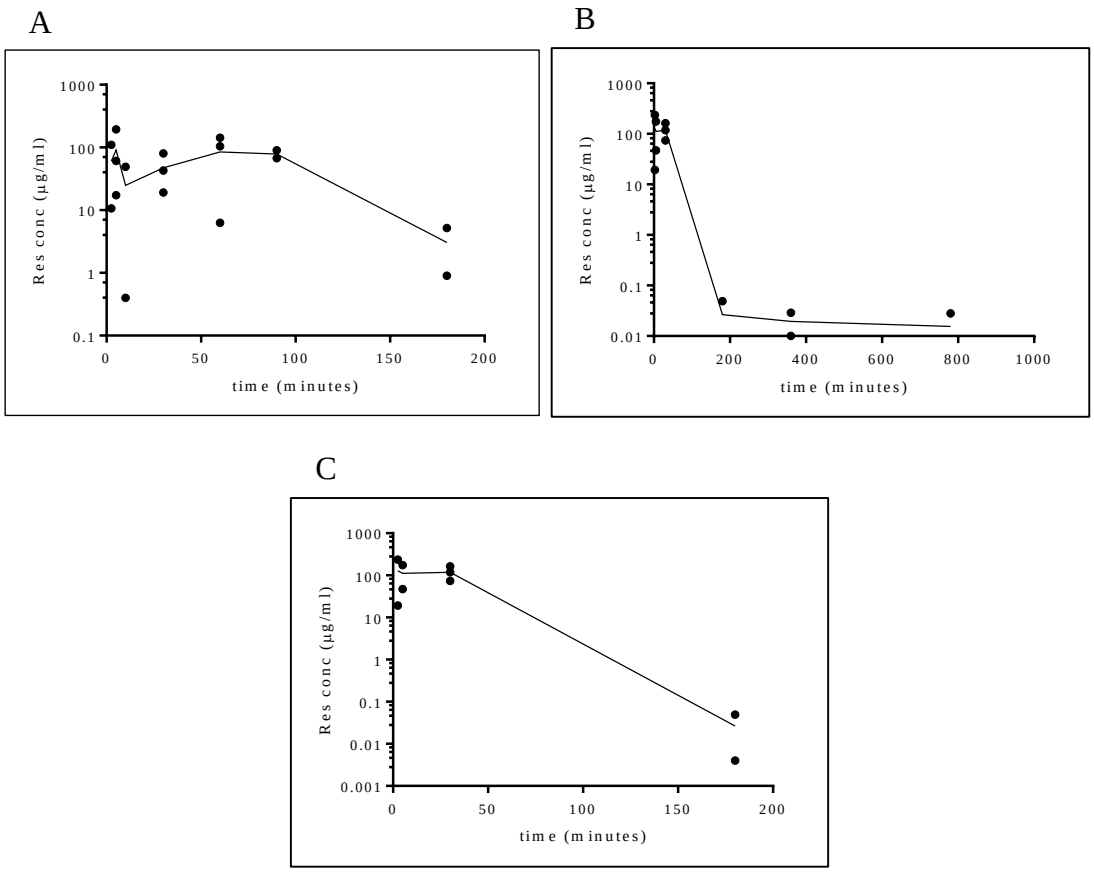

Figure F1. Concentration time profile of resveratrol (A) without, (B) with antibiotics and (C) with antibiotics (initial time points of plot (B) t=0-180). Data represented as replicates. The solid line represents the mean data.

F 2. Concentration time profile of R3G with and without antibiotics (resveratrol dosed i.p. 60mg/kg).

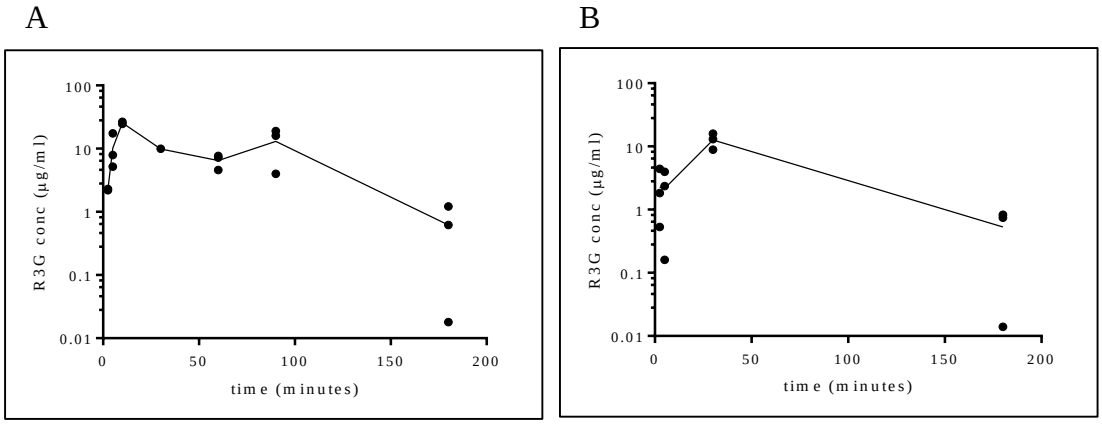

Figure F2. Concentration time profile of R3G (A) without and (B) with antibiotics. Data represented as replicates. The solid line represents the mean data.

F 3. Concentration time profile of R3S with and without antibiotics (resveratrol dosed i.p. 60mg/kg).

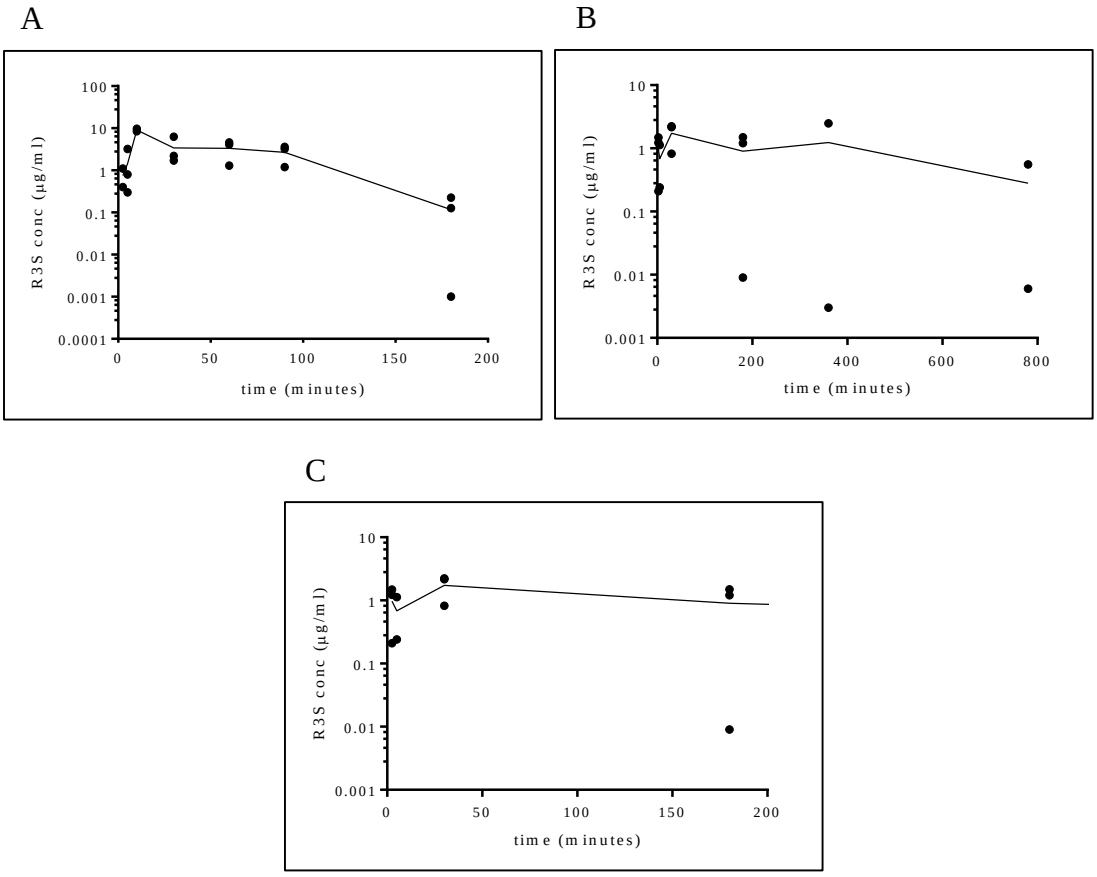

Figure F3. Concentration time profile of R3S (A) without, (B) with antibiotics and (C) with antibiotics (initial time points of plot (B) t=0-180). Data represented as replicates. The solid line represents the mean data.